

Title: Optimising Time Trial Helmet Design for Enhanced Aerodynamics in Cycling Through CFD Techniques

Name: Robert Campbell

Student ID: [REDACTED]

Supervisors: Assoc Prof Andrew Wandel (Lead), Dr Khalid Saleh (Second)

University of Southern Queensland
School of Engineering

ENP4111 Dissertation Project

(This is a 2-unit research project in Bachelor of Engineering Honours Program)

Limitations of Use

The Council of the University of Southern Queensland, its Academic Affairs, and the staff of the University of Southern Queensland, do not accept any responsibility for the truth, accuracy or completeness of material contained within or associated with this dissertation. Persons using all or any part of this material do so at their own risk, and not at the risk of the Council of the University of Southern Queensland, its Faculty of Health, Engineering and Science or the staff of the University of Southern Queensland.

This dissertation reports an educational exercise and has no purpose or validity beyond this exercise. The sole purpose of this dissertation project is to contribute to the overall education within the student's chosen degree program. This document, the associated hardware, software, drawings, and other material set out in the associated appendices should not be used for any other purpose: if they are so used, it is entirely at the risk of the user.

Certification

I certify that the ideas, designs and experimental work, results, analyses and conclusions set out in this dissertation are entirely my own effort, except where otherwise indicated and acknowledged.

I further certify that the work is original and has not been previously submitted for assessment in any other course or institution, except where specifically stated.

Student Name:

Robert Campbell

Student Number:

[REDACTED]

[REDACTED]

Signature

Date

Abstract

Keywords: Cycling, road cycling, sports engineering, aerodynamics, mechanical engineering, computational fluid dynamics, CFD, bicycle, helmet, time trial

Throughout the history of cycling, advancements in aerodynamics through design have given the rider ‘free’ speed without having to exert any additional energy. In the context of professional cycling, athletes and their multi-million-dollar budget teams are striving to gain any advantage over competitors through aerodynamics in the form of improved design, clothing, helmets, shoes, socks, and of course the sleek shaved legs that most professional cyclists show off in the peloton. The first race that shocked the world for aerodynamics was the 1989 Tour De France. This final stage consisted of a 25 km TT event, in which Greg Lemond went from second to first place by utilising a TT helmet, disc wheel and ‘aero’ bars, something unheard of at the time.

The literature review provided the governing equations to construct a theoretical model to set a reference for helmet dimensions and performance. From this, a TT time savings model was derived to show how the helmets performed over a 40km TT when used by a rider of the same size and output of 400 W. ANSYS Spaceclaim was used to design a control helmet for testing to set a reference point for all other helmets. Three commercially available designs were replicated for testing which included the BELL Javelin, HJC Adwatt and POC Tempo. Three prototypes were designed and tested against the replicas. ANSYS Fluent was selected to perform the simulations at a velocity of 13 m/s (46.8 km/h) utilising a $k - \epsilon$ model to maintain computational efficiency and an appropriate wake and enclosure dimensions were defined. The simulations included the use of a human model which consisted of a larger male size torso, arms and head only, in which simulations for each helmet were performed at angles of 20 and 30 degrees.

Overall, the top performing helmet was the version 3 prototype at 20 degrees with a 13.7% efficiency improvement than the control helmet. When ranked in the TT time savings model it was 15.15 seconds in front of second place and 48.48 seconds in front of last place. The worst performing helmet was the BELL Javelin at 30 degrees. Further work was identified to validate the results from this research which included 3D printed prototyping helmets for WT testing followed by human testing in WT and on road testing. The main finding was that helmet

performance is heavily reliant on rider position and yaw angle, even in extreme or irregular designs. Further designs would need to consider this with the potential for future projects of technology which provides data to the cyclist in real time on how to adjust their position whilst riding to obtain an optimal aerodynamic efficiency.

Acknowledgements

Thanks to my wife and family, whose support has been critical to my success throughout my degree. Assistance and guidance from my supervisor facilitated this research paper being taken to the next level in quality.

Thanks also to my network of fellow peers. Having people to discuss ideas and go through the same journey was helpful in the final stage of my study.

R. Campbell

Nomenclature

Term Glossary and Abbreviations		
Term	Description	Units
CFD	Computational Fluid Dynamics	-
aero	Aerodynamic	-
FEA	Finite Element Analysis	-
TT	Time Trial	-
TTT	Team Time Trial	
UCI	Union Cyclist International (International cycling governing body)	-
WT	Wind tunnel	-
C_{dA}	Aerodynamic resistance	N
C_d	Drag Coefficient	-
m/s	metres per second	-
km/h	Kilometres per hour	-
v	Displacement Velocity	m/s
v_f	Velocity Relative to Fluid	m/s
W	Watts	-
P	Cyclist Power	W
h_b	body height	cm
m_b	body mass	kg
m_c	Bicycle mass	kg
M	Cyclist-bicycle system mass	kg
A	Frontal Area	m^2
A_{BSA}	Body Surface Area	m^2
A_p	Frontal area using aero handlebars and TT helmet	m^2
α_1	TT helmet inclination on the horizontal	$^\circ$
L	Length of TT helmet	m
A	Frontal Area	m^2
ρ	Air density	kg/m^3
ρ_0	Air density at 760 mmHg and 273 K	kg/m^3
PB	Barometric Pressure	Pa
q	Dynamic Pressure	Pa
T	Temperature of air	$^\circ C$

R_{RC}	Rolling Resistance coefficient	-
R_R	Rolling Resistance	N
R_T	Total resistive forces	N
R_D	Drag Force	N
TKE	Turbulent Kinetic Energy	-
k	Turbulent Kinetic Energy	-
e	Dissipation rate of Turbulent Kinetic Energy	-
ω	Specific Dissipation rate	-
Ahmed Body	Generic car body (simplified car model)	-
Climb(ing)	Riding a bicycle on an inclined surface	

Table of Contents

Limitations of Use	ii
Certification	iii
<i>Abstract</i>	iv
Acknowledgements	vi
<i>Nomenclature</i>	vii
Chapter 1 – Introduction	1
1.1 – Aim	1
1.2 – Background	1
1.3 – Problems	5
1.4 – Research Goals	6
Chapter 2 – Literature Review: Established Knowledge	7
2.1 – Cycling Aerodynamics	7
2.1.1 – Governing Equations	7
2.1.2 – Forces and moments	9
2.1.3 – Drag Coefficient	11
2.1.4 – Frontal Area	12
2.1.5 – Air Density	14
2.1.6 – Velocity	14
2.1.7 – Drafting	15
2.2 – Automotive aerodynamics	18
2.2.1 – Topology Optimisation	18
2.2.2 – Active Aerodynamics	20
2.2.3 – Surface Roughness and Texturing	21
2.3 – Cyclist Profile	24
2.3.1 – Power	24
2.3.2 – Head angle	26
2.3.3 – Helmet Types	27

2.3.4 – Anthropometric Data	30
2.4 – Aerodynamic Testing	32
2.4.1 – CFD.....	32
2.4.2 – Wind Tunnel Testing	35
2.5 – Mathematical Formulation.....	37
2.5.1 – Turbulence	38
2.5.2 – Reynolds-averaged Navier Stokes (RANS) Equation.....	39
2.5.3 – Turbulent Kinetic Energy k	41
2.5.4 – Dissipation rate of Turbulent Kinetic Energy e	42
2.5.5 – Specific Dissipation rate ω	42
2.5.6 – Standard $k - e$ model	42
2.5.7 – Standard $k - \omega$ model.....	42
2.5.8 – Transitional $SST k - \omega$ model.....	43
2.5.9 – Steady State vs Transient Solver.....	44
2.6 – Design Regulations.....	44
2.6.1 – Australian Standards.....	44
2.6.2 – UCI Regulations.....	45
2.7 – Knowledge Gap	47
2.7.1 – Research Justification	47
2.7.2 – Project Feasibility Analysis	48
Chapter 3 – Methodology.....	49
3.1 – Chapter Overview	49
3.2 – Theoretical Model	49
3.3 – ANSYS Fluent.....	51
3.4 – Control helmet and Body	52
3.5 – Preliminary Simulations	55
3.6 – Current Design Replication.....	57
3.7 – Project Simulations	58

3.7.1 – Scope	58
3.7.2 – Geometry	59
3.7.3 – Enclosure and Wake	60
3.7.4 – Named Selections	60
3.7.5 – Mesh	61
3.7.6 – Model Selection	62
3.7.7 – CFD conditions	63
3.7.8 – Report Definitions	64
3.7.9 – Solution Setup.....	65
3.7.10 – FLUENT Outputs	66
3.8 – TT time savings.....	67
3.9 – Risk Assessment	67
3.10 – Summary.....	67
Chapter 4 – Results	68
4.1 – Chapter Overview	68
4.2 – Project Simulation	68
4.2.1 – 20 degree position	68
4.2.2 – 30 degree position	69
4.2.3 – Changes in Velocity	70
4.2.4 – Visualisations	71
4.3 – Time Savings Model	73
4.4 – Steady State vs Transient Solver.....	74
4.5 – Chapter Summary	76
Chapter 5 – Discussion.....	77
5.1 – Chapter Overview	77
5.2 – Results Analysis.....	77
5.2.1 – Best Performing helmet	77
5.2.2 – Worst Performing helmet	78

5.2.3 – Remaining helmets performance	79
5.2.4 – Optimal helmet shape designs.....	80
5.2.5 – Time savings results	82
5.2.6 – Change in head angle	82
5.2.7 – Change in velocity.....	83
5.2.8 – UCI Design Compliance.....	83
5.2.9 – Average of Results.....	85
5.2.10 – Transient Result Comparison	86
5.3 – Chapter Summary	90
Chapter 6 – Conclusion and Further Work	91
6.1 – Conclusion	91
6.2 – Performance Analysis	91
6.3 – Further Work	93
6.3.1 – Commercial Design Replication	94
6.3.2 – Human model.....	94
6.3.3 – Bicycle model	94
6.3.4 – Simulation refinements	95
6.3.5 – Non-uniform wind flow	96
6.3.6 – Simulations of cyclist in paceline	96
6.4 – Further testing.....	96
6.4.1 – 3D Prototype WT	97
6.4.2 – Human WT	97
6.4.3 – Strength and safety testing	97
6.4.4 – On road testing	99
6.4.5 – Helmet designs	99
References.....	100
Appendix A.....	109
A.1 – Project Specification and Work Plan	109

A.2 – Timeline	111
A.3 – Risk Assessment	112

List of Figures

Figure 1 – Greg Lemond 1989 TT	1
Figure 2 – Chris Boardman on Lotus ‘Superbike’	2
Figure 3 – Evolution of the hour record average speed.....	3
Figure 4 – Filippo Ganna breaking the hour record in 2022	4
Figure 5 – The detailed design for aerodynamic advantage of Ganna’s bicycle and helmet ..	4
Figure 6 – Team Visma and their new Giro TT helmet	5
Figure 7 – Team Quickstep and their new Specialized TT helmet	5
Figure 8 – FBD of rider to obtain frontal area..	8
Figure 9 – Aerodynamic forces and moments of cyclist	10
Figure 10 – Diagram showing forces when the cyclist is riding uphill	10
Figure 11 – Diagram showing forces calculated relative to wind velocity	11
Figure 12 – Different rider positions.....	13
Figure 13 – Diagram showing all components of total air velocity and the yaw and pitch angle definitions	15
Figure 14 – Professional cycling Peloton during road race.....	16
Figure 15 – Examples of a TTT paceline	16
Figure 16 – Percentage drag compared to lead rider in a paceline	17
Figure 17 – CFD velocity visualisation showing the benefit of drafting in a peloton	17
Figure 18 – Examples of different CFD simulations in automotive industry.....	19
Figure 19 – Example of topology optimisation in the automotive industry	20
Figure 20 – Examples of active aerodynamics in the automotive industry in the form of movable wings	20
Figure 21 – Example of dimples applied to Ahmed body in dimple effect research and testing	21
Figure 22 – Velocity magnitude contour comparing dimple effect	22
Figure 23 – Bugatti Bolide (bottom) and the dimple system on the air intake (top)	23
Figure 24 – Graph showing records of maximum sustainable power as a function of effort duration	24
Figure 25 – Different helmet designs and head angles tested in previous research	26
Figure 26 – Result of head angle on pressure coefficient.....	27
Figure 27 – Result of head angle on velocity streamline	27
Figure 28 – Popular Road and TT helmets.....	28
Figure 29 – Side view of TT helmet illustration	28

Figure 30 – Average Tour De France cyclist weight.....	30
Figure 31 – Average Tour De France cyclist height.....	31
Figure 32 – Tour De France winner weight.....	31
Figure 33 – Tour De France winner height	31
Figure 34 – Boundary Domain for CFD simulation of cyclist	32
Figure 35 – Larger boundary domain for CFD simulation of cyclist.....	33
Figure 36 – Examples of poly-hexcore and tetrahedral mesh applied to TT cyclist.....	33
Figure 37 – CFD vs WT testing.....	34
Figure 38 – Diagram of a closed circuit WT at Eindhoven University in the Netherlands.....	35
Figure 39 – Diagram of a 3/4 open-jet WT at Monash University Clayton Campus	36
Figure 40 – Team Jumbo Visma testing team TT aerodynamics in a WT	36
Figure 41 – Scale model of cyclist manufactured by 3D printer for WT testing	37
Figure 42 – Relationship of Reynolds number and flow transitions.....	39
Figure 43 – Comparing turbulent kinetic energy when using different models within CFD ...	41
Figure 44 – Increase in computational cost per iteration of RANS based models.....	43
Figure 45 – Extract from AusCycling Technical Regulations on helmets	45
Figure 46 – UCI helmet design regulations.....	45
Figure 47 – UCI prototype equipment application form	46
Figure 48 – Rider head angle impact on cyclist power	50
Figure 49 – TT helmet length impact on cyclist power.....	51
Figure 50 – ANSYS Fluent workspace	51
Figure 51 – Control body with no helmet.	53
Figure 52 – Control helmet design.....	53
Figure 53 – Dimensions of the body for the human model	54
Figure 54 – Dimensions of the head from the human model.....	54
Figure 55 – Preliminary simulations mesh convergence study.....	55
Figure 56 – Mesh quality for preliminary simulations.....	55
Figure 57 – Model in setup showing correct direction for flow	56
Figure 58 – (a) Velocity streamline showing flow separation, (b) Velocity vector showing flow direction	57
Figure 59 – Current Designs to be replicated.	57
Figure 60 – Replication process of current designs.....	58
Figure 61 – Final product of replica helmets.....	58
Figure 62 – Different head angles that will be tested during project.....	59
Figure 63 – Three versions of prototype helmets	59

Figure 64 – Enclosure with dimensions	60
Figure 65 – Wake with dimensions	60
Figure 66 – Model named selections	61
Figure 67 – Inlet named selection and coordinate system.....	61
Figure 68 – Mesh nodes and elements.....	61
Figure 69 – Mesh quality of cyclist.....	62
Figure 70 – k- ϵ model setup	63
Figure 71 – Air properties for simulation	63
Figure 72 – Inlet velocity	64
Figure 73 – Report definitions for Drag Force and Coefficient.....	64
Figure 74 – Projected area for frontal area.....	65
Figure 75 – Standard initialisation setup.....	65
Figure 76 – Scaled residuals showing solution convergence	66
Figure 77 – FLUENT outputs in ANSYS Workspace	66
Figure 78 – Percentage Drag Force Improvement for all helmets at both angles	69
Figure 79 – Graphical comparison of drag force for a range of velocity 8 to 18 m/s of control helmet with top performing helmets	70
Figure 80 – Velocity contour plot for best and worst performing helmet.....	71
Figure 81 – Velocity streamline plot for best and worst performing helmet	71
Figure 82 – Pressure contour plot for best and worst performing helmet.....	72
Figure 83 – Graphical comparison of time gap of all helmets at both angles	74
Figure 84 – Graphical representation of transient results for both angles	75
Figure 85 – Version 3 prototype visualisations	77
Figure 86 – BELL Javelin visualisations	78
Figure 87 – Velocity streamline or remaining helmets at 20 (left) and 30 degrees (right)	80
Figure 88 – Version 1 prototype helmet dimensions.....	84
Figure 89 – Version 2 prototype helmet dimensions.....	84
Figure 90 – Version 3 prototype helmet dimensions.....	85
Figure 91 – Percentage drag force improvement of the average performance of all helmets through both angles	86
Figure 92 – Steady vs transient drag force result graphical comparison at 20-degrees.....	87
Figure 93 – Steady vs transient percentage improvement graphical comparison at 20-degrees	88
Figure 94 – Steady vs transient drag force result graphical comparison at 30-degrees.....	89

Figure 95 – Steady vs transient percentage improvement graphical comparison at 30- degrees	89
Figure 96 – TTT drafting	96
Figure 97 – Jay Vine’s recent TT crash at UCI World Championship.....	98
Figure 98 – Stefan Kung’s TT crash at the European Championship	98

List of Tables

Table 1 – Evolution of the hour record showing the impact of improved aerodynamics.....	3
Table 2 – Formulas used to model cycling aerodynamics.....	7
Table 3 – Examples of different correction factors for determining aerodynamic drag in cycling.....	9
Table 4 – Examples of different objects and their drag coefficient	12
Table 5 – Results for frontal area for riders of different sizes	13
Table 6 – Percentage contribution different body parts have to the total aerodynamic resistance.....	13
Table 7 – Frontal areas of rider positions in Figure 3	14
Table 8 – Effect of air density on aerodynamic drag.....	14
Table 9 – Trueness and precision of power meters by manufacturer.....	25
Table 10 – Power output required to reach a constant velocity in the various positions.	26
Table 11 – Examples of some TT helmets over the last decade.....	29
Table 12 – Advantages and limitations of the ANSYS meshes	34
Table 13 – CFD studies on cycling aerodynamics models	38
Table 14 – Descriptions of all RANS models.....	40
Table 15 – Behaviours of all RANS models.....	40
Table 16 – CFD models using within different sports	41
Table 17 – Professional cycling team budgets per year	48
Table 18 – Theoretical model properties and calculations.....	50
Table 19 – TT time savings model inputs and formulas	67
Table 20 – 20 degree position simulation results.....	68
Table 21 – 30 degree position simulation results.....	69
Table 22 – Comparison of drag force for a range of velocity 8 to 18 m/s of control helmet with top performing helmets.....	70
Table 23 – Visualisations of remaining helmets at 20 degrees.....	72
Table 24 – Visualisations of remaining helmets at 30 degrees.....	73
Table 25 – Time savings theoretical model	74
Table 26 – 20 degree position transient simulation results.....	75
Table 27 – 30 degree position transient simulation results.....	75
Table 28 – Helmet shape designs and their characteristics	81
Table 29 – Calculated average of results from both head angles showing performance consistency	85

Table 30 – Steady vs transient result comparison at 20-degrees.....	87
Table 31 – Steady vs transient result comparison at 30-degrees.....	88
Table 32 – Examples of additional considerations for simulating with a full bicycle system..	95

Chapter 1 – Introduction

1.1 – Aim

This research project aimed to test the aerodynamics of current industry designs for road cycling TT helmets and proposed a more optimal design that assisted in providing less aerodynamic resistance, therefore, allowing competitive cyclists and similar athletes to obtain an advantage over their rival competitors. The findings in this research could be proposed to high level helmet manufacturers for future investment.

1.2 – Background

In the elite to professional levels within the world of cycling, aerodynamics can sometimes be a deciding factor in who is victorious in their sporting endeavours. Manufacturers and sponsors work with athletes to provide the most aerodynamic bicycles and helmets to obtain any marginal gains over their competitors. The critical role aerodynamics plays in cycling became evident in the 1989 Tour De France, in which Greg Lemond famously won the tour by beating Laurent Fignon. Lemond was 50 seconds behind Fignon on the last day on the tour in which the stage consisted of a 25 km TT. Lemond, competed in an aero helmet, triathlon bars and a back disc wheel, whilst Fignon competed with conventional TT bars of the time without any helmet on. Lemond was able to beat Fignon by 58 seconds, to which, began the evolving development of aerodynamics in the world of cycling.



*Figure 1 – Greg Lemond 1989 TT
(Wilson, 2022)*

Furthermore, the advantage of aerodynamics was observed during the 1992 Olympic pursuit in which Chris Boardman was able to achieve something unheard of by lapping his competitor whilst riding the Lotus 'Superbike' (Tew & Sayers, 1999).



Figure 2 – Chris Boardman on Lotus 'Superbike'
(Glendenning, 2012)

Another notable feat of the impact to performance that aerodynamics has in cycling has been observed in the evolution of the hour record. The hour record is a unique event which is performed in a velodrome on a fixed gear track bike under standard conditions. During this event a single rider attempts to travel the longest distance possible. Whilst performance in this event requires a significant contribution of physiology, training and psychology of the athlete, the constant recording breaking attempts over the years can largely be attributed to the aerodynamic performance which includes optimising the cyclists position, bicycle, components and equipment (Padilla, et al., 2000). Refer to Figure 3, which shows the evolution of the hour record average speeds. Refer to Table 1, which shows detailed data of the significant recording break occurrences.

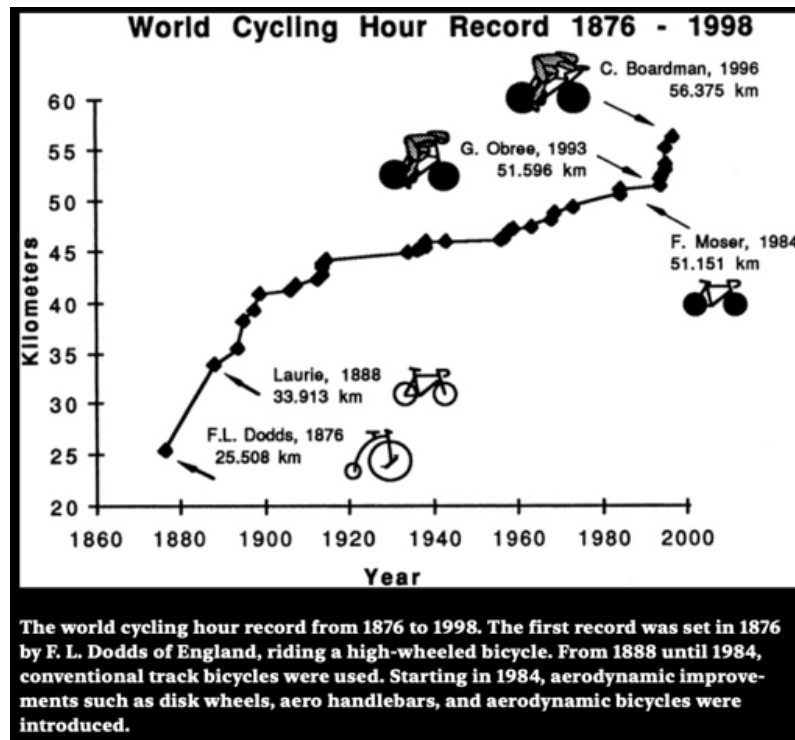


Figure 3 – Evolution of the hour record average speed

(Bassett, et al., 1999)

Table 1 – Evolution of the hour record showing the impact of improved aerodynamics

(Padilla, et al., 2000)

Table 2. Characteristics of recent 1-h cycling world record holders

Cyclist	Record, km/h	Date, mo/day/yr	Height, cm	Mass, kg	BSA, m ²	FA, m ²	C _d , m ²	C _x , m ²	Power, W
Merckx	49.432	10/25/72	184	72	1.940	0.3491	0.75	0.2618	380
Moser	51.151	01/21/84	182	76	1.969	0.3544	0.70	0.2481	400
Obree	52.713	04/27/94	182	71	1.912	0.3441	0.50	0.1720	359
Indurain	53.040	09/02/94	188	81	2.076	0.3755	0.65	0.2441	510
Rominger	55.291	11/05/94	175	65	1.791	0.3220	0.60	0.1932	456
Boardman	56.375	09/06/96	177	69	1.857	0.3342	0.55	0.1838	462

BSA, body surface area, estimated using the equation of Du Bois and Du Bois (13); FA, frontal area, considering it as a constant 18% fraction of BSA (12, 36, 46); C_d, shape coefficient, estimated from values of the literature for different riding positions and equipment (4, 5, 10, 22, 32, 33, 36); C_x, drag coefficient, measured for Moser (9) and Indurain, and estimated from FA and C_d for the rest of the cyclists; Power, mechanical power output during the record ride, estimated with the model of Menard (31).

The most recent breaking of the hour record was achieved on the 8th of October 2022, by professional road cyclist Filippo Ganna. During this record he covered 56.792 km (di Prampero & Ferretti, 2023). Refer to Figure 4, which shows Ganna during his hour record breaking attempt. From this image you can see that every component and piece of equipment in use has been optimised for aerodynamics which includes wheels, chain rings, helmet, suit, socks shoe covers, and custom made aero bars. Refer to Figure 5, which shows the level of detail for optimising aerodynamics of his bicycle and helmet. This record breaking, supported by the equipment setup, clearly emphasises the importance of aerodynamics to optimising performance within the sport of cycling.



*Figure 4 – Filippo Ganna breaking the hour record in 2022
(Laughlin, 2022)*



*Figure 5 – The detailed design for aerodynamic advantage of Ganna's bicycle and helmet
(Laughlin, 2022)*

In recent TT events this year, some teams have created some radical looking designs and have boasted their performance. Refer to Figure 6 and Figure 7, which shows some examples of the radical modern designs that the top teams are using. This suggests that there is still room for growth in this area of research and the professional teams are willing to take risks and trial unorthodox designs.



*Figure 6 – Team Visma and their new Giro TT helmet
(Croxtton, 2024)*



*Figure 7 – Team Quickstep and their new Specialized TT helmet
(Brett, 2023)*

1.3 – Problems

This research will include addressing problems of both theoretical and practical natures. The theoretical problems will include:

- Cycling Aerodynamics
- Cyclist Profile
- Aerodynamic Testing
- Mathematical Formulation
- UCI Regulations

The practical components of this problem include:

- Designing a basic control helmet inspired by current themes and designs within the industry.
- Conducting CFD simulations on all helmets.
- Assessing anthropometric data to obtain human model.
- Creation of prototypes using modelling techniques.

1.4 – Research Goals

This goal of this research project was to produce a TT helmet with a lower value of drag force than three commercially available helmets selected for testing. The design method chosen was CFD with a human model wearing the helmet. The design dimensions were set by the cycling governing body known as the UCI. Observations from the performance of each helmet were discussed to determine design features that enhance aerodynamics. From the results, further work required is discussed.

Specific Objectives:

1. Conduct literature review to build a theoretical model for cycling aerodynamics to determine helmet performance
2. Design a basic control helmet to compare all tests to
3. Obtain 3 commercially available designs for testing
4. Design a prototype helmet which performs optimally compared to the control and commercial designs
5. Rank the performance of all helmets in a race scenario of a 40km TT

Chapter 2 – Literature Review: Established Knowledge

2.1 – Cycling Aerodynamics

2.1.1 – Governing Equations

In the context of cycling, there are multiple forces resisting against the rider preventing them from reaching their optimal speed. Among these, aerodynamic drag provides the greatest resistance. Some studies have shown that travelling at race speeds of 14 m/s (50.4 km/h), 90% of the resisting forces can be attributed to aerodynamic drag (Debraux, et al., 2011). Refer to Table 2, which shows the main formulas required to solve aerodynamics of the model. Refer to Figure 8, which shows a free body diagram of the model used in the formulas from Table 2. The main terms considered for this research are expanded in the following sections.

Table 2 – Formulas used to model cycling aerodynamics
(Debraux, et al., 2011)

Formulas for calculating cycling Aerodynamics	
Description	Formula
Displacement Velocity	$v = \frac{P}{R_T}$
Aerodynamic Drag	$R_D = 0.5 \times A_p \times C_D \times \rho \times v_f^2$
Air density	$p = p_0 \times \left(\frac{PB}{760}\right) \times \left(\frac{273}{T}\right)$
Barometric Pressure	$PB = 760 \times e^{-0.124 \times Alt}$
Body surface area	$A_{BSA} = 0.00949 \times (h_b^{0.655}) \times (m_b^{0.441})$
Projected frontal area	$A_p = 0.107 \times (h_b^{1.6858}) + 0.329 \times (L \sin(\alpha_1))^2 - 0.137 \times (L \sin(\alpha_1))$
Drag Coefficient relationship	$C_D = \frac{R_D}{q} \times A_p$
Dynamic Pressure	$q = \frac{1}{2} \times \rho \times v_f^2$
Drag coefficient	$C_D = 4.45 \times m_b^{-0.45}$
Velocity relative to fluid	$v_f = v + v_r$
Total Resistive Forces	$R_T = R_D + R_R$
Rolling Resistance	$R_R = C_R \times M \times g$
Cyclist-bicycle system mass	$M = m_b + m_c$

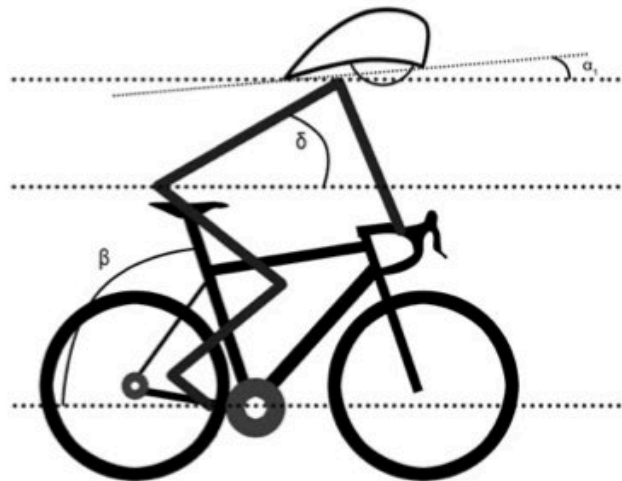


Figure 1. Illustration of the seat tube angle (β , in degree) and the trunk angle (δ , in degree) used by Heil (2001) to determine the projected frontal area of a cyclist and bicycle, and the helmet inclination angle (α_1 , in degree) used by Barelle et al. (2010).

Figure 8 – FBD of rider to obtain frontal area..

(Debraux, et al., 2011)

The formulas listed in Table 2 provide the main points of interest that were considered in this research and were used to build the theoretical model in which the TT time savings models were derived from. Refer to Table 3, which shows how changes to location, bicycle, components, positions, helmets and clothing requires adjusting through correction factors to obtain more accurate results. This emphasises how complex it can be for determining suitable control points for testing that could be utilised in this area of research and performance.

Table 3 – Examples of different correction factors for determining aerodynamic drag in cycling
(Bassett, et al., 1999)

Density ratio	K_d
Sea level	1.0
Colorado Springs, 1829 m	0.836
Mexico City, 2340 m	0.794
Bogata/Duitama, Colombia, 2500 m	0.781
Rider position	K_{po}
Standard position with aero bars, elbows in (inside body contour)	1.0
Standard position with aero bars, elbows wide (outside body contour)	1.07–1.11
Historic racing position with drop bars, varying torso and head angle	1.08–1.18
Obree Position	0.96
Superman Position	0.95
Bicycle and components	K_b
Round tube standard track bike, aero bars, disk or composite wheels	1.0
Round tube standard track bike, drop bars, wire-spoke wheels	1.07
Composite double triangular frame, oval frame members (Corima)	1.0
Aluminum aero tube bike (Hooker, USA-SB1)	0.93
Lotus composite aero bike (1992 Olympic, Boardman)	0.93
Advanced composite aero bike, USA SB2, 1996 Merckx (Boardman)	0.925
Bicycle clothing	K_c
Short Sleeves, 3/4 legs, nylon Spandex skin suit	1.0
Same design, optimum weave material	0.98
Cotton jersey, separate shorts	1.02
Wool jersey, full tights, full sleeves	1.09
Bicycle helmets	K_h
Aero time-trial helmet (USA, England, German, French, Italian)	1.0
Modern slotted protective helmet	1.025
Historic leather strap helmet	1.04

The above correction factors to the aerodynamic drag assume an average air drag for a rider and bicycle of approximately 2.5 kg (24.5 N) at 48 kph. By multiplying the above factors together, an overall correction K_i may be obtained.

2.1.2 – Forces and moments

When analysing the aerodynamics of cycling, 6 actions are observed. Refer to Figure 9, which shows the three forces and three moments. The main force of interest when analysing aerodynamics is drag, R_D (shown as F_D), which acts in the opposing direction that the cyclist is travelling along. The other forces of interest are side force and vertical lift force. The moments considered are the roll moment, yaw moment and pitching moment which are all defined relative to the centre of the wheelbase. All force and moment coefficients are normalised by dynamic pressure and frontal area. However, normalisation of moment coefficients occurs due to the wheelbase length and frontal area (Crouch, et al., 2017).

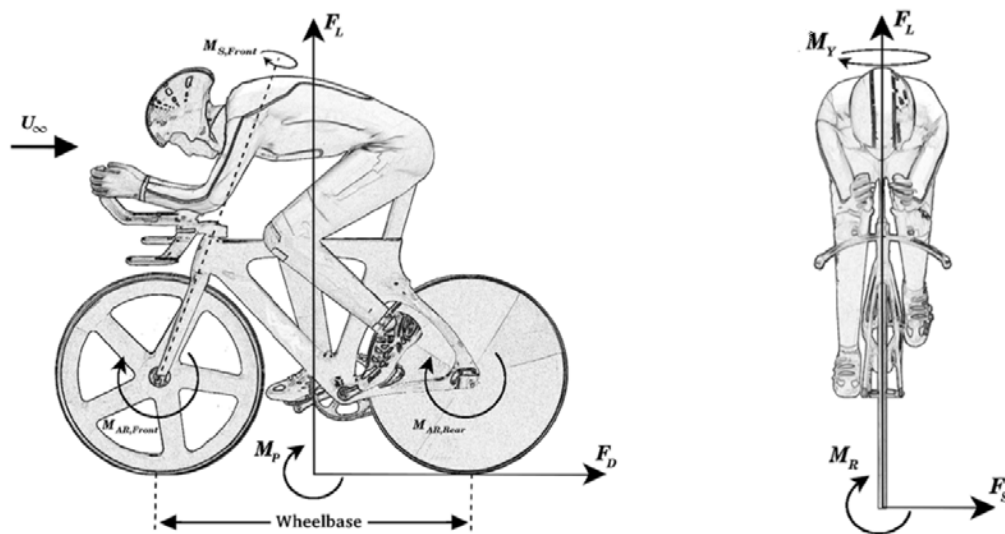


Fig. 2 Diagram showing cyclist and bicycle aerodynamic forces (F_L , F_D , F_s) and moments (M_p , M_R , M_y) about the centre of the wheelbase, along with steering and aerodynamic moments acting on the wheels

Figure 9 – Aerodynamic forces and moments of cyclist
(Crouch, et al., 2017)

Refer to Figure 10, which shows a diagram of the forces considered when the cyclist begins riding uphill. As a cyclist begins to ride up an inclined surface, the cyclist's weight begins to act in the direction of motion. As a result, this makes it harder to pedal uphill as a greater force is pulling you back (Malizia & Blocken, 2020).

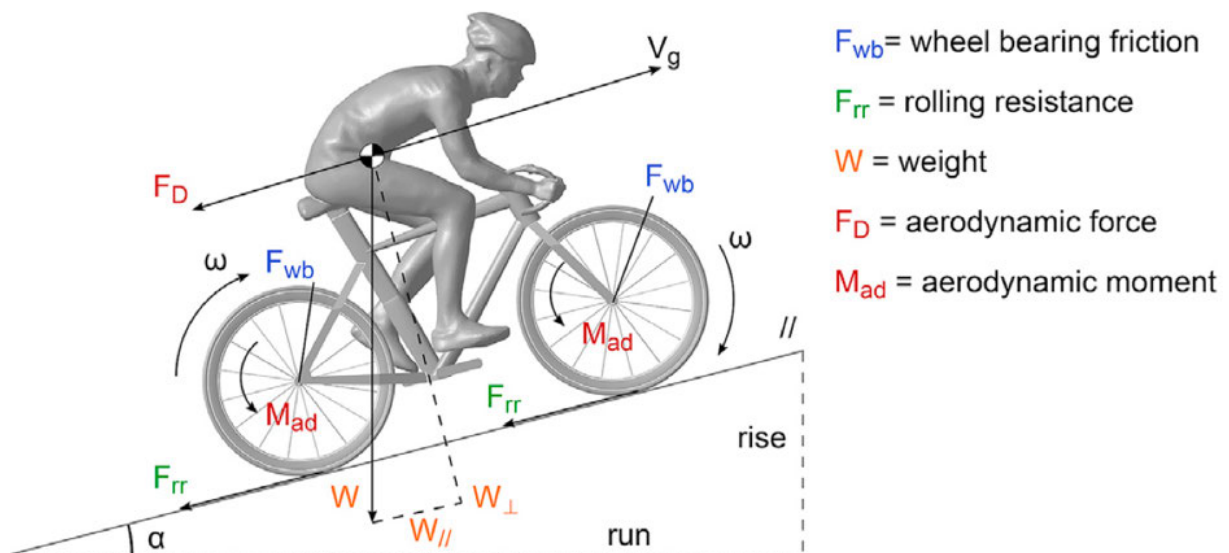


Figure 10 – Diagram showing forces when the cyclist is riding uphill
(Malizia & Blocken, 2020)

Refer to Figure 11, which shows the forces calculated relative to wind velocity. The forces that act on the front wheel generate a steering moment which requires a counteracting force from the cyclist through the handlebar from their hands (Malizia & Blocken, 2020). Further research shows a greater depth of understanding of all the forces present in a cyclist-bicycle system, however, the above mentioned covered a sufficient understanding for this project. The main considerations for CFD in this project is aerodynamic drag force, which is a function of the frontal area of the cyclist and the drag coefficient (Crouch, et al., 2017).

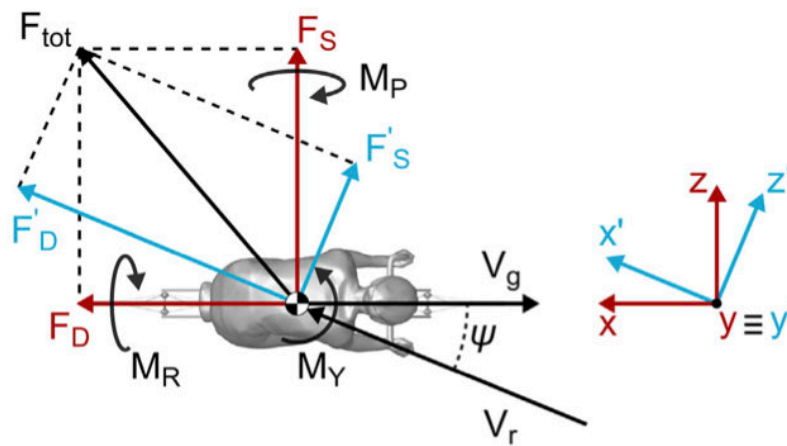


Fig. 7. Forces in relative wind axes (blue) and in body axes (red). Moments in body axes are also presented. (For interpretation of the references to color in this figure legend, the reader is referred to the Web version of this article.)

*Figure 11 – Diagram showing forces calculated relative to wind velocity
(Malizia & Blocken, 2020)*

2.1.3 – Drag Coefficient

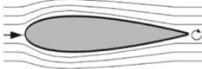


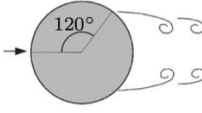


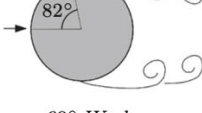


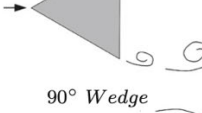
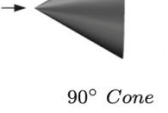







The drag coefficient, C_d , can be defined as the aerodynamic efficiency of an object, regardless of its size. When considering a position of a rider, also known as frontal area, the objective is to reduce the drag coefficient which as a result will lower the total resistive forces. This can be influenced by multiple factors which include orientation, body shape, free-stream flow conditions, surface roughness, and the Reynolds number (Crouch, et al., 2017).

Often, the frontal area and drag coefficient are paired into a single term known as C_{dA} . Furthermore, the drag coefficient can also be a function of the external wind velocity direction, however, this effect is usually ignored (Malizia & Blocken, 2020). Refer to Table 4, which shows examples of different objects and their C_d .

Table 4 – Examples of different objects and their drag coefficient

(Couch, et al., 2017)

Table 1 Drag coefficients of simple 2D, 3D, and more complex 3D geometries for a range of Reynolds numbers [4–7]

2-D Geometry	3-D Geometry	Complex 3-D Geometry
 <p><i>Air foil</i></p> <p>$x = \text{chord } (c)$ $A = c(b)$ $Re \approx 1 \times 10^5$ $C_D \approx 0.1$</p>	 <p><i>Elipsoid</i></p> <p>$x = \text{diameter } (d)$ $A = \frac{\pi}{4} d^2$ $Re \approx 1 \times 10^5$ $C_D \approx 0.05$</p>	 <p><i>Faired – HPV</i></p> <p>$x = \sqrt{A}$ $A = \text{frontal}$ $Re \approx 1.5 \times 10^6$ $C_D \approx 0.07$</p>
 <p><i>Circular Cylinder</i></p> <p>$x = \text{diameter } (d)$ $A = d(b)$ $Re \approx 5 \times 10^5$ $C_D \approx 0.4$</p>	 <p><i>Sphere</i></p> <p>$x = \text{diameter } (d)$ $A = \frac{\pi}{4} d^2$ $Re \approx 5 \times 10^5$ $C_D \approx 0.1$</p>	 <p><i>Fast – Back Car</i></p> <p>$x = \sqrt{A}$ $A = \text{frontal}$ $Re \approx 4 \times 10^6$ $C_D \approx 0.28$</p>
 <p><i>Circular Cylinder</i></p> <p>$x = \text{diameter } (d)$ $A = d(b)$ $Re \approx 1 \times 10^4$ $C_D \approx 1.2$</p>	 <p><i>Sphere</i></p> <p>$x = \text{diameter } (d)$ $A = \frac{\pi}{4} d^2$ $Re \approx 1 \times 10^4$ $C_D \approx 0.5$</p>	 <p><i>Small Bus</i></p> <p>$x = \sqrt{A}$ $A = \text{frontal}$ $Re \approx 3.5 \times 10^6$ $C_D \approx 0.42$</p>
 <p><i>60° Wedge</i></p> <p>$x = \text{width } (w)$ $A = w(b)$ $Re \approx 1 \times 10^5$ $C_D \approx 1.4$</p>	 <p><i>60° Cone</i></p> <p>$x = \text{diameter } (d)$ $A = \frac{\pi}{4} d^2$ $Re > 1 \times 10^4$ $C_D \approx 0.8$</p>	 <p><i>Cyclist – Time Trial</i></p> <p>$x = \sqrt{A}$ $A = \text{frontal}$ $Re \approx 7 \times 10^5$ $C_D \approx 0.60$</p>
 <p><i>90° Wedge</i></p> <p>$x = \text{width } (w)$ $A = w(b)$ $Re \approx 1 \times 10^5$ $C_D \approx 1.6$</p>	 <p><i>90° Cone</i></p> <p>$x = \text{diameter } (d)$ $A = \frac{\pi}{4} d^2$ $Re > 1 \times 10^4$ $C_D \approx 1.15$</p>	 <p><i>Semi – Trailer</i></p> <p>$x = \sqrt{A}$ $A = \text{frontal}$ $Re \approx 6 \times 10^6$ $C_D \approx 0.70$</p>
 <p><i>Flat Plate</i></p> <p>$x = \text{width } (w)$ $A = w(b)$ $Re \approx 1 \times 10^5$ $C_D \approx 2.0$</p>	 <p><i>Disk</i></p> <p>$x = \text{diameter } (d)$ $A = \frac{\pi}{4} d^2$ $Re > 1 \times 10^3$ $C_D \approx 1.1$</p>	 <p><i>Cyclist – Upright</i></p> <p>$x = \sqrt{A}$ $A = \text{frontal}$ $Re \approx 7 \times 10^5$ $C_D > 0.80$</p>

2.1.4 – Frontal Area

It is a key consideration, that the main contributor to increasing frontal area and thereby increasing aerodynamic drag is the position of the rider themselves. Whilst this is not something that can be designed and adjusted through engineering concepts, it is important to consider and assist in building the foundation for improving aerodynamics in cycling. Understanding rider position will be critical in designing an optimal helmet, as the head angle of the rider could drastically impact the C_{dA} (Crouch, et al., 2017). Refer to

Table 5, which shows the difference in results for frontal area of riders of different sizes. Refer to Table 6, which shows how each body part contributes to the total aerodynamic resistance.

Table 5 – Results for frontal area for riders of different sizes

(Bassett, et al., 1999)

Subject	Height (m)	Mass (kg)	Total Frontal Area (m ²)	Surface Area (m ²)
11	1.82	80.0	0.368	2.01
12	1.85	78.1	0.355	2.02
13	1.76	57.9	0.294	1.71
14	1.73	63.1	0.294	1.75
15	1.78	79.4	0.315	1.97
16	2.00	94.0	0.386	2.31
17	1.78	75.8	0.354	1.94
18	1.70	61.2	0.301	1.71

Table 6 – Percentage contribution different body parts have to the total aerodynamic resistance

(Crouch, et al., 2017)

Table 2 Relative contribution of various parts of the body and the bicycle to the total aerodynamic resistance

Study	Key variable	Simulation	Position	Crank	Head (%)	Arms (%)	Torso (%)	Left leg (%)	Right leg (%)	Bicycle (%)
[36]	Position	Steady-k – ϵ	U, D, TT	0°	14–20	15–26	12–24	21–28	17–25	–
[38]	Multi-riders	Steady-k – ϵ	TT	0°	7–16	22–24	7–14	21–30	27–35	–
[14]	Leg position	Steady-SST	TT	0°–180°	14–17	23–31	23–32	11–22	11–23	17–20

Cycling position is indicated by *U*, *D*, and *TT* which represent Upright, Down, and Time-Trial positions, respectively. Note that % given for Defraeye et al. [36, 38] do not include the bicycle and have been condensed for brevity. For a more detailed breakdown of the magnitude of the aerodynamic forces acting on the body, the reader is referred to these articles

Refer to Figure 12, which shows different riding positions that can be utilised for testing aerodynamic efficiency within cycling. Overall, understanding rider positions and posture can give researchers guidance for improving aerodynamic efficiency, by understanding sources of drag and nature of the wake (Barry, et al., 2015). Refer to Table 7, which shows the resultant frontal area for each of these positions seen in Figure 12.



Figure 12 – Different rider positions

(Barry, et al., 2015)

Table 7 – Frontal areas of rider positions in Figure 3

(Barry, et al., 2015)

Table 1. Description of riding postures tested covering both cycling and draft-legal triathlon postures.

	Posture and description	Frontal area (m ²)
1	Hands on hoods – reference posture	0.4941
2	Drops – conventional racing posture	0.4720
3	Drops and crouched torso – arms bent to lower torso angle	0.4594
4	Drops and crouched torso with eyes looking down	0.4520
5	Hoods grip – gripping brake hoods with horizontal forearms	0.4365
6	Aerobars – typical ITU draft-legal short aerobars	0.4174
7	Aerobars with head lowered and shoulders shrugged	0.3855
8	Aerobars with eyes looking down	0.4126
9	Aerobars with head tucked between arms	0.3850

2.1.5 – Air Density

The air density, ρ , can change according to the surrounding atmospheric pressure and temperature (Bassett, et al., 1999). Refer to Table 8, which shows how the air density can directly impact the aerodynamic efficiency of a cyclist. This was observed during the 1972 record breaking of the hour record by Eddy Merckx. Merckx took advantage of the lower air density of Mexico City (Crouch, at al., 2017).

Table 8 – Effect of air density on aerodynamic drag

(Debraux, et al., 2011)

Track	Alt (km)	PB (mmHg)	ρ^a (kg/m ³)	R_D^b (N)
Bordeaux (France)	0	760	1.20	29.8
Colorado Springs (USA)	1.84	605	0.96	23.9
Mexico City (Mexico)	2.25	575	0.91	22.6

Alt = Altitude; PB = Barometric Pressure; ρ = Air density; R_D = Aerodynamic drag; A_p = Projected frontal area; C_D = Coefficient of drag; v_f = Velocity relative to the fluid.; ^aWith a temperature equal to 20°C; ^bBased on Equation 2, for a cyclist with $A_p C_D = 0.221 \text{ m}^2$ and $v_f = 15 \text{ m/s}$.

2.1.6 – Velocity

It is evident through the literature review that velocity is considered as a direct headwind. However, this is not the case in a real world scenario as wind comes from all directions, thus creating an angle between the cyclists motion and airflow known as yaw or pitch angle. Refer to Figure 13, which shows a diagram of all components of the total air velocity and yaw and pitch angle definitions. Yaw is defined as the lateral angle in the transverse plane, while pitch is the vertical angle in the sagittal plane. These are important considerations for determining aerodynamic performance outdoors. However, they are often neglected in track cycling where no natural wind is present (Fitzgerald, et al., 2019).

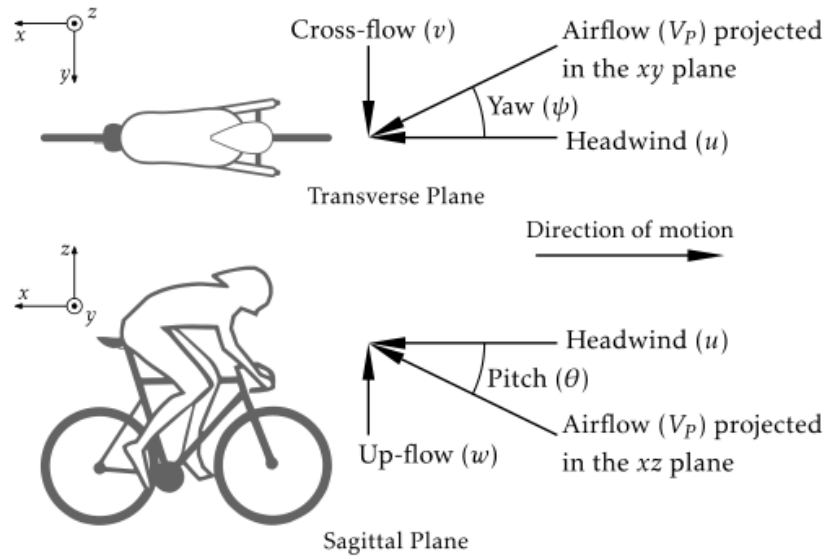


Figure 13 – Diagram showing all components of total air velocity and the yaw and pitch angle definitions
(Fitzgerald, et al., 2019)

For this research displacement velocity v was considered, which is the speed the cyclist is travelling in m/s. Also for consideration, the velocity relative to fluid v_f , which is the speed of the surrounding air in m/s (Debraux, et al, 2011). These both contributed to understanding and application of the theoretical model. However, only displacement velocity was considered for the final CFD simulations.

2.1.7 – Drafting

Within the sport of cycling the main group in a road race is known as the peloton. Refer Figure 14, which shows an example of a peloton in a road race. Riding in the peloton provides an aerodynamic benefit to those who are not at the front as their power output is less due to being in the wake of the lead cyclists and the disturbed air flow in front of them. Studies on smaller groups have shown that cyclists riding in-line can reduce their power required by 50 – 70% (Blocken, et al., 2018).



*Figure 14 – Professional cycling Peloton during road race
(Blocken, et al., 2018).*

Within TTT races cyclists are grouped together, usually a group of four, to set the fastest time possible. Refer to Figure 15, which shows various professional teams in a paceline format for a TTT. By having additional riders, it provides a drafting benefit to the riders behind to allow them time to recover after spending time on the front and having a higher power output to combat the wind resistance.



*Figure 15 – Examples of a TTT paceline
(Blocken, et al., 2018)*

The impact drafting has to riders behind the lead cyclist has been widely studied and its benefits are significant. Refer to Figure 16, which shows the percentage of drag compared to the lead rider for those within the draft all the way up to 9 cyclists in a paceline. Refer to Figure 17, which shows the drafting benefit cyclists experience relative to their position in the peloton.



Fig. 9. Drag of every rider in pacelines of 2 up to 9 riders, as a percentage of the drag of an isolated rider. Wheel-to-wheel distance $d = 0.05$ m. Right column gives average drag percentage for the whole paceline.

Figure 16 – Percentage drag compared to lead rider in a paceline
(Blocken, et al., 2018)

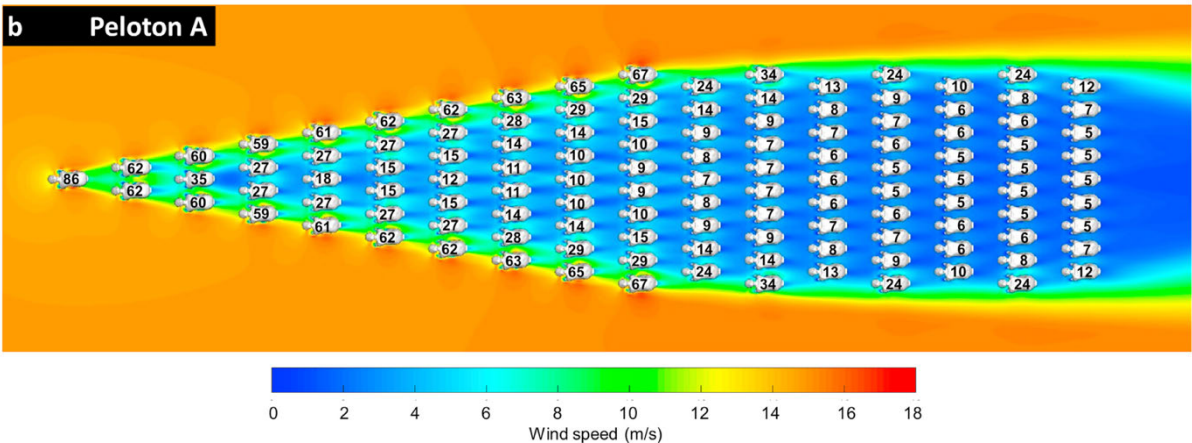


Figure 17 – CFD velocity visualisation showing the benefit of drafting in a peloton
(Blocken, et al., 2018)

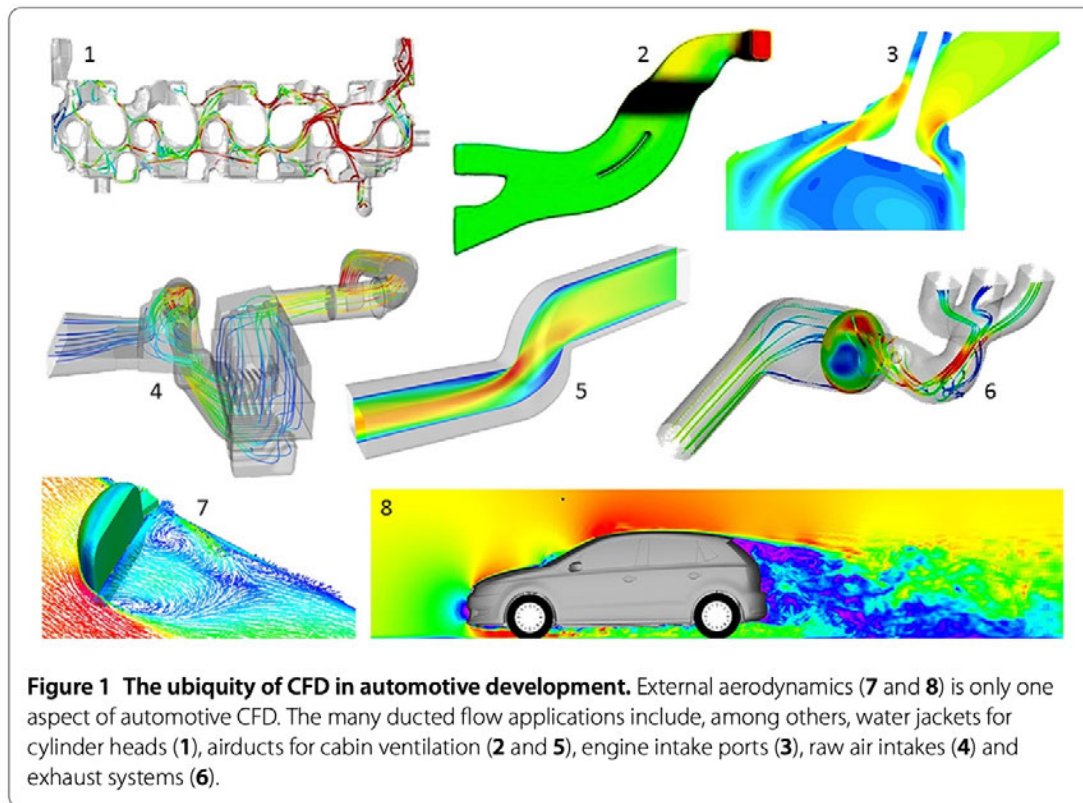
2.2 – Automotive aerodynamics

The optimisation of cycling aerodynamics is arguably in its infancy when compared to the evolution and advancements made in the automotive industry. Having a better understanding of aerodynamics in the automotive industry would facilitate adopting their advancements to the optimisation of cycling performance. The following sections elaborate on some automotive techniques that could be used to improve aerodynamics for cycling.

In the automotive industry, drag creation was first discovered through experimental methods. Fuel consumption is drastically impacted by drag, which has been shown to reach up to 75% when travelling at a speed of 120 km/h. The most significant contributing factor of drag is due to the emergence of flow separation at the rear of a vehicle. Often neglected in aeronautics, the occurrence of this cannot be avoided for ground vehicles. Furthermore, the three-dimensional flow that can be observed behind a car in its wake demonstrates a complex behaviour which proves challenging to manage due to reactions to vehicle geometry which cause recirculation and separation to occur (Dumas, 2008).

2.2.1 – Topology Optimisation

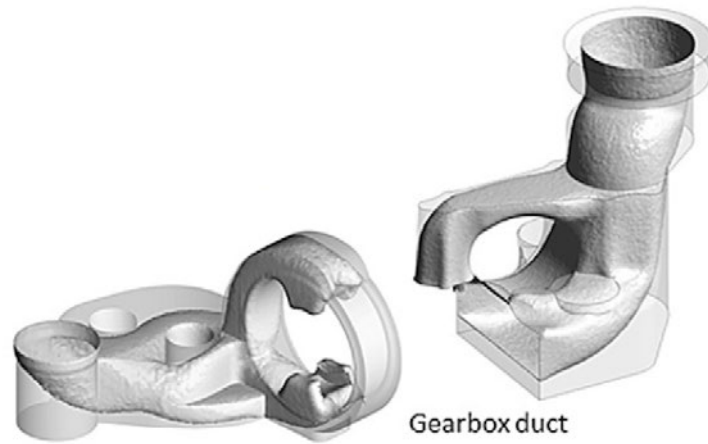
In modern day vehicles, CFD is a critical element for the design and development process. However, CFD is utilised to predict behaviour of much more complex objects and flows than obtaining values for lift and drag force. Refer to Figure 18, which shows some examples which include ventilation airducts, exhaust systems, engine intakes, air intakes, cooling plates, and cylinder heads to name a few (Othmer, 2014). The literature review identified a gap in which no internal flow is modelled for helmets, yet all modern helmets incorporate these into their design. Therefore, helmet performance could be enhanced by adopting this technique into CFD analysis of designs.



*Figure 18 – Examples of different CFD simulations in automotive industry
(Othmer, 2014)*

A method available within CFD that the automotive industry utilises to optimise their designs is known as topology optimisation. This is an advanced computational technique which can optimise design by improving the material structure and layout for a stipulated set of loading, boundary conditions and design objectives (Othmer, 2014). Refer to Figure 19, which shows an example of topology optimisation for a gearbox duct where material has been removed from the original design. In the context of designing a TT helmet, this could facilitate multiple optimisations, some of which include:

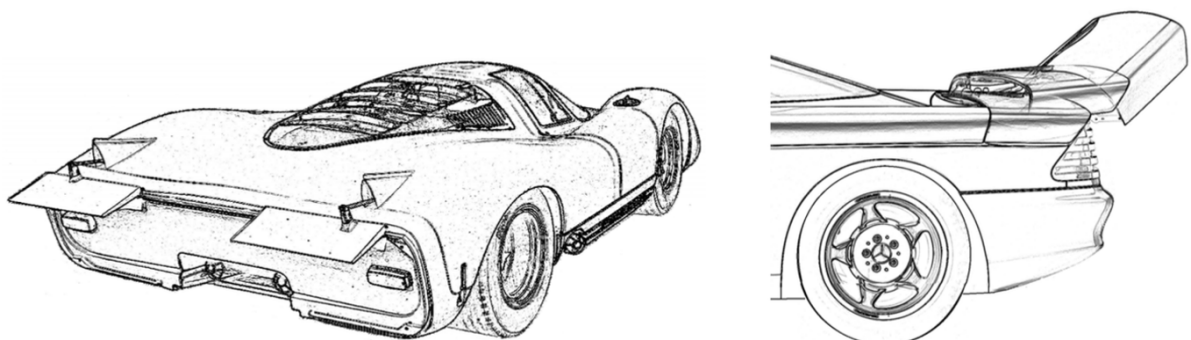
- Reduction of drag: Reshape the design to facilitate lesser value of drag force.
- Reduction of weight: Remove excessive material that doesn't compromise structural integrity.
- Enhanced ventilation: Addition of ventilation gaps without increasing drag force or reducing overall performance which will improve comfort and heat dissipation of the rider.
- Custom design: Providing a method to custom fit and shape for an individual, which can assist athletes with



*Figure 19 – Example of topology optimisation in the automotive industry
(Othmer, 2014)*

2.2.2 – Active Aerodynamics

In the automotive industry, a method for improving aerodynamics whilst the vehicle is operational is known as active aerodynamics. Refer to Figure 20, which shows an example of this where movable wings are fitted to the rear of vehicles. This is most common in high performance vehicles where the addition of the active components can offer functions which include improving down force, reducing lift force, or reducing drag force. An example of this was seen on the race car Chaparral 2F, which was known for being smooth at moderate speeds, however, reacted aggressively at higher speeds. To address this issue, an adjustable rear wing was added in which the driver could operate. It incorporated an aerodynamic profile, therefore increasing the down force generation. Furthermore, the vehicles performance was enhanced due to a lower aerodynamic drag when travelling straight at high speeds and an improved downforce in cornering (Piechna, 2021).



*Figure 20 – Examples of active aerodynamics in the automotive industry in the form of movable wings
(Piechna, 2021)*

Whilst the addition of active aerodynamics can offer improvements in performance, incorporating them into design can provide its own set of challenges. Piechna (2021) highlighted that studies pertaining to safety and comfort are usually conducted by researchers working on control problems whilst studies to improve aerodynamics from utilising active components are conducted by researchers in the domain of numerical flow simulations. This can lead to some conflicting ideas as the two groups have different considerations and approaches to incorporating active aerodynamics into the design. This area could provide some revolutionary improvements to the cycling industry, however, applying this into helmet designs must be done in accordance with UCI regulations.

2.2.3 – Surface Roughness and Texturing

Another method of optimising aerodynamics which has been utilised in the automotive industry is adjusting surface roughness and texture. A common application referred to throughout the literature is the additions of dimples to the outer surface, also known as the dimple effect. Refer to Figure 21, which shows an example in research that was applied to a large Ahmed body.

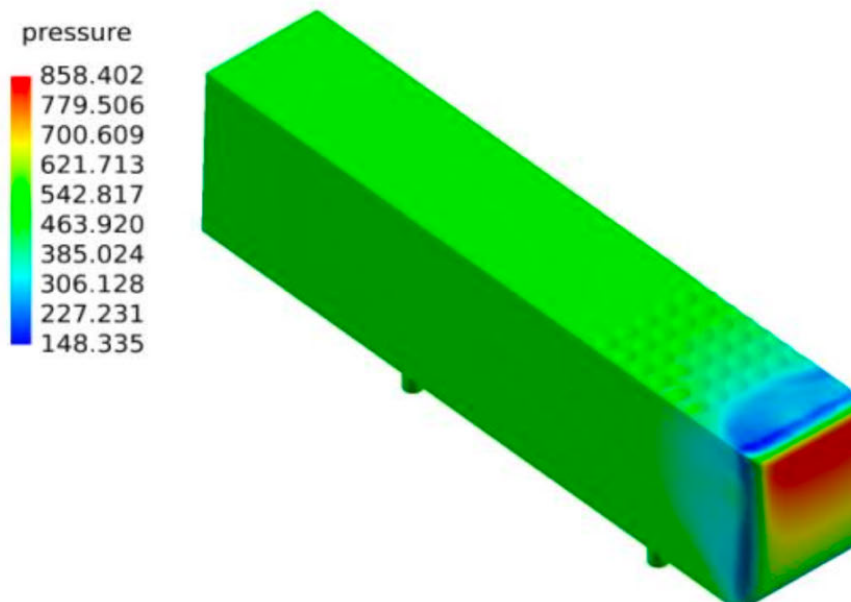


Figure 21 – Example of dimples applied to Ahmed body in dimple effect research and testing
(Shaw, et al., 2020)

This technique was adopted from golf balls which provides a method for creating a turbulent boundary layer around the body which facilitates a reduction in drag and enhanced downforce. When this is applied to automotive design, the thin, turbulent boundary layer becomes more attached to the surface of the vehicle. As a result, this allows air flow to follow along the vehicles surface for longer around the rear of the vehicle which decreases the size of the wake (Shaw, et al., 2020). Refer to Figure 20, for the CFD results for the dimple effect applied to the Ahmed body in Figure 22 which shows that the wake region is reduced with the addition of the dimple.

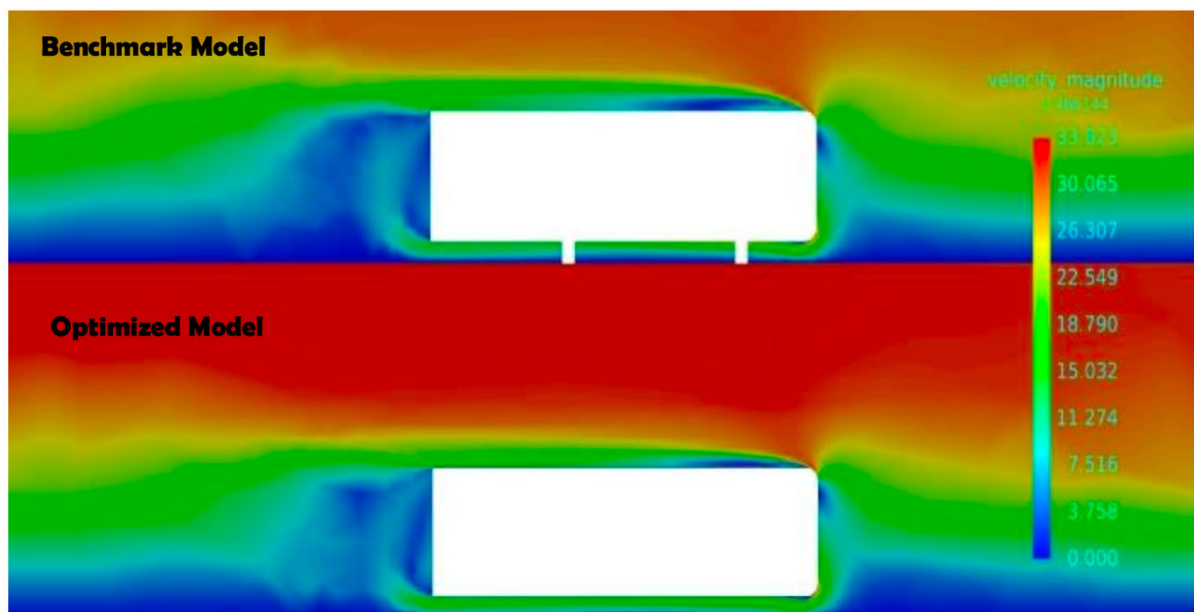


Figure 22 – Velocity magnitude contour comparing dimple effect
(Shaw, et al, 2020)

A recent example of the dimple effect was seen in the Bugatti Bolide. Refer to Figure 23, which shows the addition of the dimples to the air intake cover and an image of the vehicle for reference. This technology took the dimple effect further by providing a method for controlling the dimples in relation to the vehicle speed. At lower speeds the dimples remain retracted as the flow does not detach enough to require their use. However as speed increases, the dimples extend to form bubbles which provides small pressure differentials which facilitates turbulent air attaching to the vehicle (Donut, 2021). The maximum effectiveness of the bubbles has been reported to be over speeds of 119 km/h and Bugatti has tested and determined a 10% drag reduction (Edelstein, 2021). Furthermore, the dimples also provide a function of air braking by increasing the amount of drag forces and downforce (Dave, 2024).

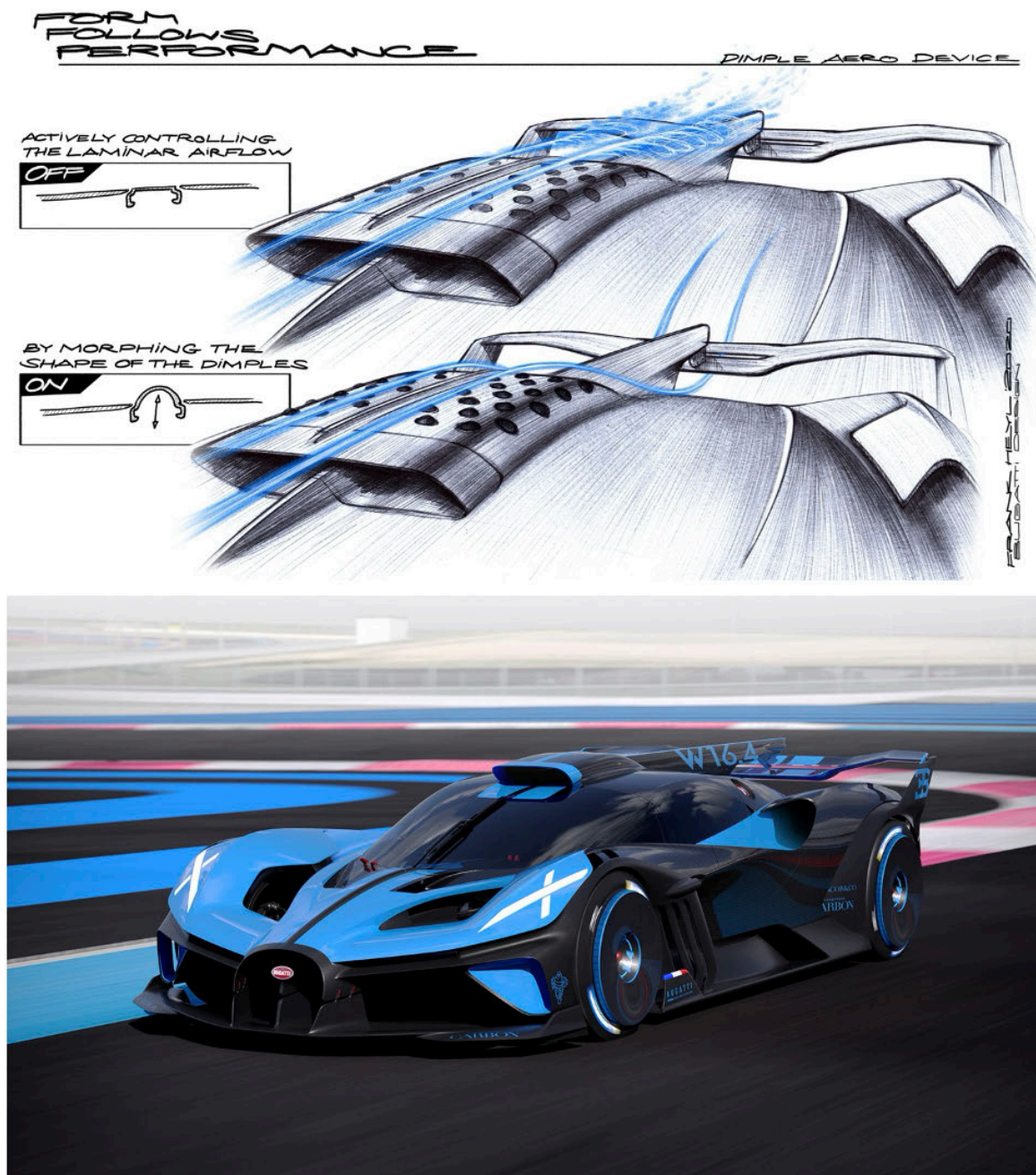


Figure 23 – Bugatti Bolide (bottom) and the dimple system on the air intake (top)
(Edelstein, 2021)

2.3 – Cyclist Profile

2.3.1 – Power

To understand how output performance is measured from the cyclist, it is critical to understand the 'power' generated by them. This key metric is measured in Watts. The power generated comes from the muscular activity of the cyclists legs through pedalling, however, only up to 30% is converted to mechanical power at the crank with the remainder being lost to heat. This is achieved by the body's ability to store chemical energy from food to use it for the required metabolic processes such as sprinting or sustained efforts over time. This metric is individual to each cyclist and is influenced by their physiology and training background (Malizia & Blocken, 2020). Refer to Figure 24, which shows the maximum sustainable power as a function of effort duration of some well-known records.

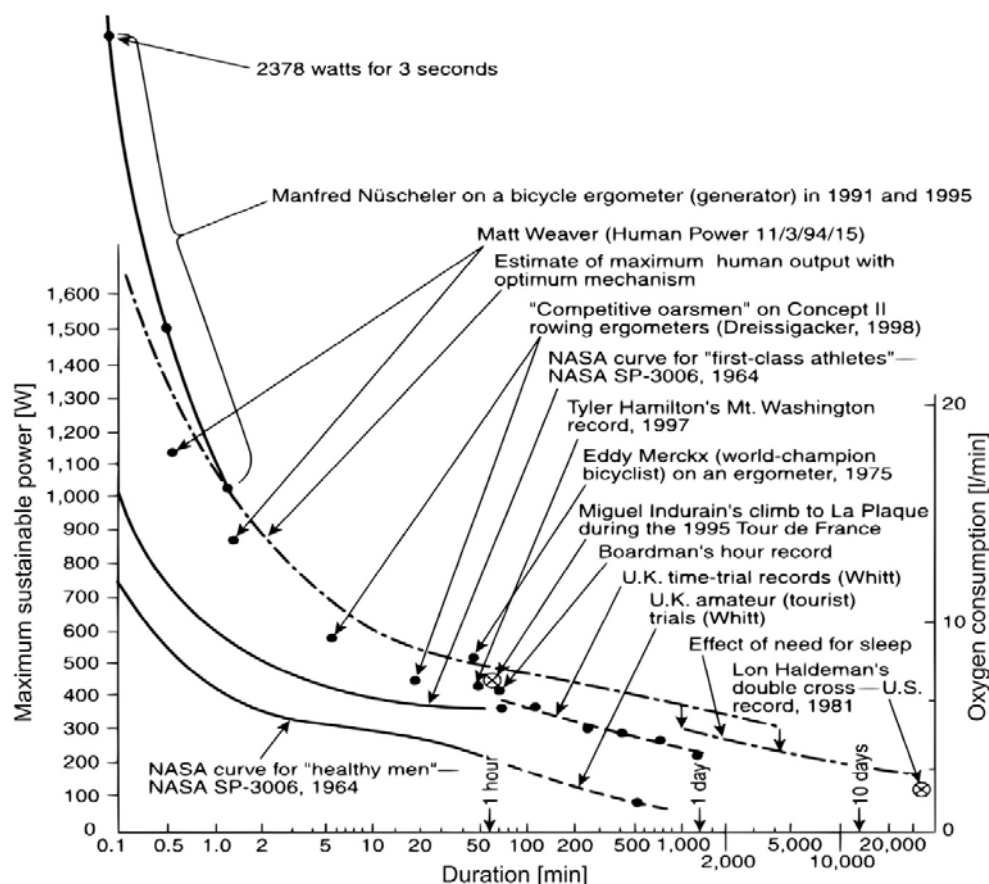


Figure 24 – Graph showing records of maximum sustainable power as a function of effort duration
(Malizia & Blocken, 2020)

The cyclist can obtain their power data instantly by use of a power meter on their bicycle which can come in various forms which include, shoes, pedals, rear hub, or cranks. Most popular power meters in use today measure torque directly at the crank. For any testing conducted using a power meter, it is critical to ensure it is calibrated prior to use. Furthermore, different studies showed that different power meters which will give a variance in results (Passfield, et al., 2017). Refer to Table 9, which shows the difference in results for various power meters which highlights their accuracy.

*Table 9 – Trueness and precision of power meters by manufacturer
(Maier, et al., 2017)*

n	Manufacturer	Mean deviation (%)	Coefficient of variation (%)	Cadence (RPM)
12	SRM	-0.5 ± 2.4	0.8 ± 0.4	83 ± 14
10	PowerTap	0.9 ± 2.1	0.8 ± 0.2	87 ± 5
11	Quarq	0.5 ± 3.0	1.3 ± 0.8	87 ± 6
13	Stages Cycling	-2.9 ± 3.9	$2.0 \pm 1.4^*$	89 ± 6
3	Verve Cycling	-1.7 ± 1.1	0.6 ± 0.4	88 ± 3
2	power2max	-4.8 ± 3.4	1.5 ± 0.4	87 ± 16
1	Garmin	-2.0	1.6	86
1	Polar	-3.9	2.6	93
1	Rotor	2.1	0.4	84
54	All	-0.9 ± 3.2	1.2 ± 0.9	87 ± 8
Values are presented as mean \pm standard deviation (if $n > 1$). * Different from SRM and PowerTap $p < 0.05$				

The main goal of reducing aerodynamic drag for the cyclist is to improve performance by using the same mechanical output from the cyclist (Debraux, et al., 2011). Whilst the power the cyclist can generate is not something that will be specifically analysed during this research, there are some important factors that must be considered. Furthermore, a relationship always exists between aerodynamics and the cyclist power. Refer to Table 10, which shows power output required to reach a desired velocity from different riding positions. Prior to testing helmets, it is critical to select the optimal position that the rider will be in during racing.

Table 10 – Power output required to reach a constant velocity in the various positions.

(Barry, et al., 2015)

Table 3. Drag coefficient area and simulated power required for each posture (see Table 1 and Figures 1 and 2).

Posture	$C_D A$ (m ²)	Power required (W)	Delta $C_D A$ (m ²)	Delta power (W)
1	0.343	430		
2	0.332	417	0.011	13.0
3	0.306	385	0.037	43.9
4	0.321	403	0.022	25.9
5	0.295	372	0.048	56.0
6	0.289	365	0.054	63.6
7	0.283	358	0.060	70.1
8	0.295	372	0.048	56.5
9	0.287	363	0.056	65.1

Delta values are for the change in $C_D A$ and power referenced to Posture 1.

2.3.2 – Head angle

The cyclists head angle plays a critical role in contributing to aerodynamics when a TT helmet is being used. Due to the highly intense output required for the sport, cyclists are constantly adjusting their head which can have significant impact to the aerodynamic performance of the helmet. Beaumont et al. (2018) tested 3 different helmet designs which returned minimal changes in projected frontal area. However, changing the head angle of the rider made significant changes to aerodynamic performance. Refer to Figure 25, which shows the different helmets tested in this study which shows how the performance of different designs can decline as the head angle changes. Furthermore, refer to Figure 26, for the pressure coefficient and Figure 27 for the velocity streamline as changes in the head angle occur.

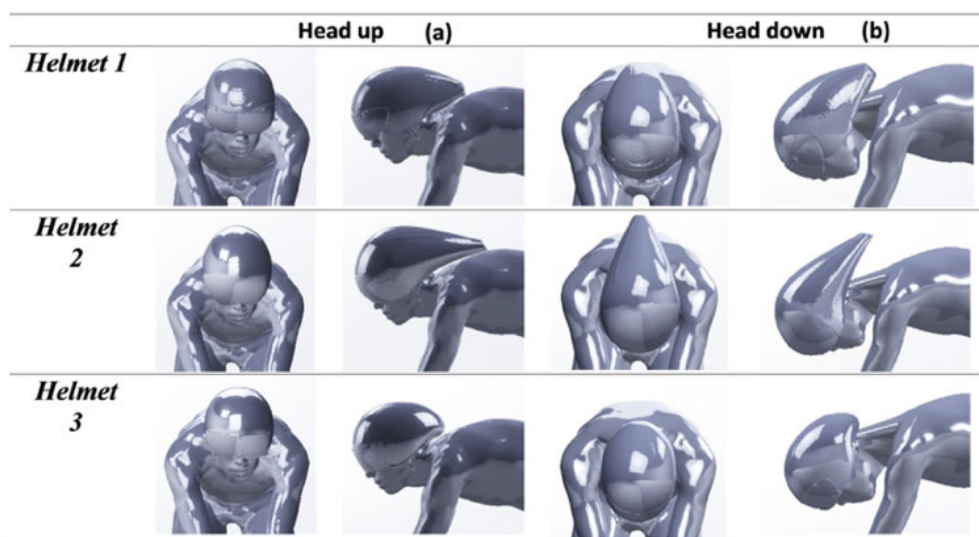


Fig. 1. Defining the geometry of the test subject. For each time trial helmet: Head-up position (a), head-down position (b).

Figure 25 – Different helmet designs and head angles tested in previous research

(Beaumont, et al., 2018).

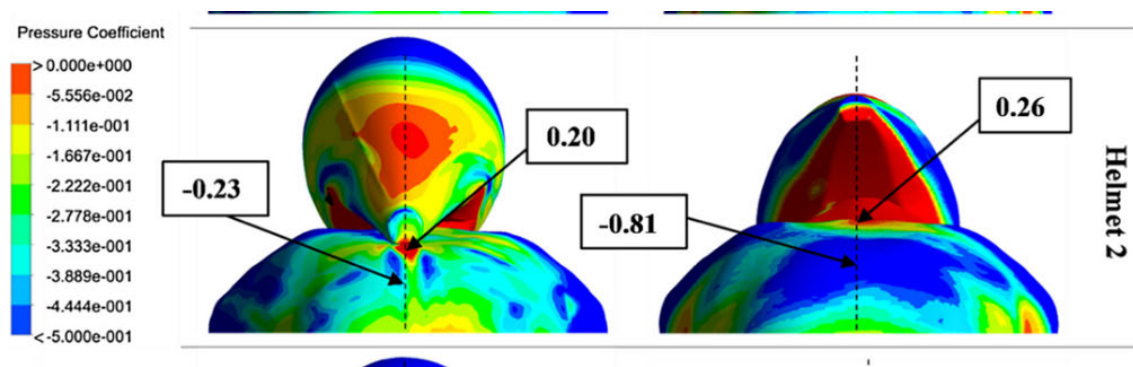


Figure 26 – Result of head angle on pressure coefficient
(Beaumont, et al., 2018).

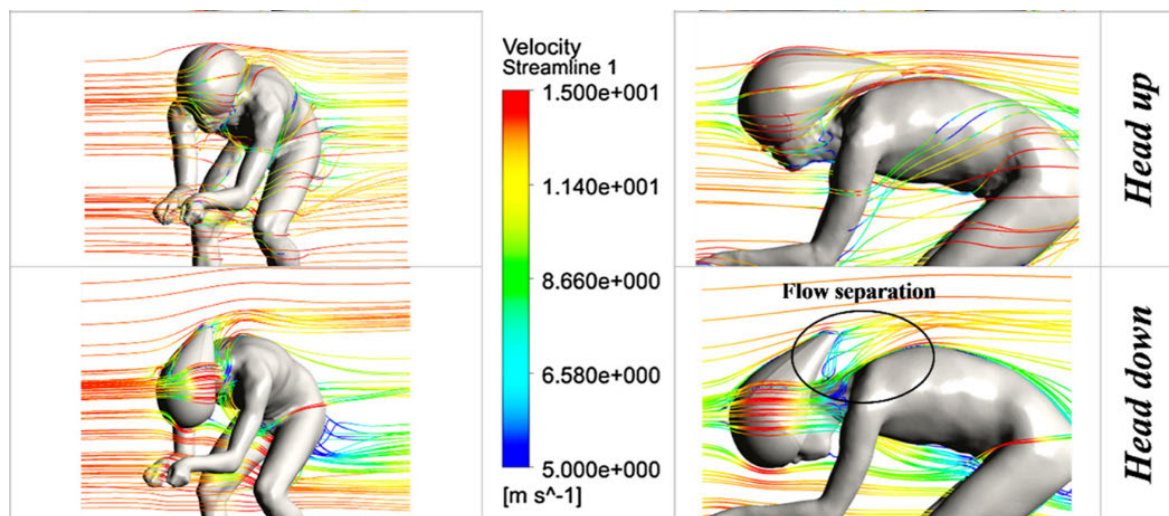


Figure 27 – Result of head angle on velocity streamline
(Beaumont, et al., 2018).

2.3.3 – Helmet Types

In relation to the total drag the cyclist experiences whilst riding, the helmet can contribute up to 8% depending on shape and size. Worth mentioning is that 65 – 80% is due to the rider and their position (Alam, et al., 2014). This research only focused on TT helmets; however, review of standard road helmets was considered for reference. Refer to Figure 28, which shows some variations of TT and road helmets highlighting their differences.



Figure 28 – Popular Road and TT helmets
(Alam, et al., 2014).

When comparing the use of TT helmets to regular road racing helmets, a TT helmet can provide drag savings of more than 40% less than their counterparts. Most TT helmets available for purchase today can be seen to have a tear drop shape to allow for a more aerodynamic flow of air around the cyclist (Alam, et al., 2014). Refer to Figure 29, which shows an illustration of the side view of a typical TT helmet design.

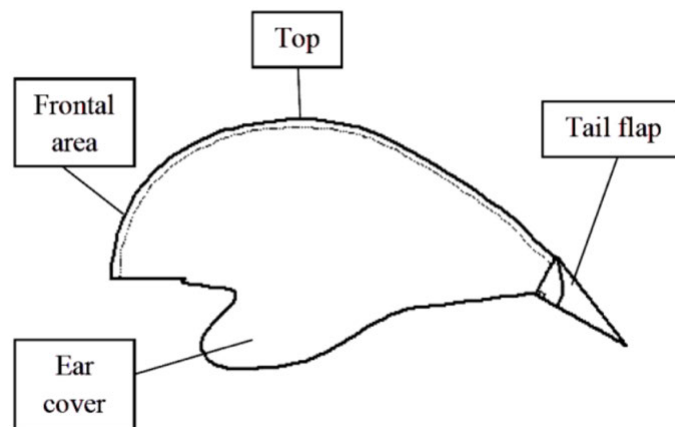


Figure 29 – Side view of TT helmet illustration
(Kamarudin, et al., 2020).

To facilitate an understanding of the difference in TT helmets, extensive research was conducted to obtain what helmets are available for commercial purchase. This highlighted key features that manufacturers incorporate within their design to obtain a performance advantage. Three helmets were selected from this group for further testing. Refer to Table 11, which shows examples of TT helmets over the last decade.

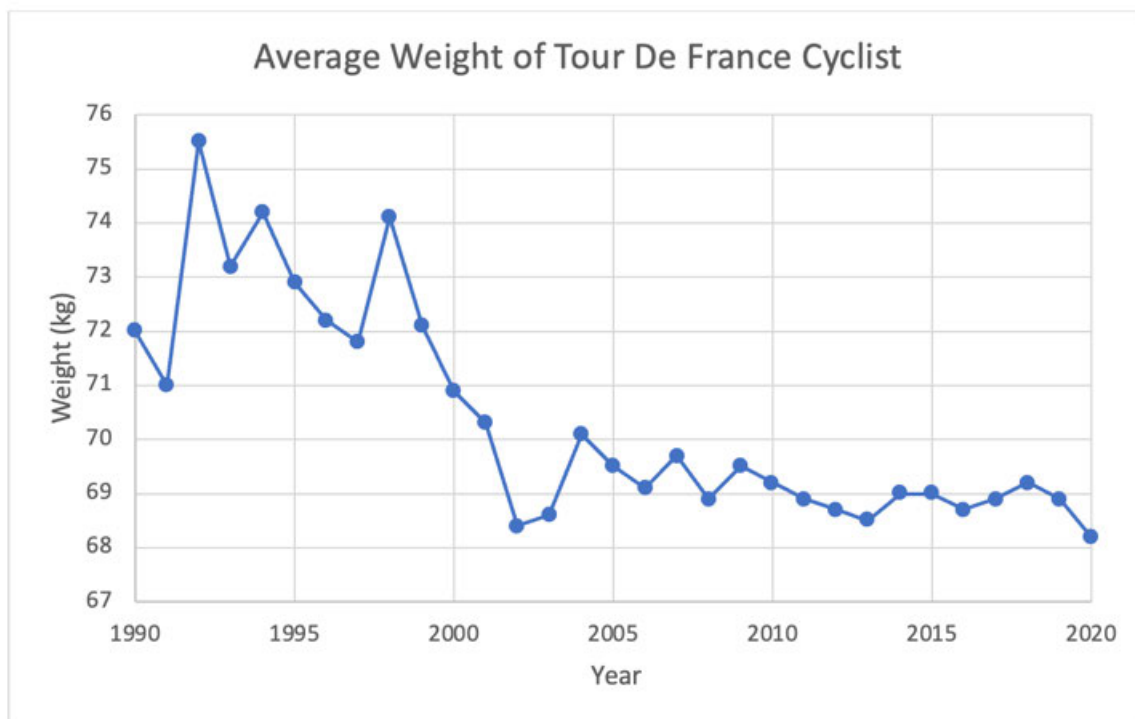
Table 11 – Examples of some TT helmets over the last decade

TT Helmets		
HJC Adwatt  <i>(HJC Sports, 2024)</i>	BELL Javelin  <i>(Cyclestore, 2016)</i>	POC Tempor  <i>(Arthur, 2015)</i>
KASK Mistral  <i>(KASK, 2022)</i>	MET Cordatronca  <i>(MET Helmets, 2024)</i>	RUDY Project Wing  <i>(RUDY Project, 2024)</i>
LAZER Victor  <i>(LAZER Sports, 2024)</i>	GIRO Aerohead  <i>(GIRO Helmets, 2024)</i>	SMITH Jetstream  <i>(SMITH, 2024)</i>

2.3.4 – Anthropometric Data

Road cycling has commonly known for lean athletes of a small stature, so they have a greater ability to climb up the mountain stages in the Tour De France. A cyclist's ability to ride up hills can be determined by their Functional Threshold Power (FTP) in terms of their bodyweight which is measured in Watts/kg, and this can be a decisive factor for performance in cycling (Van Dijk, et al., 2017). Malizia and Blocken (2021) identified during WT testing that a larger rider experiences a greater 14% drag than their smaller counterparts. However, Jobson, et al. (2007) identified that larger cyclists appear to benefit from fixed resistance laboratory testing as opposed to field testing where the drag force increases due to the larger body size.

Refer to Figure 30, which shows an average of Tour De France professional cyclists' weight since 1990. Refer to Figure 31, which shows an average of their heights. Refer to Figure 32 and Figure 33, which shows the weight and height of Tour De France winners over this period respectively.



*Figure 30 – Average Tour De France cyclist weight
(Wood, 2019)*

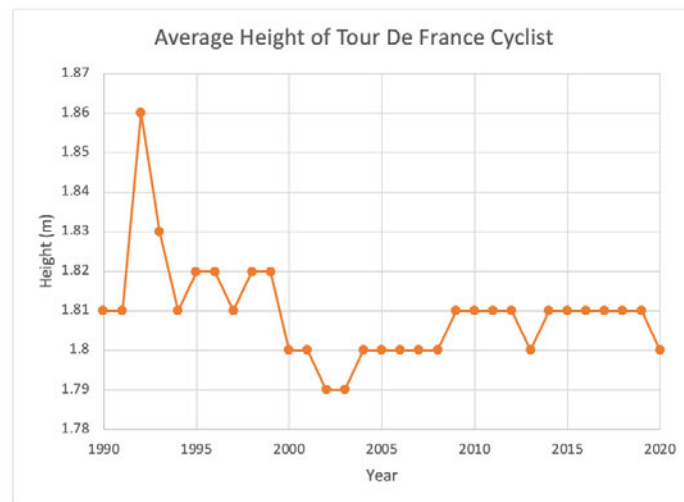


Figure 31 – Average Tour De France cyclist height
(Wood, 2019)

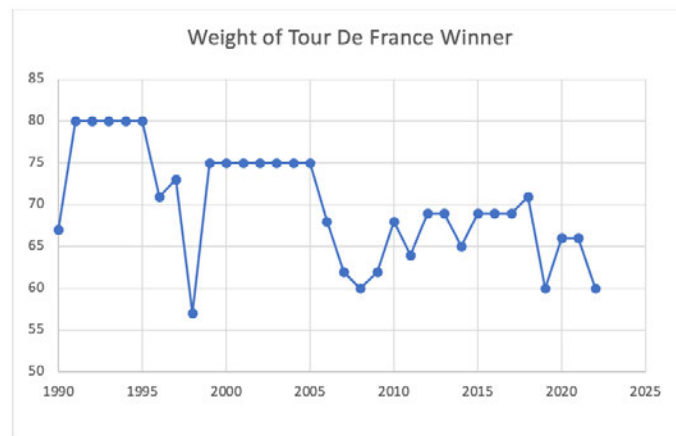


Figure 32 – Tour De France winner weight
(Wood, 2019)

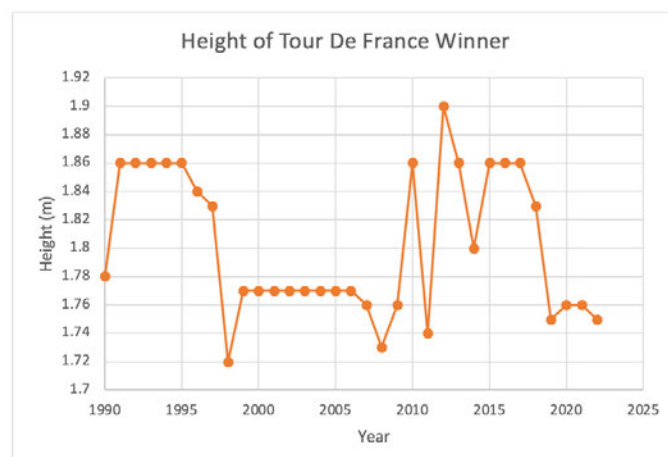


Figure 33 – Tour De France winner height
(Wood, 2019)

2.4 – Aerodynamic Testing

Within aerodynamic testing for cycling and required equipment, there are multiple methods of testing available. Designs can be tested using CFD software platforms, WT testing (model scale and full size), or on road testing (Malizia & Blocken, 2020). CFD is a powerful tool for analysing aerodynamics of a bicycle helmet, however, it does have its limitations (Luke, et al., 2005). WT testing can facilitate the use of 3D printed prototype frames or helmets (Yang, et al., 2017), which would facilitate testing the models to actual wind speeds of 45 km/h and measuring drag force by utilising air-bearing-type force balance. However, not all WTs provide a measurement of cross winds (Barry, et. Al., 2015).

2.4.1 – CFD

Through review of various studies it was evident that CFD is relied on heavily to simulate the aerodynamic characteristics of a cyclist whilst riding. The current literature indicates the strong advantage that CFD offers which facilitates obtaining detailed information on the flow field, which proves difficult to obtain from WT testing (Defraeye, et al., 2010a). However, it was evident that there are some considerations. Blocken, et al (2018), highlighted that a model cyclist being used in CFD should have the cranks almost horizontal resulting in similar dynamic drag of a pedalling cyclist. Refer to Figure 34, which shows an example of the boundary domain used for performing CFD simulations, which is similar size to a WT testing facility.

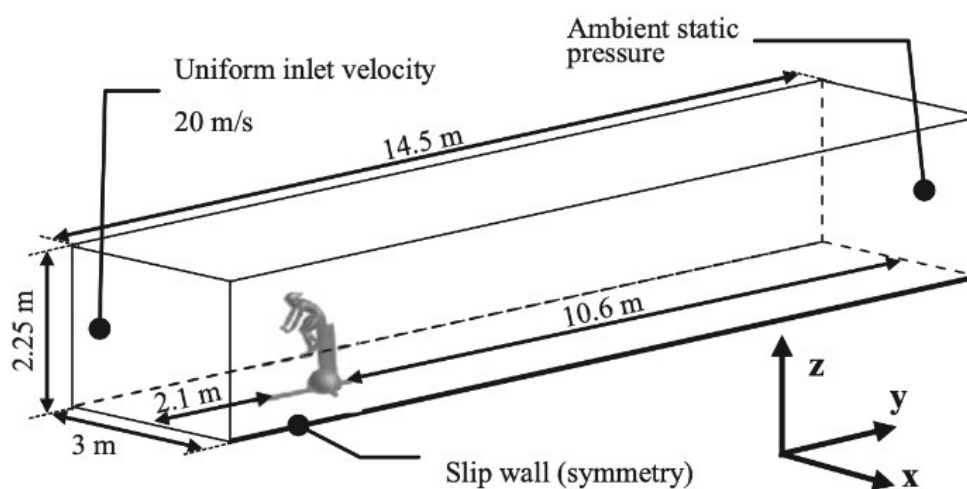
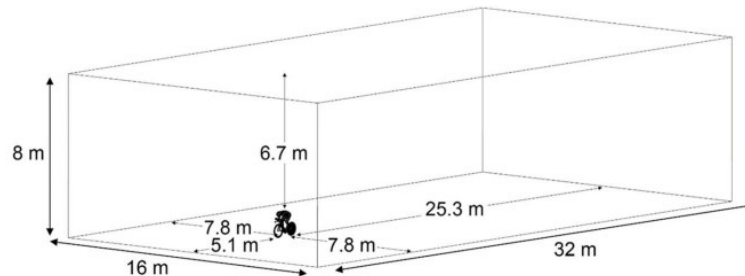


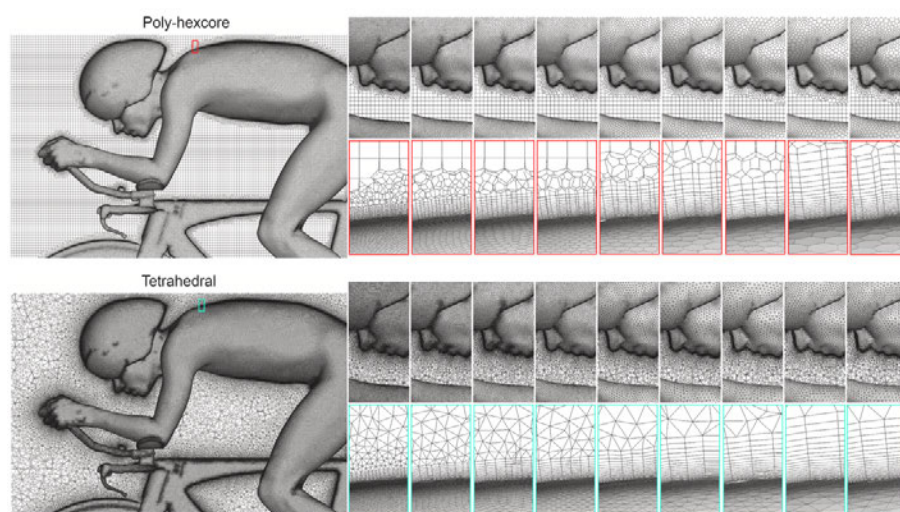
Figure 34 – Boundary Domain for CFD simulation of cyclist
(Fintelman, et al 2015)

Refer to Figure 35, which shows how other researchers have utilised a much larger domain for simulations. If a domain of this size was utilised, it would require significant computational power to successfully run simulations. Due to limitations within the ANSYS Academic licence, a smaller domain was considered and utilised.



*Figure 35 – Larger boundary domain for CFD simulation of cyclist
(van Druenen & Blocken, 2024)*

For selecting an appropriate mesh for CFD, van Druenen and Blocken (2024), tested the accuracy of poly-hexcore and tetrahedral meshes on a TT cyclist. Refer to Figure 36, which shows examples of the two methods applied to the cyclist. The available meshes in CFD platforms include the hexahedral, tetrahedral and polyhedral (Wang, et al., 2021). Using the mosaic technology within ANSYS allows the user to combine all these meshes to enhance their CFD process, simulations and results (ANSYS, 2020). Refer to Table 12, which provides the advantages and limitations of each method which was considered. The literature suggests that the tetrahedral option will provide an efficient mesh application of the helmets which will reduce computational demand.



*Figure 36 – Examples of poly-hexcore and tetrahedral mesh applied to TT cyclist
(van Druenen & Blocken, 2024)*

Table 12 – Advantages and limitations of the ANSYS meshes
(ANSYS, 2020)

	Advantages	Limitations
Hexahedral	<ul style="list-style-type: none"> - Computationally Efficient - High accuracy 	<ul style="list-style-type: none"> - Not well suited to complex geometries - Ineffective characterising of boundary flows
Tetrahedral	<ul style="list-style-type: none"> - Easy to generate automatically - Accuracy has increased due to improved solvers 	<ul style="list-style-type: none"> - Accuracy is questionable - Requires many cells to obtain good convergence and small boundary layer gaps
Polyhedral	<ul style="list-style-type: none"> - Requires a fraction of cells compared to tetrahedral - Efficiently captures the boundary layer on no-slip walls - Easy to generate automatically 	<ul style="list-style-type: none"> - Increased computational time - Not suitable for simple geometries

CFD provides a similar method of testing to that from a WT by facilitating testing in a controlled environment with repeatable conditions. However, CFD is best supported with the data from WT testing. Refer to Figure 37, which shows the difference in drag force between CFD and WT testing. Furthermore, it provides a significant advantage where detailed flow field information is available which provides a better insight into causes of drag force (Defraeye, et al., 2010a).

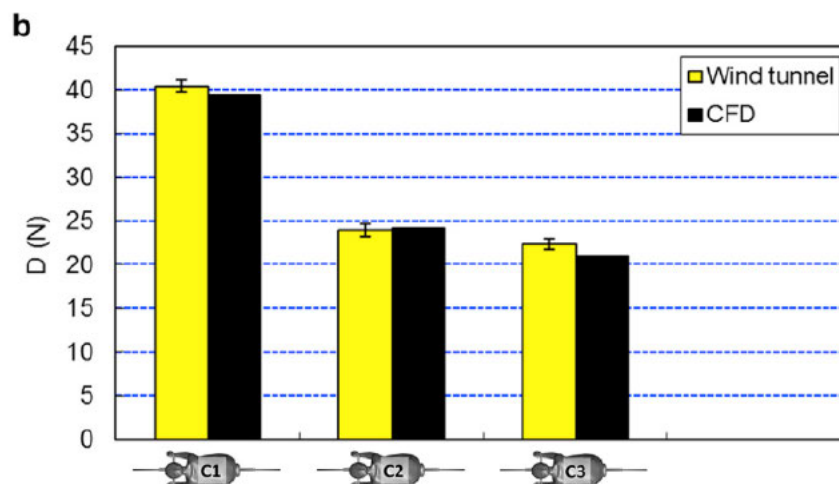


Figure 37 – CFD vs WT testing
(Blocken, et al., 2018)

Whilst CFD has its advantages as listed above, there are still issues which must be highlighted to understand its limitations and areas for improvement. It is common throughout research of CFD application for wall functions to be used to model the boundary layer. However, this can often inaccurately predict wall friction and the transition from a laminar to a turbulent boundary layer (Casey & Wintergerste, 2000).

2.4.2 – Wind Tunnel Testing

The first use of WT testing for cycling was reported to occur in 1953 in a scaled model setup. Full size testing was later performed during 1956. WT testing uses high powered fans to produce air flow at desired velocities, which provides a method of validation of results from CFD in a controlled environment. Refer to Figure 38, which shows a diagram of the closed circuit WT facility at Eindhoven University in the Netherlands. Refer to Figure 39, which shows an example of a 3/4 open-jet WT at Monash University.

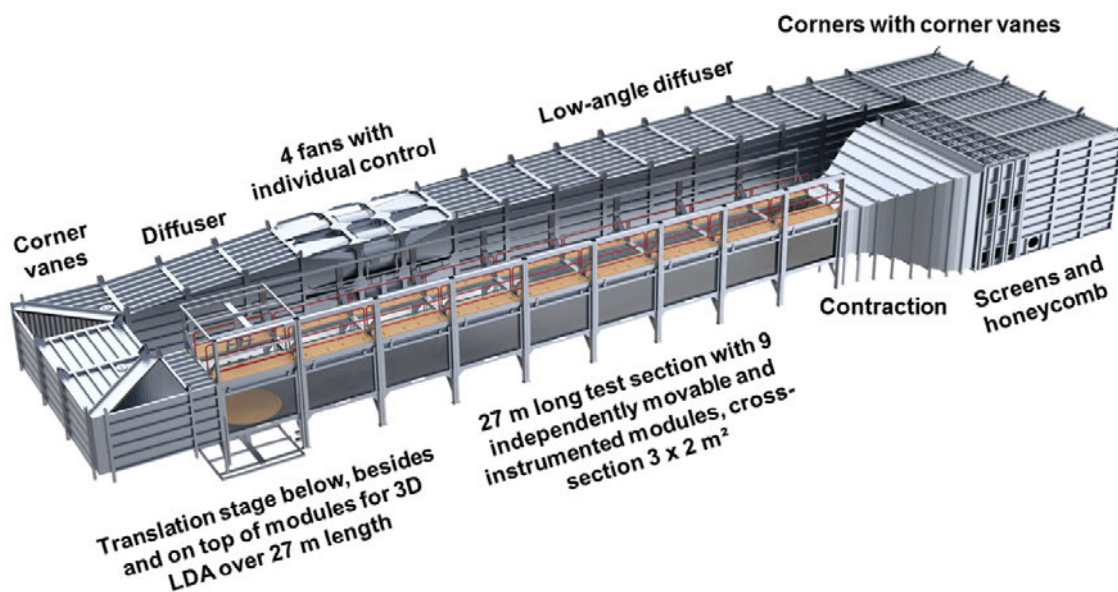


Figure 38 – Diagram of a closed circuit WT at Eindhoven University in the Netherlands

(Malizia & Blocken, 2020)

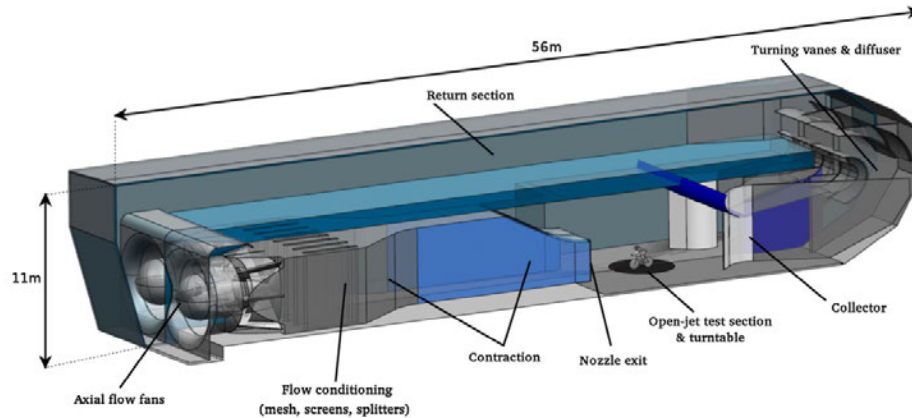


Fig. 5 Cutaway of a 3/4 open-jet wind tunnel (Monash University Clayton Campus) which is ideal for full-scale testing of athletes (note: there are many configurations and designs of open-jet wind tunnels; this is just one example)

Figure 39 – Diagram of a 3/4 open-jet WT at Monash University Clayton Campus
(Crouch, et al., 2017)

WTs are classified usually how they align with their test subjects which include, atmospheric boundary layer, aeronautical, or automobile WTs. Furthermore, their design can be an open or closed section. WT testing facilitates obtaining values for forces and moments such as aerodynamic drag in the direction of the axis that the cyclist is travelling along. The force measurements are obtained by utilising a force balance located below or on the WT floor attached by struts to the bicycle wheels. A turntable facilitates experiments that involve cross wind flows. Refer to Figure 40, which shows a professional cycling team using the Eindhoven closed circuit WT for their team TT testing.



Figure 40 – Team Jumbo Visma testing team TT aerodynamics in a WT
(Malizia & Blocken, 2020)

Throughout the literature review, it became evident how many researchers rely on 3D printing to obtain scaled models of a cyclist riding a bicycle to allow for extensive testing with the cyclist in a uniform position for each trial. Refer to Figure 41, which shows an example of a 3D printed cyclist. Furthermore, by using a scaled model of cyclist, previous studies have been able to test the drafting benefit within the peloton for a cyclist sitting at the very rear, something that would be virtually impossible to do using real cyclists for testing. As most of the research suggests when simulating aerodynamics through CFD for cyclists, the results are best validated with the use of WT testing (Luke, et al., 2005).

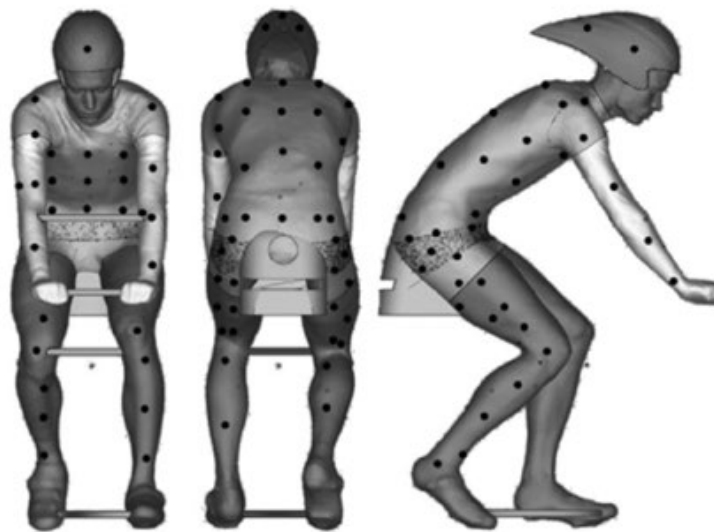


Fig. 1. Scale model of cyclist, manufactured by means of rapid prototyping. The locations of the pressure taps are shown schematically by means of black dots. The stiffening elements between the elbows and knees were not included in the actual scale model (see Fig. 2).

*Figure 41 – Scale model of cyclist manufactured by 3D printer for WT testing
(Fintelman, et al 2015)*

2.5 – Mathematical Formulation

Within modelling of aerodynamics for cycling, there have been many options selected for researchers all of which offer their own advantages and disadvantages. This section will discuss their application to cycling and elaborate on their characteristics. Refer to Table 13, which provides data that was obtained from significant researchers in this field over the last 14 years in which the model and conditions they used are listed.

Table 13 – CFD studies on cycling aerodynamics models

(van Druenen & Blocken, 2024)

CFD studies on cycling aerodynamics published in the peer-reviewed scientific literature. Overview of turbulence modeling, near-wall treatment and computational grid.

Article	Turbulence modeling and near-wall treatment	Computational grid						
		Typology	Surface cell size	Prism layers				Wake cell size max [m]
				y^+/y^+	y_p	Growth rate	# layers	
Defraeye et al. (2010a)	RANS, LES Std. k- ϵ LRNM	Pr, T, H	–	<3	–	–	–	0.03
Defraeye et al. (2011)	RANS Std. k- ϵ LRNM	Pr, T, H	–	<3	–	–	–	0.03
Blocken et al. (2013)	RANS, Std. k- ϵ LRNM	Pr, T	–	–	15 μm	–	–	0.03
Defraeye et al. (2014)	RANS, Std. k- ϵ LRNM	Pr, T, H	–	<3	–	–	–	0.03
Griffith et al. (2014)	RANS, SAS SST k- ω LRNM	Pr, T, H	–	<1	–	1.05	35–40	–
Fintelman et al. (2015)	RANS, LES, DES Std. k- ϵ SST k- ω Wall functions	Pr, Po, T, H	–	a	–	–	–	–
Blocken (2015)	RANS Std. k- ϵ Wall functions	Pr, T, H	–	4–334	30 μm	–	–	0.02
Blocken et al. (2016)	RANS Std. k- ϵ Wall functions	Pr, T, H	–	4–334	30 μm	–	–	0.03
Oggiano et al. (2016)	URANS SST k- ω LRNM	Po, H	–	<5	–	1.25	10	–
Beaumont et al. (2018)	RANS Std. k- ϵ Wall functions	T	–	21.63	–	–	–	0.03
Blocken et al. (2018a)	RANS T-SST k- ω LRNM	Pr, T, H	–	b	10 μm	1.1	40	0.03
Blocken et al. (2018b)	RANS T-SST k- ω LRNM	Pr, T, H	–	b	10 μm	1.1	40	0.03
Blocken et al. (2018c)	RANS Std. k- ϵ Wall functions	T	–	300	2000 μm	–	–	–
Blocken et al. (2019)	RANS T-SST k- ω LRNM	Pr, T, H	–	<1	10 μm	1.1	40	–
Giappino et al. (2019)	RANS SST k- ω LRNM	–	0.5–5	–	–	–	–	–
Blocken et al. (2020)	RANS, SAS SST k- ω LRNM	Pr, T, H	–	b	10 μm	–	40	0.03
Giljarhus et al. (2020)	RANS SST k- ω LRNM	Pr, H	–	2	20 μm	1.2	–	<0.36
van Druenen and Blocken (2021)	SAS SST k- ω LRNM	Pr, T, H	2–5	<1	10 μm	–	40	–
Malizia et al. (2021)	RANS SST k- ω LRNM	Pr, T	–	–	12.5 μm	c	20	–
Blocken et al. (2021)	SAS SST k- ω LRNM	Pr, T, H	–	b	10 μm	–	40	0.03
Blocken et al. (2023)	SAS SST k- ω LRNM	Pr, T, H	–	b	10 μm	–	40	0.03
Wang et al. (2022)	IDDES SST k- ω LRNM	Pr, T, H	≈ 2	5–40	–	1.2	10	–
van Druenen and Blocken (2023)	SAS SST k- ω LRNM	Pr, T, H	2–5	<1	10 μm	–	40	–

Pr: Prismatic cells at the body surface.

T: Tetrahedral cells.

H: Hexahedral cells.

Po: Polyhedral cells.

 y^+/y^+ : dimensionless wall unit. y_p : distance of wall-adjacent cell center point to the wall.

– not provided.

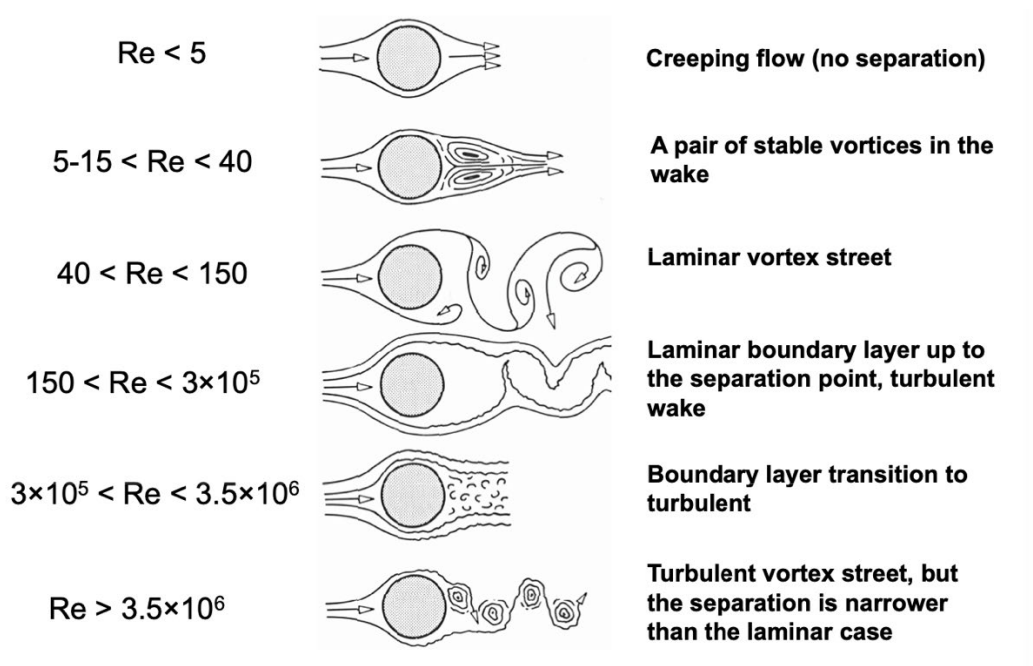
^a When assessing different turbulence modeling approaches, average y^+ values were 43 for RANS, 5.2 for DES, and 3.4 for LES.^b Generally lower than 1, locally max 5.^c Growth rate defined by last-ratio approach.

2.5.1 – Turbulence

Throughout the literature, it highlights there is no formal definition of turbulence. It is a complex phenomenon which has been described as a syndrome with some key behaviours that separate it from non-turbulent flow which include:

- Chaotic flow
- Rotational flow – Possesses three-dimensional vorticity
- Dissipative flow – Kinetic energy lost through friction
- Diffusive flow – fluid properties like heat, momentum and other scalar properties are rapidly intermixed
- Non-linear flow
- Energy is moved from large-scale to small-scale eddies
- High Reynolds number for flow

It must be clear when referring to turbulence that it is a property of flow, not the fluid itself. In turbulent flows, kinetic energy from large-scale flow transfers to smaller turbulent fluctuations resulting in large eddies. The limiting factor for size of these eddies is set by the boundaries or the flow's stratification. Furthermore, a key process that converts energy from the main flow into turbulence is the shear instability (Lueck, 2018). Refer to Figure 42, which shows the relationship between Reynolds number and flow transitions in which it can be observed when it becomes turbulent.



*Figure 42 – Relationship of Reynolds number and flow transitions
(ANSYS, 2010)*

2.5.2 – Reynolds-averaged Navier Stokes (RANS) Equation

Within modelling of cycling for CFD, it can be observed that there will laminar flow when travelling at low speeds. However, as speed increases, like racing conditions, the flow will become turbulent. RANS provides a method for describing the turbulent flow present during simulations. From the application of the Reynolds decomposition, turbulent flows are conceptualised as having every instantaneous variable given as the total of a fluctuating and mean component. Therefore, by time averaging these instantaneous equations, a result for averaged equations is given (Zaidi, et al., 2008). Refer to Table 14 and Table 15, which shows descriptions of all RANS models and their behaviours respectively. Refer to Table 16, which shows the models used in various sports including cycling.

Table 14 – Descriptions of all RANS models
(ANSYS, 2010)

Model	Description
Spalart – Allmaras	A single transport equation model solving directly for a modified turbulent viscosity. Designed specifically for aerospace applications involving wall-bounded flows on a fine near-wall mesh. FLUENT's implementation allows the use of coarser meshes. Option to include strain rate in k production term improves predictions of vortical flows.
Standard $k-\epsilon$	The baseline two-transport-equation model solving for k and ϵ . This is the default $k-\epsilon$ model. Coefficients are empirically derived; valid for fully turbulent flows only. Options to account for viscous heating, buoyancy, and compressibility are shared with other $k-\epsilon$ models.
RNG $k-\epsilon$	A variant of the standard $k-\epsilon$ model. Equations and coefficients are analytically derived. Significant changes in the ϵ equation improves the ability to model highly strained flows. Additional options aid in predicting swirling and low Reynolds number flows.
Realizable $k-\epsilon$	A variant of the standard $k-\epsilon$ model. Its "realizability" stems from changes that allow certain mathematical constraints to be obeyed which ultimately improves the performance of this model.
Standard $k-\omega$	A two-transport-equation model solving for k and ω , the specific dissipation rate (ϵ / k) based on Wilcox (1998). This is the default $k-\omega$ model. Demonstrates superior performance for wall-bounded and low Reynolds number flows. Shows potential for predicting transition. Options account for transitional, free shear, and compressible flows.
SST $k-\omega$	A variant of the standard $k-\omega$ model. Combines the original Wilcox model for use near walls and the standard $k-\epsilon$ model away from walls using a blending function. Also limits turbulent viscosity to guarantee that $\tau_T \sim k$. The transition and shearing options are borrowed from standard $k-\omega$. No option to include compressibility.
Reynolds Stress	Reynolds stresses are solved directly using transport equations, avoiding isotropic viscosity assumption of other models. Use for highly swirling flows. Quadratic pressure-strain option improves performance for many basic shear flows.

Table 15 – Behaviours of all RANS models
(ANSYS, 2010)

Model	Behavior and Usage
Spalart – Allmaras	Economical for large meshes. Performs poorly for 3D flows, free shear flows, flows with strong separation. Suitable for mildly complex (quasi-2D) external/internal flows and boundary layer flows under pressure gradient (e.g. airfoils, wings, airplane fuselages, missiles, ship hulls).
Standard $k-\epsilon$	Robust. Widely used despite the known limitations of the model. Performs poorly for complex flows involving severe pressure gradient, separation, strong streamline curvature. Suitable for initial iterations, initial screening of alternative designs, and parametric studies.
RNG $k-\epsilon$	Suitable for complex shear flows involving rapid strain, moderate swirl, vortices, and locally transitional flows (e.g. boundary layer separation, massive separation, and vortex shedding behind bluff bodies, stall in wide-angle diffusers, room ventilation).
Realizable $k-\epsilon$	Offers largely the same benefits and has similar applications as RNG. Possibly more accurate and easier to converge than RNG.
Standard $k-\omega$	Superior performance for wall-bounded boundary layer, free shear, and low Reynolds number flows. Suitable for complex boundary layer flows under adverse pressure gradient and separation (external aerodynamics and turbomachinery). Can be used for transitional flows (though tends to predict early transition). Separation is typically predicted to be excessive and early.
SST $k-\omega$	Offers similar benefits as standard $k-\omega$. Dependency on wall distance makes this less suitable for free shear flows.
Reynolds Stress	Physically the most sound RANS model. Avoids isotropic eddy viscosity assumption. More CPU time and memory required. Tougher to converge due to close coupling of equations. Suitable for complex 3D flows with strong streamline curvature, strong swirl/rotation (e.g. curved duct, rotating flow passages, swirl combustors with very large inlet swirl, cyclones).

Table 16 – CFD models using within different sports

(Defraeye, 2010b)

Overview of turbulence and boundary-layer modelling approaches of previous CFD studies in sports.

Author	Application	2D/3D	Steady/unsteady	Turbulence and BL modelling	Validation
Bixler and Schloder (1996)	Swimming (hand)	2D	Steady/unsteady ^b	sk-ε, rngk-ε, RSM	Drag force ^a
Bixler and Riewald (2002)	Swimming (arm)	3D	Steady	sk-ε (NWF)	Drag and lift force ^a
Dabnichki and Avital (2006)	Bobsleighbing (bob and riders)	3D	Steady	sk-ω (WF)	Drag and lift force+FV
Gardano and Dabnichki (2006)	Swimming (arm)	3D	Steady	–	Drag and lift force
Meile et al. (2006)	Ski jumping (skier)	3D	Steady	sk-ε	Drag and lift force
Rouboa et al. (2006)	Swimming (arm)	2D	Steady/unsteady ^b	sk-ε	Drag and lift force ^a
Bixler et al. (2007)	Swimming (swimmer)	3D	Steady	sk-ε (NWF)	Drag force
Barber et al. (2009)	Soccer (balls)	3D	Steady	rk-ε (LRNM)	Drag force+FV
Lecrivain et al. (2008)	Swimming (swimmer)	3D	Unsteady ^c	–	Drag force ^a
Zaidi et al. (2008)	Swimming (swimmer)	2D	Steady	sk-ε (NWF)	–
Zaidi et al. (2010)	Swimming (swimmer)	3D	Steady	sk-ε (NWF), sk-ω (WF)	Drag force ^a +FV
Defraeye et al. (2010)	Cycling (cyclist)	3D	Steady/unsteady ^d	sk-ε (LRNM), LES (LRNM)	Drag force and surface pressures

sk-ε: standard k -ε model; sk-ω: standard k -ω model; rngk-ε: RNG k -ε model; RSM: Reynolds stress model; rk-ε: realizable k -ε model; WF: wall functions; NWF: non-equilibrium wall functions; FV: flow visualisation; BL: boundary-layer.

^a Validation was performed by comparison with data of previous experimental studies of other researchers.

^b Accelerated flow.

^c Movement of arm during simulation.

^d Steady approach flow but unsteady wake flow.

2.5.3 – Turbulent Kinetic Energy k

The turbulent kinetic energy, k , more commonly referred to as TKE throughout the literature is defined as the mean kinetic energy per unit mass. It represents the intensity of the turbulence in a fluid by its association with the eddies present in the turbulence of the flow (Li, et al., 2022). This term provides a method of estimating the energy dissipation rate. An example application of this is seen in analysing WT performance through various conditions which include flow turbulence and atmospheric stability (Albornoz, et al., 2022). Refer to Figure 43, which shows the different behaviours of turbulent kinetic energy when different models are utilised for CFD simulations.

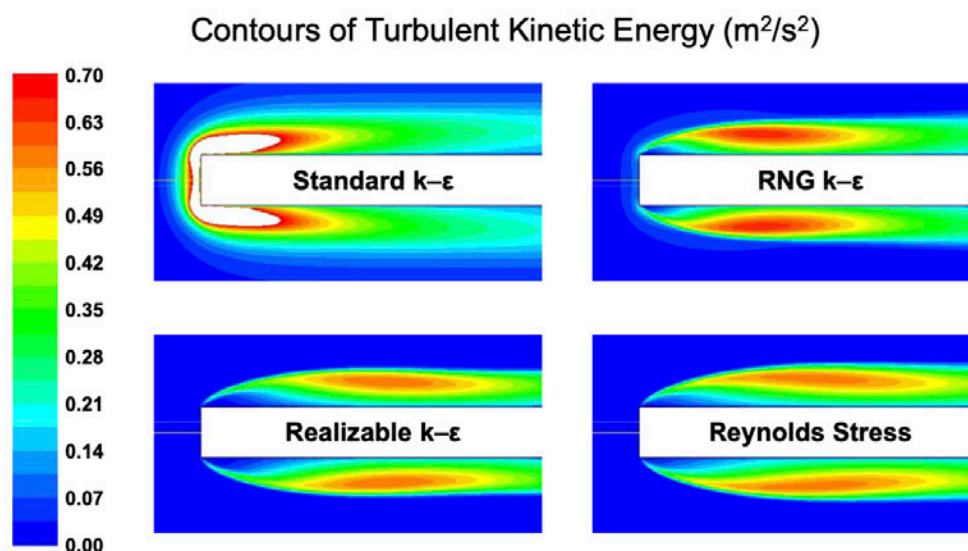


Figure 43 – Comparing turbulent kinetic energy when using different models within CFD

(ANSYS, 2010)

2.5.4 – Dissipation rate of Turbulent Kinetic Energy e

Another factor for determining the behaviour of turbulence is the dissipation rate of the turbulent kinetic energy, e . Often referred to as one of the significant fundamental aspects in turbulence it can be used to estimate additional relevant features of turbulent flow, some of which include Kolmogorov length scale, Taylor-scale Reynolds number, and the energy injection scale. The literature shows some experimental studies in which the energy dissipation rate of a turbulent flow often relies on measurements of one-dimensional flow velocity fluctuations in time (Schröder, et al., 2024).

2.5.5 – Specific Dissipation rate ω

The rate at which the turbulent kinetic energy dissipates per turbulent kinetic energy is known as ω , the specific dissipation rate. This term provides a method for scaling the dissipation rate in relation to the amount of turbulent kinetic energy in the flow turbulent kinetic energy (Mathieu, et al., 2019).

2.5.6 – Standard $k - e$ model

Within modelling turbulent flow in CFD, the standard $k - e$ model is commonly used. Using this model, it assumes a fully turbulent flow throughout the entire domain, however, it is known that turbulent flow is altered by presence of a body within the simulation (Zaidi, et al., 2010). Defraeye et al. (2010b), identified that RANS $k - e$ model with a low Reynolds number underestimated C_{dA} by 11%, whilst Large Eddy Simulation (LES) underestimated by 7% after both were validated by WT results. Furthermore, this may model flow for bluff bodies poorly, especially in the wake (Casey & Wintergerste, 2000).

2.5.7 – Standard $k - \omega$ model

A known weak point of the standard $k - e$ model is the dissipation rate is challenging to specify when modelling the near-wall region. This problem is overcome when using the $k - \omega$ model by solving the transport equation of the specific dissipation rate which facilitates this model being well suited to wall bounded flows, like those in which cyclists are modelled with (Zaidi, et al., 2010). Fintelman et al. (2015), conducted research in which the impact of crosswinds on the cyclists were simulated using RANS, Detached Eddy Simulation (DES) and LES. This

showed that the $k - \omega$ model could effectively capture flow separation around the cyclist with increasing yaw angles. Furthermore, this model is suitable for an adverse pressure gradient and is often used in the aerospace and turbomachinery industry. However, it can be easily affected by free-stream conditions (ANSYS, 2010).

2.5.8 – Transitional $SST\ k - \omega$ model

During a study of cycling pelotons, Blocken et al. (2018) utilised the $\gamma - Re$ transitional $SST\ k - \omega$ model which showed how accurate this model is by obtaining only a 0.8% difference in results from WT testing. This model is formed by the coupling of the $SST\ k - \omega$ model with an additional two transport equations, representing transition onset criteria and intermittency in terms of their Reynolds number and momentum thickness. (Blocken, et al., 2018).

This model utilises a blending function to allow a smooth transition from the $k - \omega$ model near the wall to a version of the $k - \epsilon$ model with a high Reynolds number at the outer region of the boundary layer. Furthermore, this model provides accuracy in predicting the size and onset of separation when pressure gradient is severe (ANSYS, 2010). Refer to Figure 44, which shows the order of computational requirements per iteration of the available models within ANSYS.

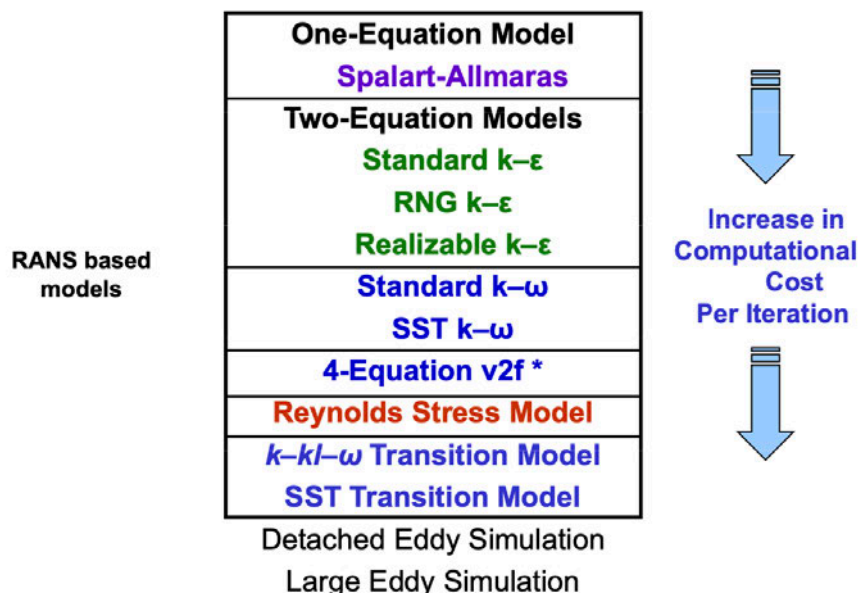


Figure 44 – Increase in computational cost per iteration of RANS based models
(ANSYS, 2010)

2.5.9 – Steady State vs Transient Solver

When utilising RANS models within CFD platforms, there are two available solvers to consider; steady state and transient. Steady state is widely used throughout engineering due to the benefits it offers which include computational efficiency, simplicity and time averaged results that can be easily validated. Some known applications of this method include aircraft wings under normal flying conditions, or heat exchangers, which can both be categorised as quasi-steady state. Some known limitations of the steady state include neglecting vortex shredding or rapid changes in flow which can often result in inaccurate predictions. For considering transient simulations, they provide an ability to capture dynamic flow behaviours such as turbulence. This method provides greater insight into simulations and results, however, it limitations include increased computational demand paired with the requirement of the correct knowledge and understanding of how to interpret the results (Resolved Analytics, n.d).

2.6 – Design Regulations

A known issue with TT helmets is they tend to prioritise performance over safety. Currently, most TT helmets commercially available do not comply with minimum standards required to protect the users head in case of a crash. Unfortunately, insufficient data exists for TT helmets for both their safety rating as well as their aerodynamic performance. Furthermore, manufacturers tend to praise all their benefits without providing any hard scientific evidence to support it (Chowdhury and Alam, 2014).

2.6.1 – Australian Standards

Australia is known for having very strict rules and design standards when it comes to bicycle helmets. When participating in road or track cycling events/races within Australia, helmets must meet the regulations set out in AS2063. However, riders can wear UCI approved helmets for events such as individual pursuit and TT's.

Within the context of professional cycling within Australia, riders must wear helmets that meet the above standard (Chowdhury and Alam, 2014). All helmets must display a sticker from the manufacturer showing compliance with the standard. Refer to Figure 45, which shows the international equivalents that are excepted as listed in the AusCycling Technical Regulations.

- 1.03.05 All riders are required to wear a helmet meeting AS2063/NZ 2063 or equivalent. Helmets must have a manufacturers mark stating its compliance with the Standard. Helmets may be inspected at any time by a Commissaire.

The following are also accepted as an international equivalent to the Australian/New Zealand Standard 2063:

- NSI Z90.4
- Snell "B" or "N" series
- ASTM F1447
- Canadian CAN/CSAD113.2M
- U.S. CPSC standard for bicycle helmets
- European CEN standard for bicycle helmets (EN1078)

Figure 45 – Extract from AusCycling Technical Regulations on helmets

(AusCycling, 2020)

2.6.2 – UCI Regulations

Refer to Figure 46, which shows the UCI's requirements for all road and track helmets. However, riders and/or teams can submit a request through the UCI to wear their own prototype equipment. Refer to Figure 47, which shows the application for prototype approval.

4. For road and track disciplines, the dimensions of the helmet (including accessories) must not exceed the below dimensions:

Length (L) can be less or equal to 450 mm ;

Width (W) can be less or equal to 300 mm ;

Height (H) can be less or equal to 210 mm ;

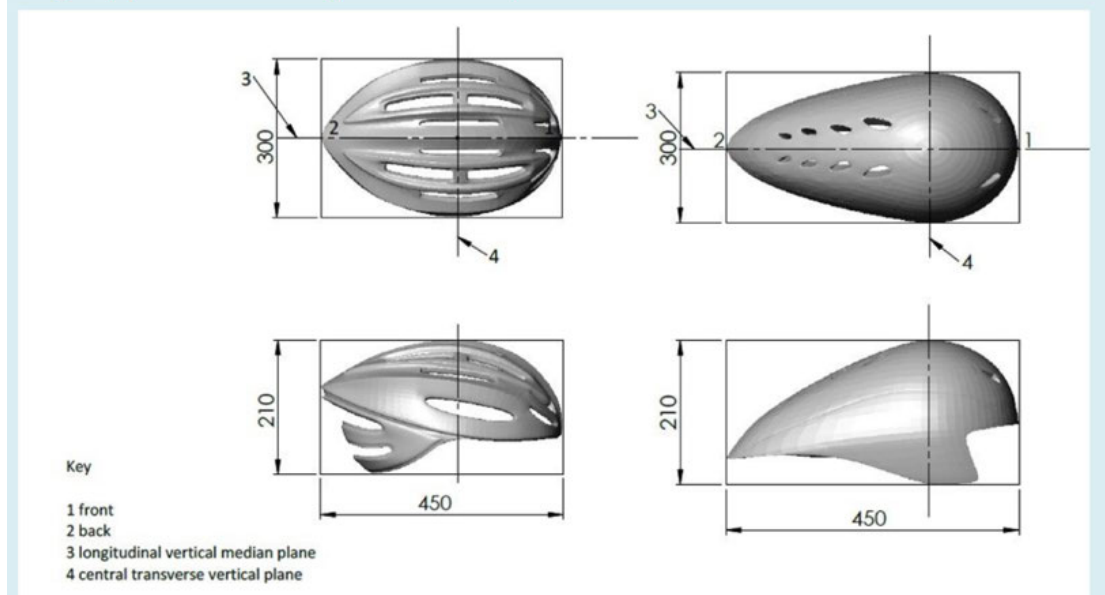


Figure 46 – UCI helmet design regulations

(UCI, 2023)

UCI | **PROTOTYPE APPLICATION FORM**

Applications must be submitted 45 days prior to the products first UCI sanctioned event use.

CONTACT INFORMATION

Company name:

Contact:

Postal address:

Billing address:

Country:

Email address:

Telephone number: Fax number:

Website:

Date of submission:

UCI | **PROTOTYPE APPLICATION FORM**

Applications must be submitted 45 days prior to the products first UCI sanctioned event use.

Materials used:

Others:

DECLARATION OF COMMITMENT

BY SIGNING, THE MANUFACTURER UNDERTAKES TO:

- Respect the approval procedure and to follow the rules of the UCI scrupulously at all stages of the Approval Protocol.
- Contribute to the administrative and research costs of the UCI, as provided in the Approval Protocol.
- Certify that all the information provided on the present form is complete and accurate. The same apply to plans, drawings and any other information which the manufacturer may subsequently give the UCI.
- Produce all new models in accordance with the final Approval Certificate issued by the UCI.

All information provided to the UCI by the manufacturer will be strictly for use during the approval procedure and will remain confidential.

The manufacturer declares that the signatories below are duly individually or collectively authorised to sign binding agreements on behalf of the company under the terms of this form.

Date: Signature:

PLEASE SEND FORM at: materiel@uci.ch

UCI | **PROTOTYPE APPLICATION FORM**

Applications must be submitted 45 days prior to the products first UCI sanctioned event use.

Date of commercialisation:

Piece of Equipment, Textile:

Crankset	<input type="checkbox"/>	Saddle	<input type="checkbox"/>
Frameset	<input type="checkbox"/>	Seatpost	<input type="checkbox"/>
Fork	<input type="checkbox"/>	Stem	<input type="checkbox"/>
Groupset	<input type="checkbox"/>	Pedals	<input type="checkbox"/>
Handlebar, mass start	<input type="checkbox"/>	Tires	<input type="checkbox"/>
Handlebar, against the clock	<input type="checkbox"/>	Textile	<input type="checkbox"/>
Helmet	<input type="checkbox"/>	Wheel	<input type="checkbox"/>

Type: Road ☐ Time trial ☐ Track ☐ Cyclo-cross ☐ Mountain Bike ☐

Model name:

Number and description of sizes:

General description:

Manufacturing process:

UCI | **PROTOTYPE APPLICATION FORM**

Applications must be submitted 45 days prior to the products first UCI sanctioned event use.

Fees:

Piece of Equipment	Amount, CHF
Frameset, Frame + Fork	1000
Groupset	500
Handlebar RR, Road Race	Mold 500
Handlebar TT, Time Trial	Mold 500
Handlebar RR, Road Race	Regular 250
Handlebar TT, Time Trial	Regular 250
Fork	250
Textile, per technology	250
Wheel, per item	250
Stem	250
Seatpost	250
Saddle	250
Crankset	250
Pedals	250
Tires	250
Helmet	250

Figure 47 – UCI prototype equipment application form
(UCI, 2024)

2.7 – Knowledge Gap

2.7.1 – Research Justification

To date there have been many different research projects into improving aerodynamics of cycling through various methods. Blocken et al. (2013) utilised CFD to observe the drag when cyclists are drafting each other. Defraeye et al. (2010, 2011) utilised CFD to determine the aerodynamic characteristics of cyclists riding in various positions. Sims and Jenkins (2011) utilised CFD to improve road cycling performance through aerodynamics of road helmets. There is limited research on the impact of TT helmets within the sport of cycling, however, Beaumont et al. (2018) has briefly touched on this area. This was a key consideration when moving forward to selecting TT helmets as the main point of analysis for this research.

Throughout the literature review it appears to be inconsistent as to standardised testing where a realistic bicycle and human are also modelled and tested through CFD. Through various studies it highlights the difference in drag when testing helmets with or without the rider. This emphasised the need for this research and ensuring that a rider is included in simulations to ensure the resulting drag does not increase with their presence. The lack of research could be due to manufacturers conducting most of the testing and keeping their designs confidential, to gain a performance and market advantage over their competitors (Crouch, et al., 2017).

Throughout all the literature review for this research, there was a reoccurring theme in which cross winds were not always analysed. When using a WT for testing, not all facilities provide a method for testing cross winds, therefore, this must be achieved by CFD. The cross wind can impact the cyclists roll moment, side force and yaw moment (Barry, et al., 2015). The following section will address the practical problem in which suitable control helmets were selected and how aerodynamics was analysed for this research. Refer to Table 17, which shows the budget for the top 5 cycling teams in the world currently. This suggests there is money to be made from these teams who are willing to invest to gain any advantage over their competitors that they can.

*Table 17 – Professional cycling team budgets per year
(Pompliano, 2023)*

Team	Budget
INEOS Grenadier	\$55 million
UAE Team Emirates	\$38 million
Jumbo-Visma	\$29 million
Quick-Step	\$27 million
AG2R-Citroen	\$25 million

2.7.2 – Project Feasibility Analysis

Through the literature review, it is evident of the effective ways of conducting these tests utilising CFD software that will yield accurate results that could be later used to compliment WT and on road testing. Due to the lack of physical work, testing or setup required, achieving the research outcomes seemed highly probable. The most challenging aspect of the research was obtaining control helmets from current industry designs and then altering their geometry to design more aerodynamic shapes. Furthermore, obtaining a human model to be added to CFD testing presented additional challenges in which limitations will be further discussed in the next section.

Chapter 3 – Methodology

3.1 – Chapter Overview

This chapter provides information on the methods used to obtain the results in later sections of the report. It will include the theoretical model for solving the resulting drag forces for the cyclist and will then clarify the CFD setup and methods used to perform simulations within ANSYS Fluent.

3.2 – Theoretical Model

Prior to performing designs of helmets and subsequent CFD simulations, a theoretical model was created to obtain characteristics of helmets of various head angles and lengths and their resulting drag force power output requirements. The theoretical model was created using Microsoft Excel and came from the formulas previously listed in Table 2 of this report from Debraux, et al (2011). Refer to Table 18, which shows the model in which all assumptions are highlighted in red. For the velocity, 13 m/s was selected as it equates to 46.8 km/hr, which is a common average speed throughout TT races. Refer to Figure 48 and Figure 49, which shows how the theoretical model highlighted the relationship of head angle and length of helmet and power required from the cyclist to maintain a velocity of 13 m/s.

Table 18 – Theoretical model properties and calculations

Cyclist Properties and calculations				
Description	Term	Value	Units	Notes
Rolling resistance coefficient	C_R	0.005	-	Assumption
Barometric Pressure	PB	760	mmHg	Assumption
Air density at 760 mmHg and 273K	p_0	1.293	kg/m ³	Assumption
Gravity	g	9.81	m/s ²	Assumption
Temperature	T	20	°C	Assumption
Air density	ρ	1.2041	kg/m ³	Assumption
Velocity of air	v_r	8	km/h	Assumption
		2.22222222	m/s	Result
Height of cyclist	h_b	190	cm	Input
Mass of cyclist	m_b	90	kg	Input
Mass of bicycle	m_c	7	kg	Input
Mass of cyclist-bicycle system	M	97	kg	Input
Length of TT helmet	L	0.15	m	Input
TT helmet inclination on the horizontal	α_1	30	°	Input
		0.52359878	radians	Result
Displacement velocity	v	46.8	km/h	Input
		13	m/s	Input
velocity relative to fluid	v_f	15.2222222	m/s	Result
Body Surface area	A_{BSA}	0.10511647	m ²	Result
Dynamic Pressure	q	139.504648	Pa	Result
Rolling Resistance	R_R	4.75785	N	Result
Aerodynamic drag	R_D	27.5152677	N	Result
Resistive Forces	R_T	32.2731177	N	Result
Frontal area using aero bars + helmet	A_p	0.33576404	m ²	Result
Drag Coefficient	C_D	0.58742291	-	Result
Cyclist power	P	419.55053	W	Input

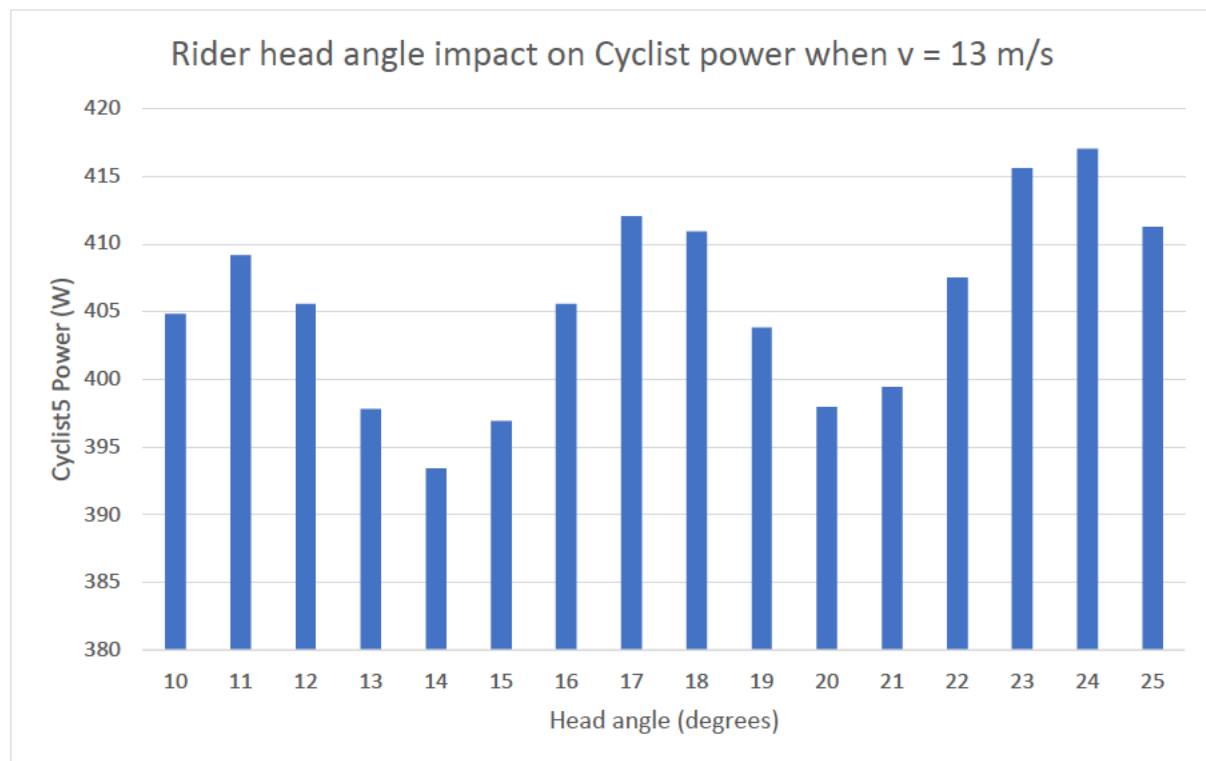


Figure 48 – Rider head angle impact on cyclist power

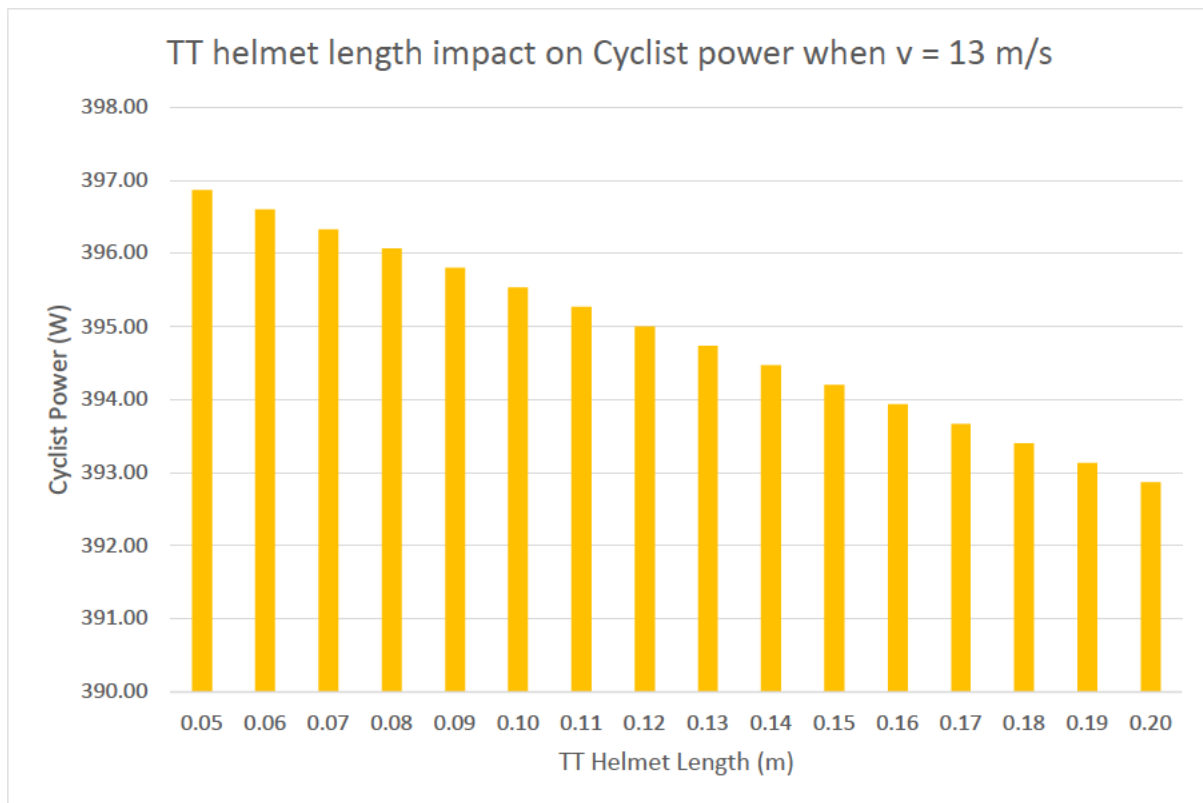


Figure 49 – TT helmet length impact on cyclist power

3.3 – ANSYS Fluent

For all geometry design and subsequent operations to perform CFD simulations, ANSYS was used. Refer to Figure 50, which shows how Fluent was selected as the CFD solver model and a representation of the schematic that was used. Each function within fluent served a purpose which include:

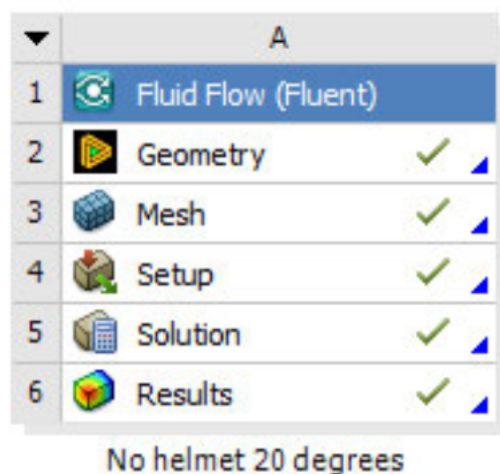


Figure 50 – ANSYS Fluent workspace

- **Geometry:** Utilised for creating helmet designs using Space Claim. During preliminary simulations, Design Modeller was utilised to create enclosures and symmetrical planes.
- **Mesh:** This tool allows for the geometry to have a mesh applied which later allows for solving. The mesh is arguably the most challenging part of the process as if your geometry is very complex, it can be difficult to mesh it. During this part of the process, named selections are allocated to inform fluent where the air is flowing from and to.
- **Setup:** This part of the process is where initial and boundary conditions are set. It allows for the user to dictate a velocity, which objects are solids/fluids. For this research, it was used to set up report plots for drag force, drag coefficient and obtain a projected area value for frontal area of the cyclist.
- **Solution:** During preliminary simulations of this research, this function was not used, however, it facilitates reviewing of the simulation and adjusting parameters to change the output to meet a desired value.
- **Results:** The results function is used to obtain visual representation of the simulations which can include contours, streamlines, vectors and videos of air particle behaviour in which size and time can be adjusted to suit user requirements.

3.4 – Control helmet and Body

The first geometry created was a control body which included a basic shape of a male torso, arms and a head. To remain consistent with the theoretical model initial conditions, a male rider of 190 cm and 90 kg was considered, and approximate values were assigned as such. Refer to Figure 51, which shows the control body that was utilised along with the reference coordinate system, which will remain consistent throughout.

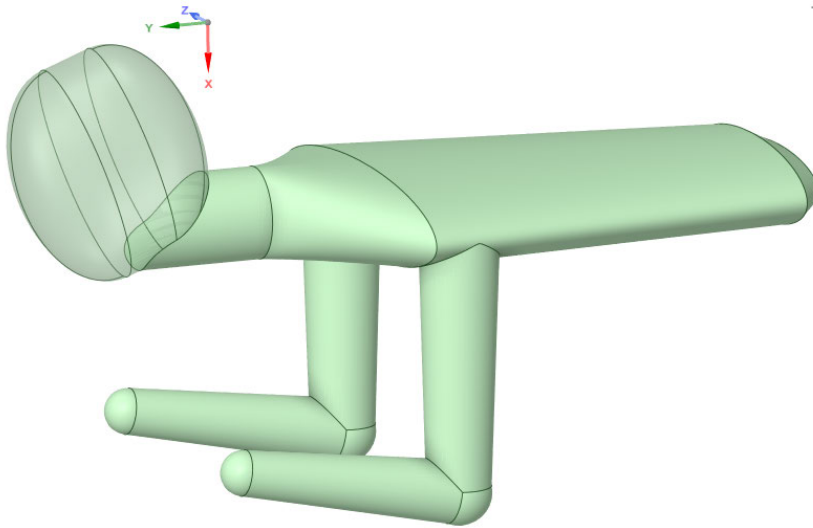


Figure 51 – Control body with no helmet.

Once the control body was created, a control helmet was designed in which all test were compared with. To obtain a design, review of popular designs was considered in which it indicates that a 'tear drop' shape of design seems to be uniform throughout various manufacturers. Refer to Figure 52, which shows how a basic tear drop design was created. Refer to Figure 53, which shows the dimensions of the body. Refer to Figure 54, which shows the dimensions of the head.

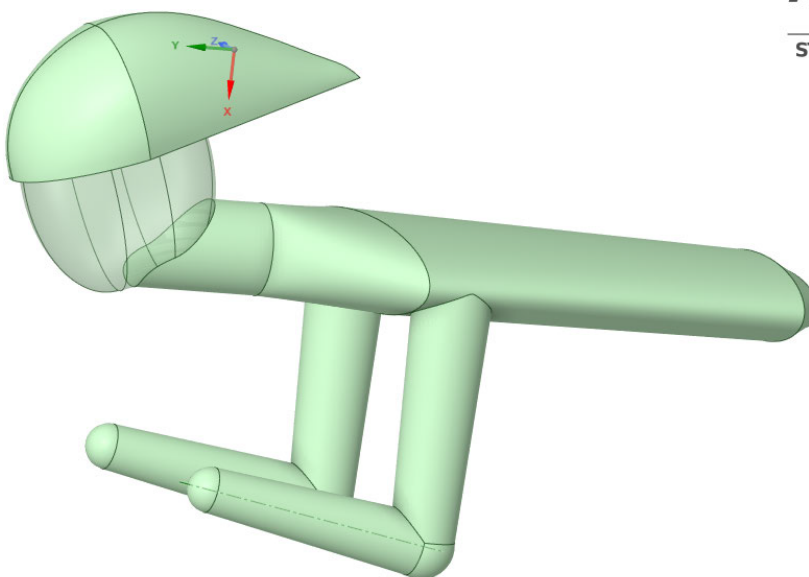


Figure 52 – Control helmet design.

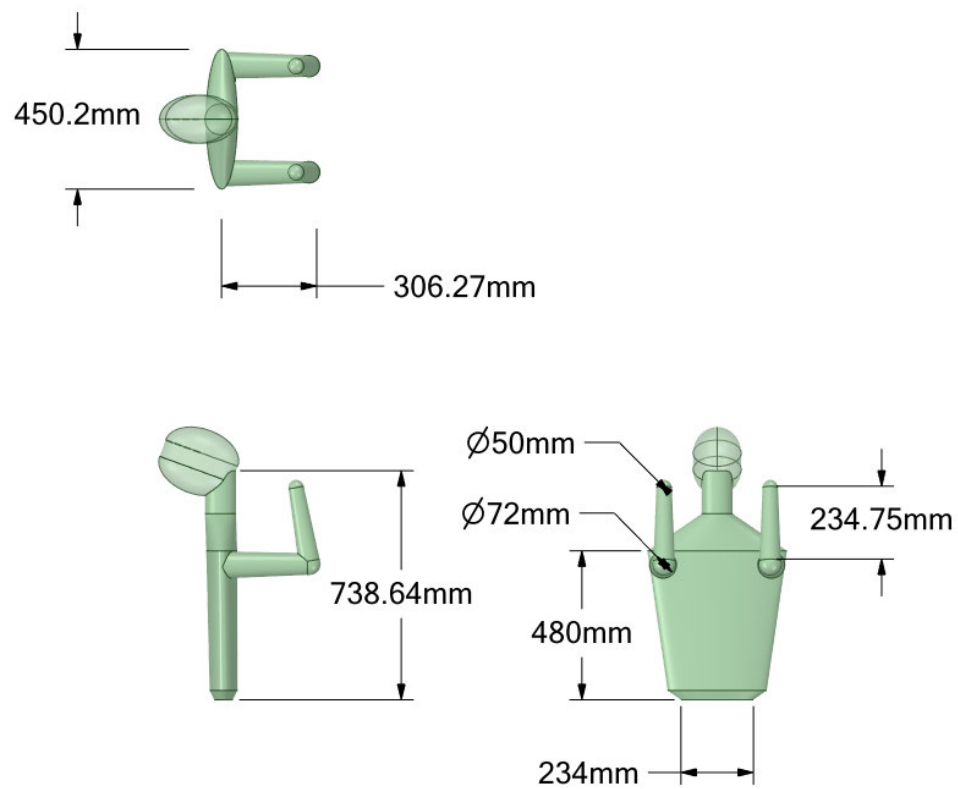


Figure 53 – Dimensions of the body for the human model

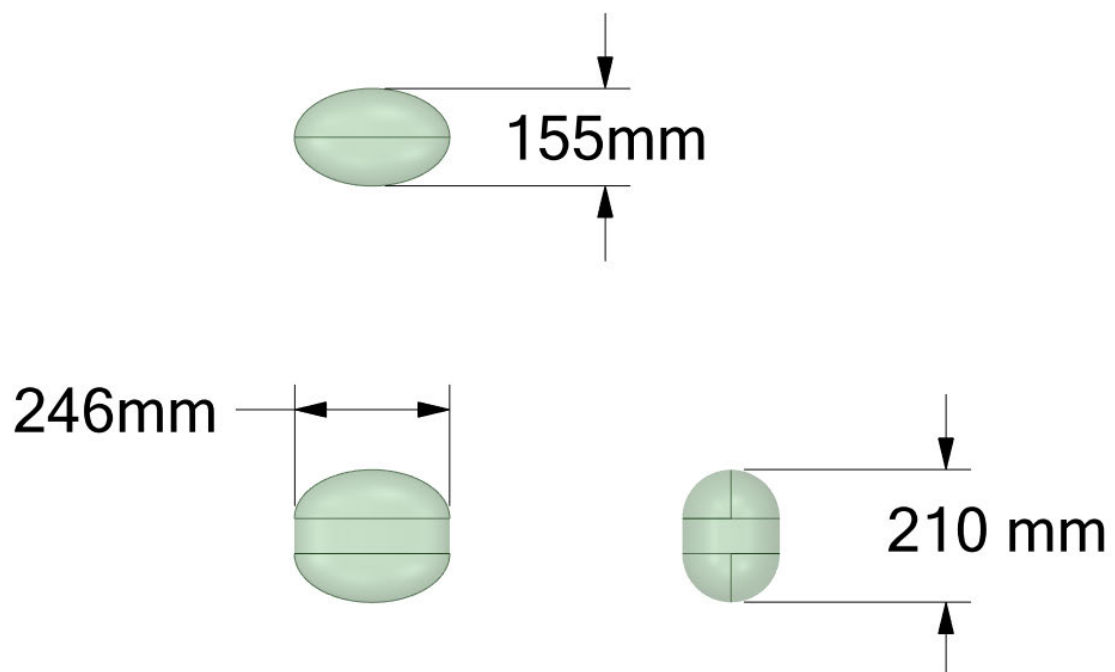


Figure 54 – Dimensions of the head from the human model

3.5 – Preliminary Simulations

To confirm the suitability of the methodology selected to this point, simulations were run using the control body and helmet. Refer to Figure 34, which shows how an enclosure was created using the dimensions obtained during the literature review. Refer to Figure 55, which shows how a singular mesh was applied to the enclosure in which a mesh convergence study identified that a mesh of 150 mm provided accurate results and that reducing the mesh size to 100 mm did not improve accuracy and increased computation time. Refer to Figure 56, which shows the mesh quality.

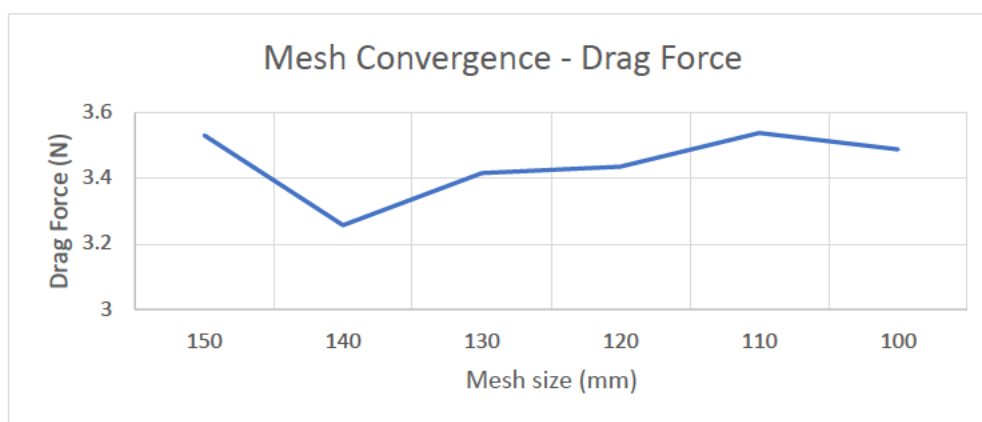


Figure 55 – Preliminary simulations mesh convergence study.

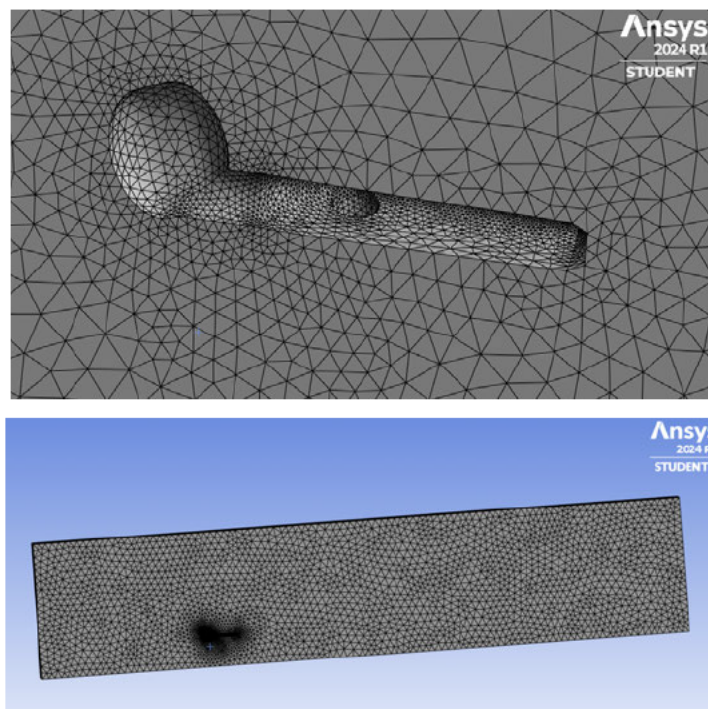


Figure 56 – Mesh quality for preliminary simulations.

Once the mesh was assigned, the named selections were allocated which included an inlet, outlet, cyclist and wall. Refer to Figure 57, which shows that the correct direction for flow was confirmed. The conditions were then dictated in Setup which included:

1. Models: viscous $k - \epsilon$ model (Steady state)
2. Materials: air as fluid.
3. Boundary Conditions: Inlet velocity 13 m/s.
4. Report Definitions: Drag force and Coefficient in y-axis.
5. Initialisation: Standard from inlet
6. Run calculation: 100 Iterations

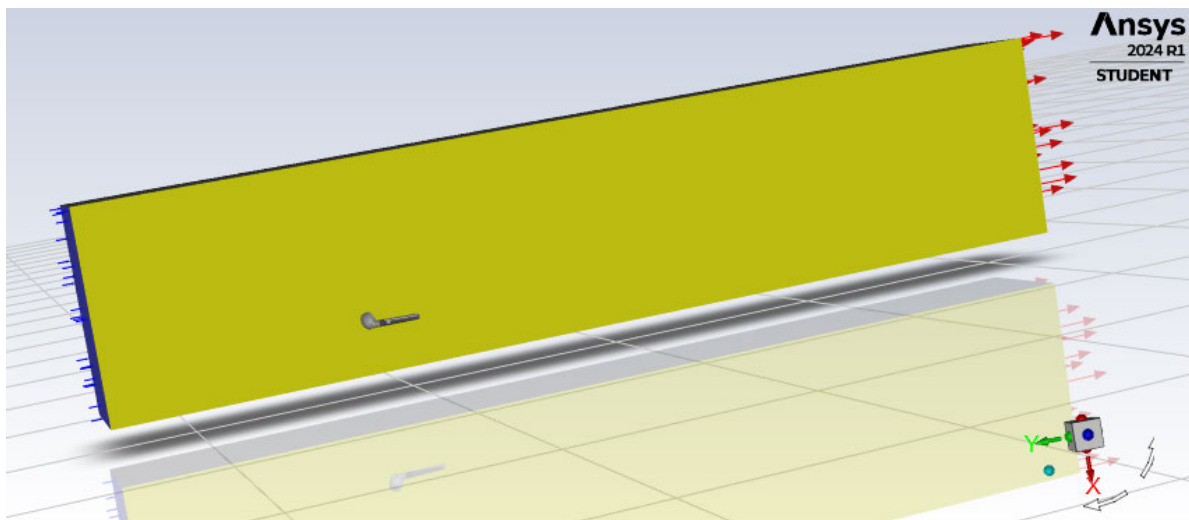


Figure 57 – Model in setup showing correct direction for flow

Refer to Figure 58(a) which shows how once the simulations were run, the results function was used to confirm the separation of flow around the cyclist. Refer to Figure 58(b), which shows that the vector function confirms the air flow direction. During the preliminary simulation, a symmetrical simulation was conducted with the intent of reducing computation time and enhancing mesh quality. This method was conducted by cutting the model in half and then doubling the result from CFD. However, during the initial simulations using symmetry it highlighted a large difference in results and a decision was made to conduct full simulations.

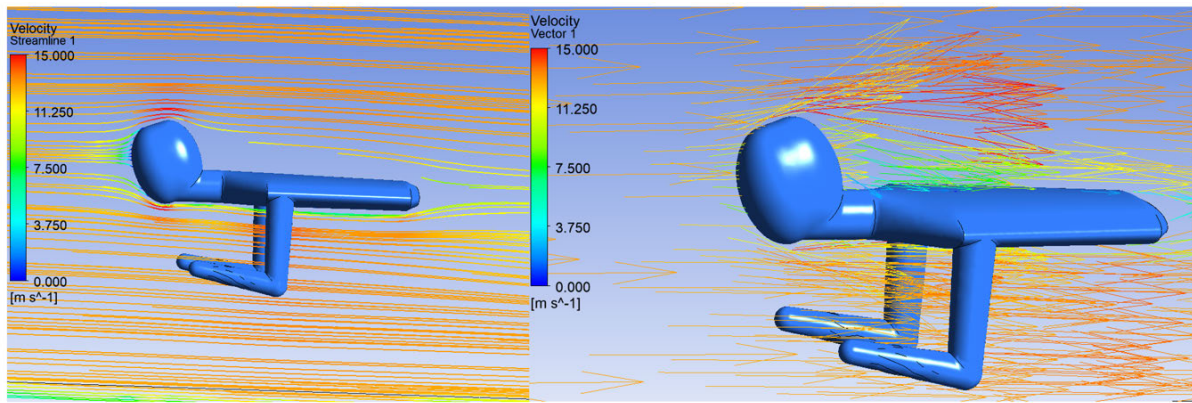


Figure 58 – (a) Velocity streamline showing flow separation, (b) Velocity vector showing flow direction

3.6 – Current Design Replication

An attempt was made to obtain files for current TT helmet designs that the public can purchase, however, it was unsuccessful most likely due to copyright and manufacturers preventing anyone from reproducing their helmet. Therefore, three popular helmet designs were considered and replicated using Space Claim. Refer to Figure 59, which shows the 3 helmets which included the POC Temporal, BELL Javelin and HJC Advant. Unfortunately, finding any test data on these helmets from credible research articles was unsuccessful, however, a popular cycling magazine states that the HJC Advant is the best on test (Opton, 2022). These three helmets were selected as they were each unique in their design and shape, and an effort was made to understand the performance of different helmet designs.



Figure 59 – Current Designs to be replicated.

To obtain the most accurate replication of the helmets, images were obtained of each helmet in the x, y and z direction. They were then pasted into Space Claim on respective axis' and carefully traced. The blend function was then used to complete the design and convert it into

a solid. Refer to Figure 60, which shows how the replication process was performed within Spaceclaim. Refer to Figure 61, which shows the final product of each replica.

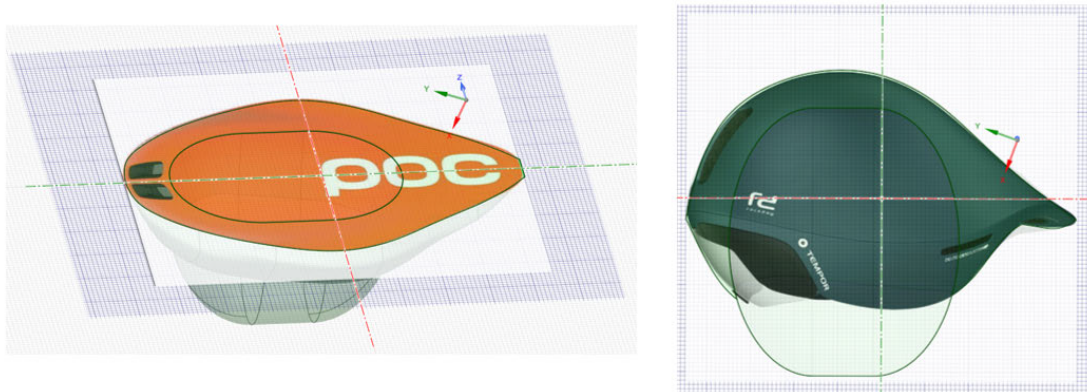


Figure 60 – Replication process of current designs

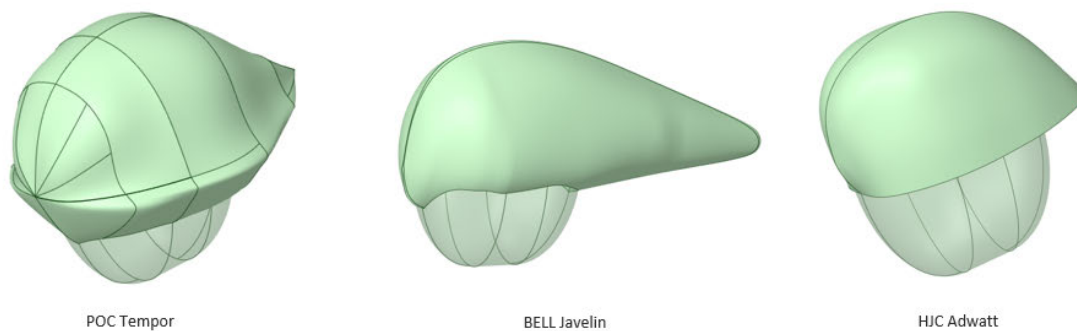


Figure 61 – Final product of replica helmets

3.7 – Project Simulations

3.7.1 – Scope

The aim of this research was to test the three current designs of TT helmets, which were identified as the POC Tempor, BELL Javelin and HJC Adwatt. From the results of these helmets, a prototype helmet design was proposed which offers a lesser value of drag force meaning greater performance for the cyclist. All helmets were tested with the control body that was identified during section 3.4 – Control helmet and Body. Helmets were tested at 2 different head positions of 20 and 30 degrees, at a velocity of 13 m/s (46.8 km/h).

Once all simulations were complete, the values for each helmet were applied to the TT savings model in Microsoft Excel, which shows the performance of all helmets over a 40 km flat TT course with a rider size of 190 cm at 90 kg, riding at a power output of 400 W.

The bicycle was omitted from the model as there are so many differences between bicycle frames and their aerodynamics. To remain impartial, only the helmet and part of the rider was considered.

3.7.2 – Geometry

Refer to Figure 62, which shows how all geometry was created using Space Claim and the two head angles that were considered and their subsequent simulations. Refer to Figure 63, which shows the three prototypes that were tested. To reduce complexity of meshing and computation time, the cyclist did not include the legs and bicycle, in which reasoning behind this is expanded later in this report.

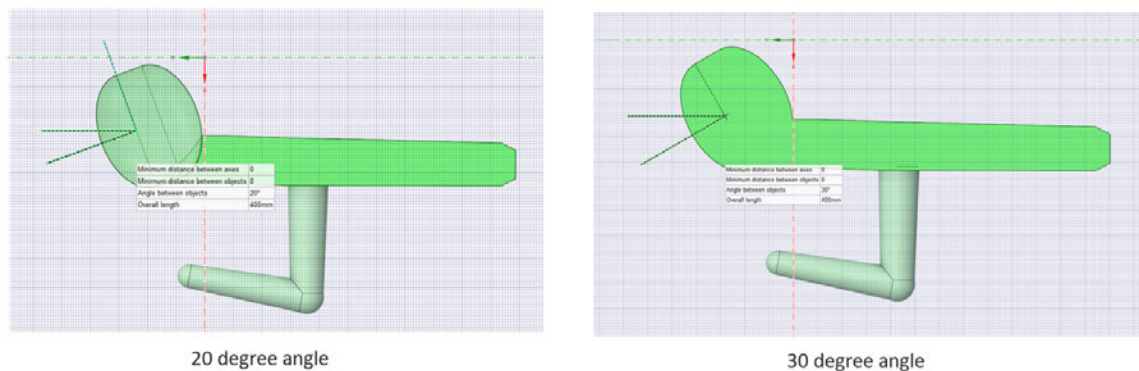


Figure 62 – Different head angles that will be tested during project

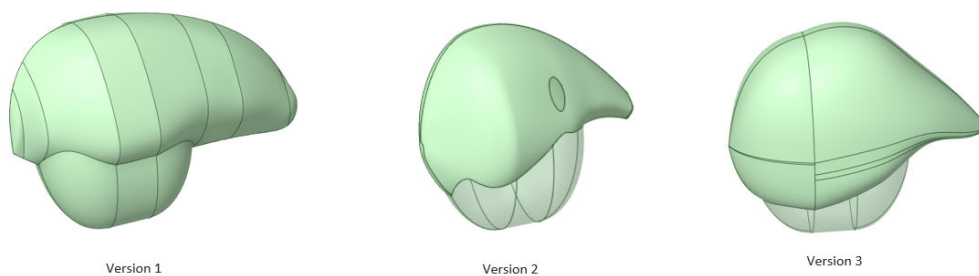


Figure 63 – Three versions of prototype helmets

3.7.3 – Enclosure and Wake

The enclosure was created identical to that shown during preliminary simulations. Refer to Figure 34, which shows the dimensions this was based off which were obtained during the literature review. However, an additional dimension was placed underneath the cyclist as this model did not encompass the legs and the bicycle of the rider. Refer to Figure 64, which shows the dimensions and visual representation of the enclosure. Refer to Figure 65, which shows the wake that was created to allow more accurate results for simulations and the dimensions by assigning a finer mesh around the cyclist.

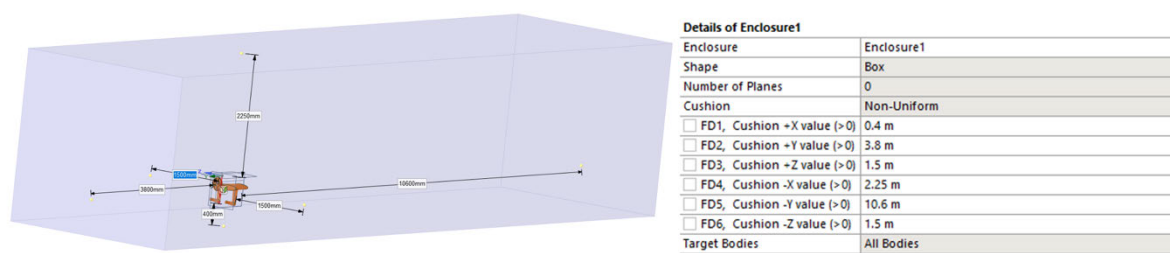


Figure 64 – Enclosure with dimensions

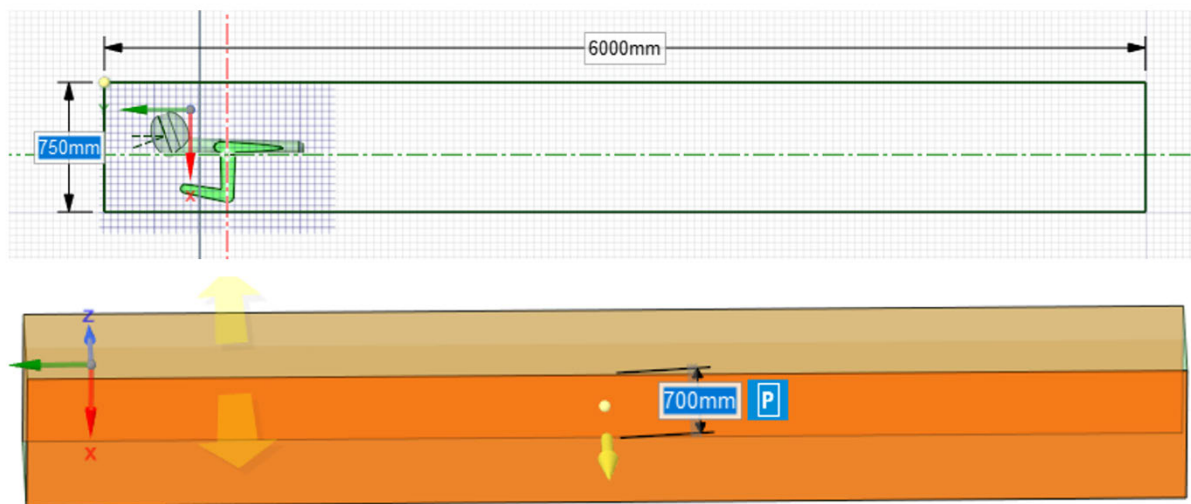


Figure 65 – Wake with dimensions

3.7.4 – Named Selections

Named selections were allocated to identify direction of air flow for ANSYS. Refer to Figure 66, which shows the named selections. Refer to Figure 67, which shows how the inlet was placed in the negative y direction. All remaining named selections were placed accordingly within that coordinate system.

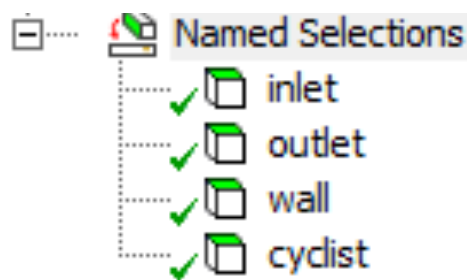


Figure 66 – Model named selections

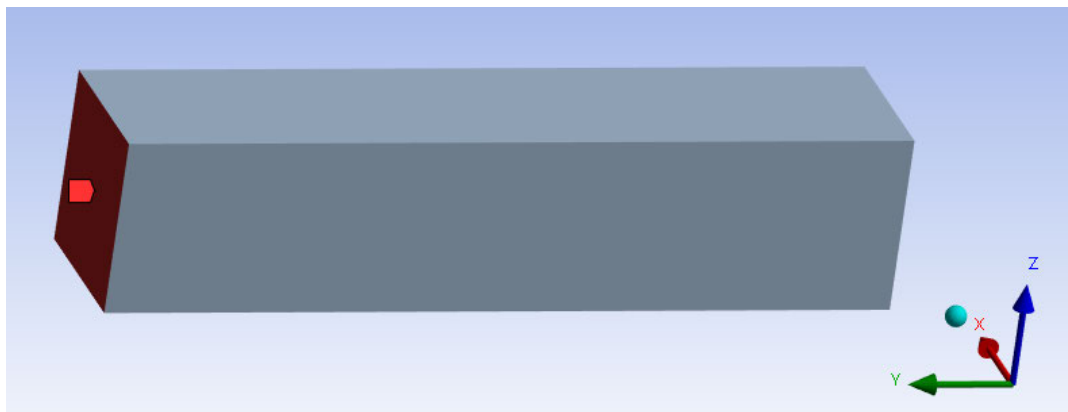


Figure 67 – Inlet named selection and coordinate system

3.7.5 – Mesh

To facilitate a higher quality mesh around the cyclist a wake was created. The wake was assigned a 20 mm mesh, the enclosure a 200 mm mesh, and a 4 mm mesh size for the cyclist. The 150 mm mesh size would have been utilised for the enclosure, however, due to ANSYS student licence restrictions, it wasn't. Refer to Figure 68, which shows the final number of nodes and elements for the version 3 prototype. The face sizing function was used to facilitate multiple mesh sizes within the model. Refer to Figure 69, which shows the mesh quality for the cyclist.

Statistics	
<input type="checkbox"/> Nodes	293213
<input type="checkbox"/> Elements	609434

Figure 68 – Mesh nodes and elements

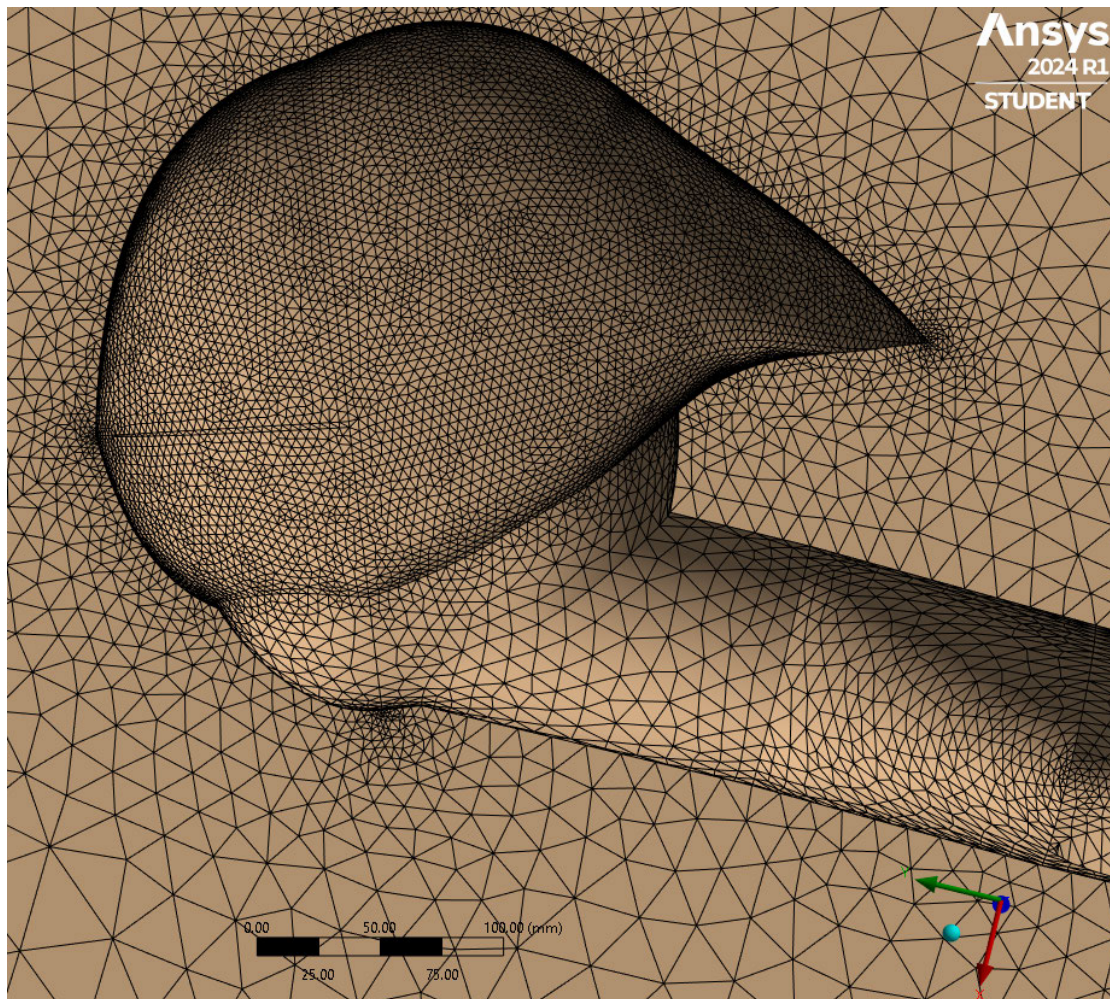


Figure 69 – Mesh quality of cyclist

3.7.6 – Model Selection

To provide a wider range of results and a greater understanding of behaviour for each helmet, steady state and transient simulations were conducted. To reduce the computational cost and facilitate project efficiency the standard $k - e$ model was selected. Refer to Figure 70, which shows its setup. Whilst other models offer superior modelling of turbulent flow, a priority of designing and simulating more helmets was selected as there has already been extensive research into the advantages and disadvantages of all RANS turbulence models available for simulation, for the sport of cycling.

The screenshot shows the 'Viscous Model' dialog box. On the left, under 'Model', the 'k-omega' option is selected. Below it, under 'k-omega Model', the 'SST' option is selected. Under 'k-omega Options', 'Low-Re Corrections' is unchecked. Under 'Near-Wall Treatment', 'correlation' is selected. Under 'Options', 'Production Limiter' is checked. Under 'Transition Options', 'Transition Model' is set to 'none'. On the right, under 'Model Constants', various parameters are set: Alpha*_inf = 1, Alpha_inf = 0.52, Beta*_inf = 0.09, a1 = 0.31, Beta_i (Inner) = 0.075, Beta_i (Outer) = 0.0828, TKE (Inner) Prandtl # = 1.176, TKE (Outer) Prandtl # = 1, SDR (Inner) Prandtl # = 2, SDR (Outer) Prandtl # = 1.168, and Production Limiter Clip Factor = 10. Under 'User-Defined Functions', 'Turbulent Viscosity' is set to 'none'.

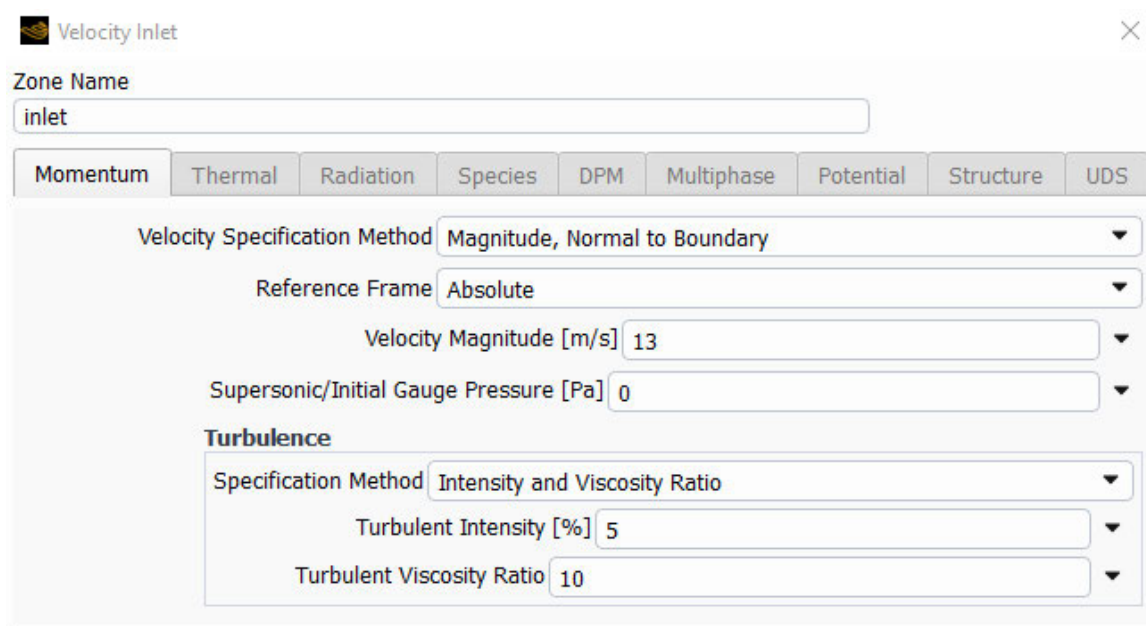
Figure 70 – k-e model setup

3.7.7 – CFD conditions

Refer to Figure 71, which shows the inputs to simulate the conditions for the cyclist which include selecting air as the fluid, which has the properties set by default. Refer to Figure 72, which shows how the inlet velocity was set at 13 m/s, as previously mentioned during preliminary simulations.

The screenshot shows the 'Air' material properties dialog box. Under 'Name', 'air' is entered. Under 'Material Type', 'fluid' is selected. Under 'Chemical Formula', it is empty. Under 'Fluent Fluid Materials', 'air' is selected. Under 'Mixture', 'none' is selected. In the 'Properties' section, 'Density [kg/m³]' is set to 'constant' with a value of 1.225. 'Viscosity [kg/(m s)]' is set to 'constant' with a value of 1.7894e-05. There are 'Edit...' buttons next to the constant values.

Figure 71 – Air properties for simulation



Velocity Inlet

Zone Name: inlet

Momentum | Thermal | Radiation | Species | DPM | Multiphase | Potential | Structure | UDS

Velocity Specification Method: Magnitude, Normal to Boundary

Reference Frame: Absolute

Velocity Magnitude [m/s]: 13

Supersonic/Initial Gauge Pressure [Pa]: 0

Turbulence

Specification Method: Intensity and Viscosity Ratio

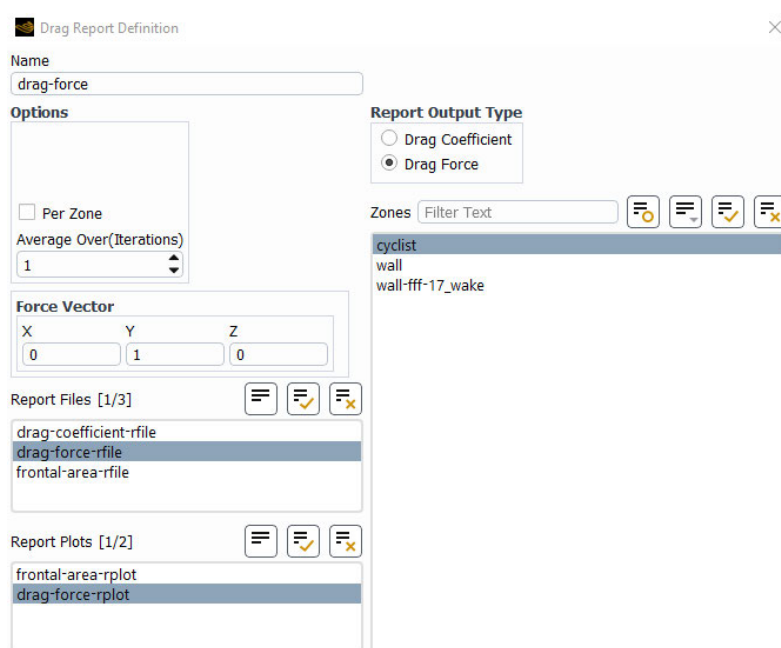
Turbulent Intensity [%]: 5

Turbulent Viscosity Ratio: 10

Figure 72 – Inlet velocity

3.7.8 – Report Definitions

The main value of interest from this project was the drag force in the y direction. Refer to Figure 73, which shows how the report definition for the drag force and drag coefficient was created. Refer to Figure 74, which shows how the projected area function was utilised to obtain the frontal area of the cyclist.



Drag Report Definition

Name: drag-force

Options

☐ Per Zone

Average Over (Iterations): 1

Force Vector

X: 0 Y: 1 Z: 0

Report Files [1/3]

drag-coefficient-rfile
drag-force-rfile
frontal-area-rfile

Report Plots [1/2]

frontal-area-rplot
drag-force-rplot

Report Output Type

☐ Drag Coefficient
☒ Drag Force

Zones: Filter Text

cyclist
wall
wall-fff-17_wake

Figure 73 – Report definitions for Drag Force and Coefficient

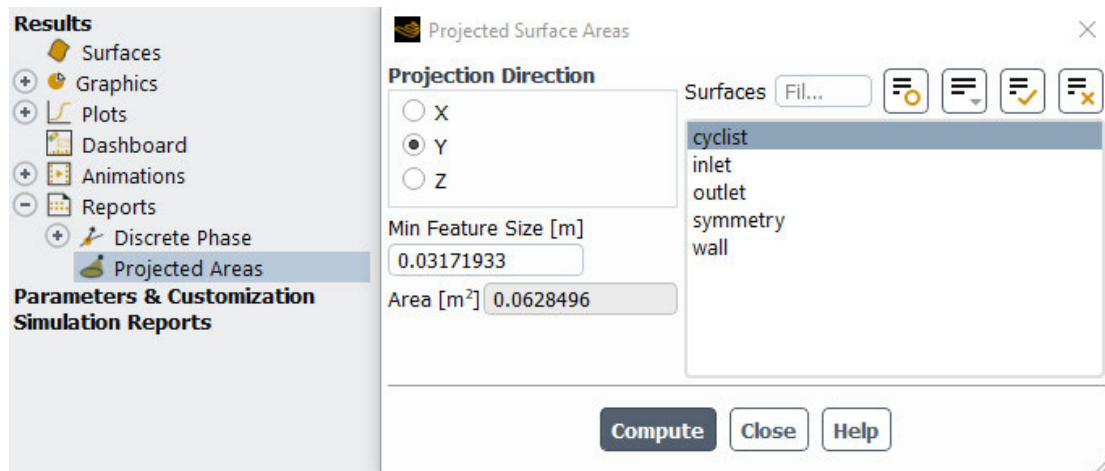


Figure 74 – Projected area for frontal area

3.7.9 – Solution Setup

Refer to Figure 75, which shows that standard initialisation was used from the inlet prior to performing simulations. Iterations were set to 1000 for the initial simulation and then later dropped down to 120. Refer to Figure 76, which shows the scaled residuals which shows how the solution stabilises around 120, thereby justifying the reduction.

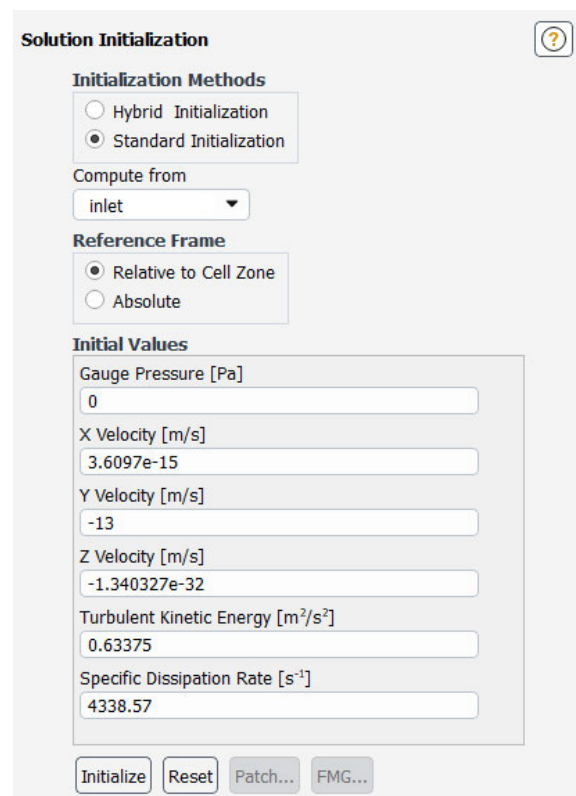


Figure 75 – Standard initialisation setup

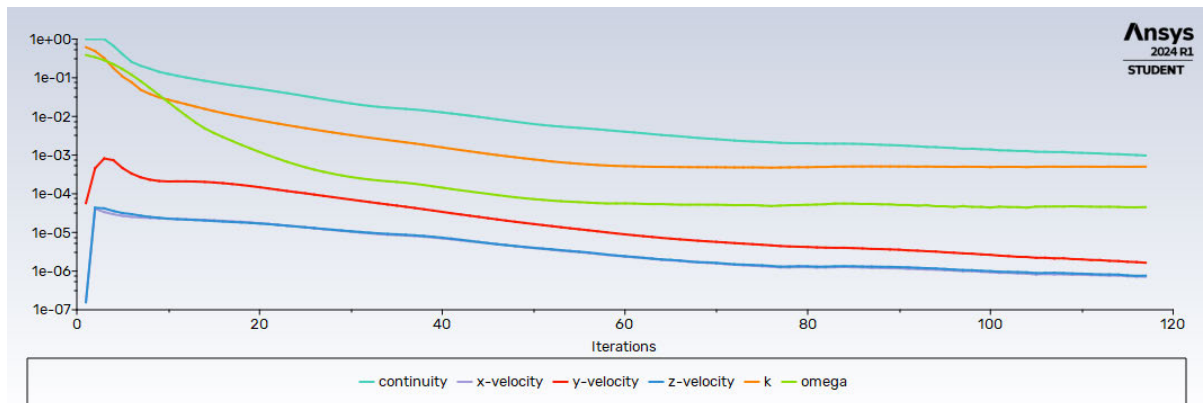


Figure 76 – Scaled residuals showing solution convergence

3.7.10 – FLUENT Outputs

Refer to Figure 77, which shows the setup in ANSYS Workspace for all the FLUENT outputs. For ease of reading the individual images have been combined, as they were displayed in an individual column in Workbench.

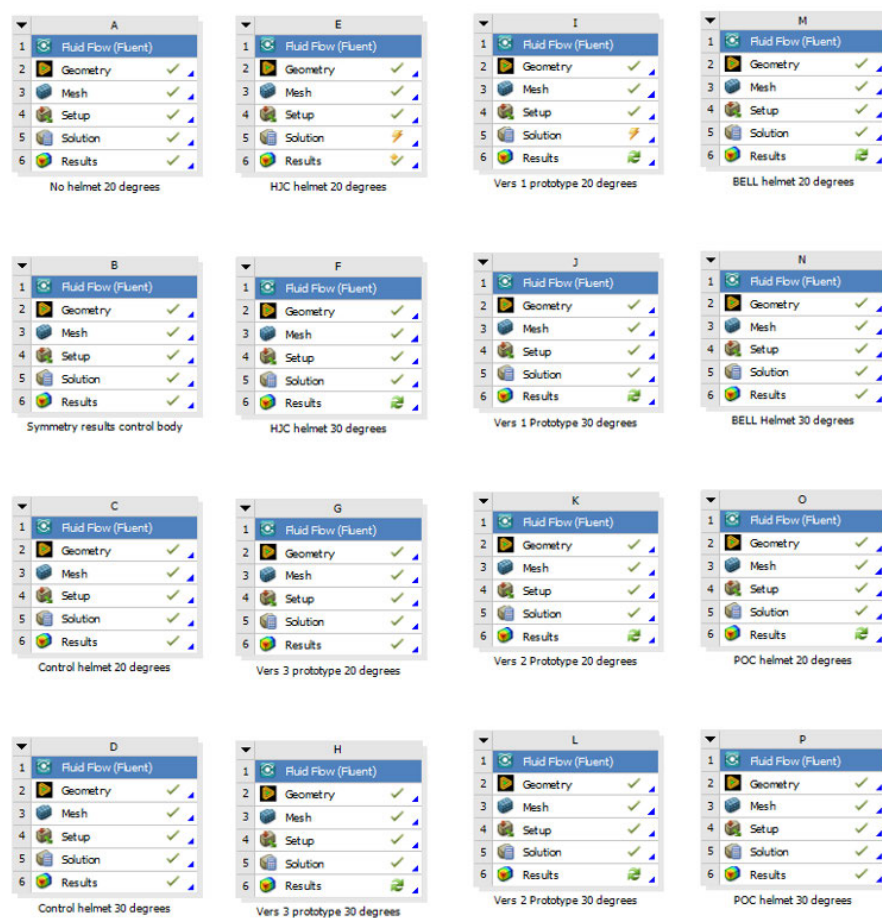


Figure 77 – FLUENT outputs in ANSYS Workspace

3.8 – TT time savings

The TT time savings was built from the formulas listed in Table 2 and derived from the theoretical model in Table 18. For this model, power was assumed to be 400 W for each cyclist and all cyclists are 190 cm and 90 kg. As the bicycle and legs were not included in simulations, it was assumed that the resulting force of their inclusion would be 25 N, which was added to the drag force from the CFD simulations for the helmets. This gave an approximate value which closely matched the total resistive forces for the bicycle and rider identified during the theoretical model. Refer to Table 19, which shows the TT time savings model, and the formulas used within it, which was built using Microsoft Excel.

Table 19 – TT time savings model inputs and formulas

TT Time Savings Formulas				
Description	Term	Formula/Value	Units	Assumption/Input/Result
Helmet Drag Force	R_{CFD}	Result from CFD	N	Input
Rider and bicycle resistive Force	R_D	25	N	Assumption
Total Resistive Forces	R_T	$R_{CFD} + R_D$	N	Result
Cyclist Power	P	400	W	Input
Course Distance	L	40	km	Input
Velocity	v	P/R_T	m/s	Input
Course time	t	$=TEXT(L/V/24, "mm:ss.ss")$	$mm:ss$	Result

*Velocity converted to km/h to calculate course time

3.9 – Risk Assessment

This risk assessment was conducted utilising the safe track portal (Ref: 4719) portal and the risk was deemed as low. The full risk assessment can be seen in Appendix A.

3.10 – Summary

This section included the methodology used to obtain the control model, current design helmets, prototype design and the CFD process through its entirety. During the next section, the results are provided and discussed.

Chapter 4 – Results

4.1 – Chapter Overview

This chapter provides information on all the results obtained from the CFD simulations for the three current designs and the three prototypes at a head angle of 20 and 30 degrees. The main results considered were the steady state simulations, however, the transient results have been considered also to obtain a greater understanding. Results for each helmet at different velocities are also shown. The results are provided in both numerical and visual representations of the simulations. All data has been collected and applied to the theoretical model to obtain the time savings of each helmet.

4.2 – Project Simulation

4.2.1 – 20 degree position

All helmets were tested at a head angle of 20 degrees at a velocity of 13 m/s using a steady state solver. The drag force (N), drag coefficient and frontal area (including rider, m^2) was obtained from the simulations. Refer to Table 20, which shows the percentage improvement and ranking of each helmet to demonstrate their performance against each other.

Table 20 – 20 degree position simulation results

CFD simulations for 20 degree head angle, v = 13 m/s						
Helmet Type	Angle (°)	Drag Force (-N)	Drag Coefficient	Frontal area incl. rider (m^2)	Percentage improvement with control (%)	Rank
None	20	3.5318612	5.766304	0.1246537		
Control	20	3.6883284	6.0217606	0.1426161		
HJC Adwatt	20	3.3940434	5.5412953	0.1332361	8.0	3
BELL Javelin	20	3.5955404	5.87027	0.1341381	2.5	6
POC Tempour	20	3.4648672	5.656926	0.1474832	6.1	4
Vers 1 Prototype	20	3.3299316	5.436623	0.13732076	9.7	2
Vers 2 Prototype	20	3.467814	5.6617372	0.1319908	6.0	5
Vers 3 Prototype	20	3.184581	5.2072786	0.1326649	13.7	1

4.2.2 – 30 degree position

Refer to Table 21, which shows how the process was repeated for all helmets at a head angle of 30 degrees using a steady state solver. Refer to Figure 78, which shows a comparison of the percentage improvement for drag force of all helmets at both angles.

Table 21 – 30 degree position simulation results

CFD simulations for 30 degree head angle, v = 13 m/s						
Helmet Type	Angle (°)	Drag Force (-N)	Drag Coefficient	Frontal area incl. rider (m ²)	Percentage improvement with control (%)	Rank
None	30	3.5912358	5.8632421	0.1267121		
Control	30	4.1048488	6.701794	0.1419186		
HJC Adwatt	30	3.313545	5.4098694	0.1326154	19.3	1
BELL Javelin	30	3.66462	5.9830531	0.1392865	10.7	6
POC Tempour	30	3.6193594	5.9091582	0.1480469	11.8	5
Vers 1 Prototype	30	3.5256653	5.7561882	0.134128	14.1	3
Vers 2 Prototype	30	3.3406666	5.4541495	0.1309996	18.6	2
Vers 3 Prototype	30	3.5942124	5.8681019	0.1332187	12.4	4

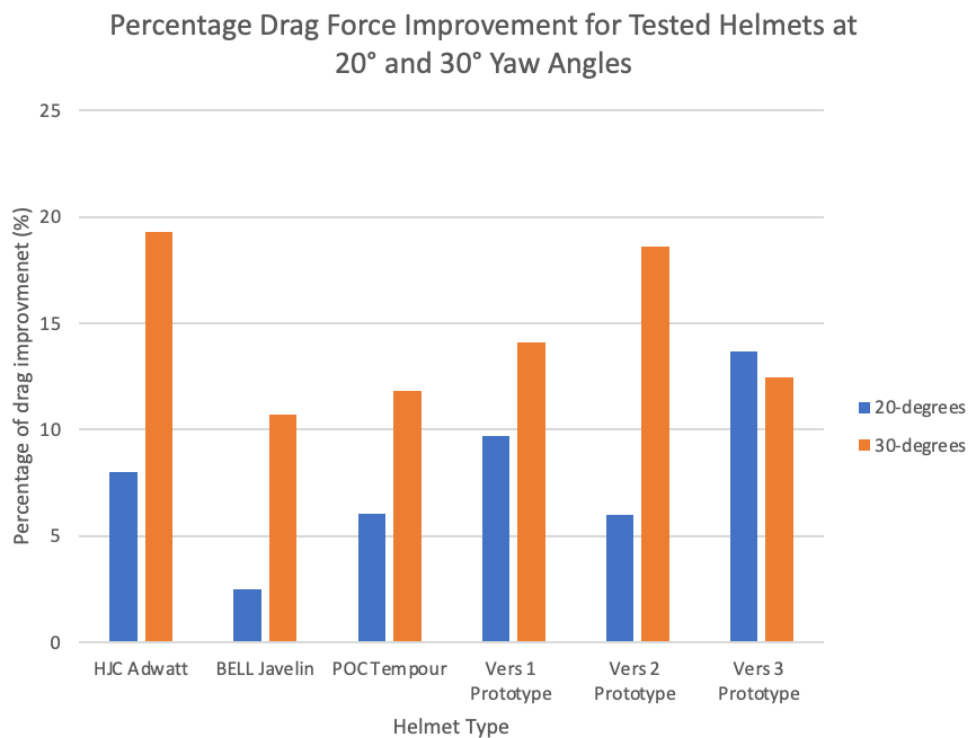


Figure 78 – Percentage Drag Force Improvement for all helmets at both angles

4.2.3 – Changes in Velocity

To determine the behaviour of the helmets as velocity increases, simulations were conducted on the control, version 3 prototype, version 1 prototype and the HJC Adwatt. The simulations were tested at 20 degrees and the velocity range started at 8 m/s and increased by 2, up to 18 m/s. Refer to Figure 79, which shows the performance of each helmet as velocity increases. Refer to Table 22, for a full list of results.

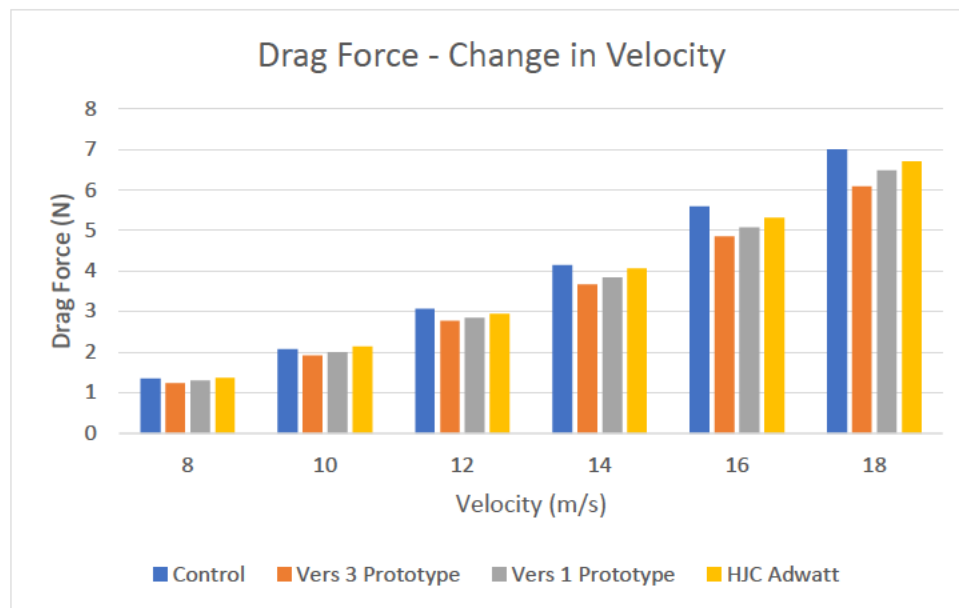


Figure 79 – Graphical comparison of drag force for a range of velocity 8 to 18 m/s of control helmet with top performing helmets

Table 22 – Comparison of drag force for a range of velocity 8 to 18 m/s of control helmet with top performing helmets

Top 3 helmets at 20 degrees different velocities					
Velocity		Drag Force (N)			
km/h	m/s	Control	Vers 3 Prototype	Vers 1 Prototype	HJC Adwatt
28.8	8	1.35	1.25	1.30	1.36
36	10	2.09	1.93	2.01	2.14
43.2	12	3.08	2.77	2.85	2.94
50.4	14	4.15	3.68	3.85	4.08
57.6	16	5.60	4.85	5.08	5.32
64.8	18	7.01	6.09	6.48	6.71

4.2.4 – Visualisations

To demonstrate the difference in performance, visualisations are displayed for the best and worst performing helmet. Refer to Figure 80, which shows the visualisations for the velocity contour. Refer to Figure 81, which shows the visualisations for the velocity streamline. Refer to Figure 82, which shows the visualisations for pressure contour plot. Refer to Table 23 and Table 24, which shows the remaining helmets and their visualisations at each angle respectively.

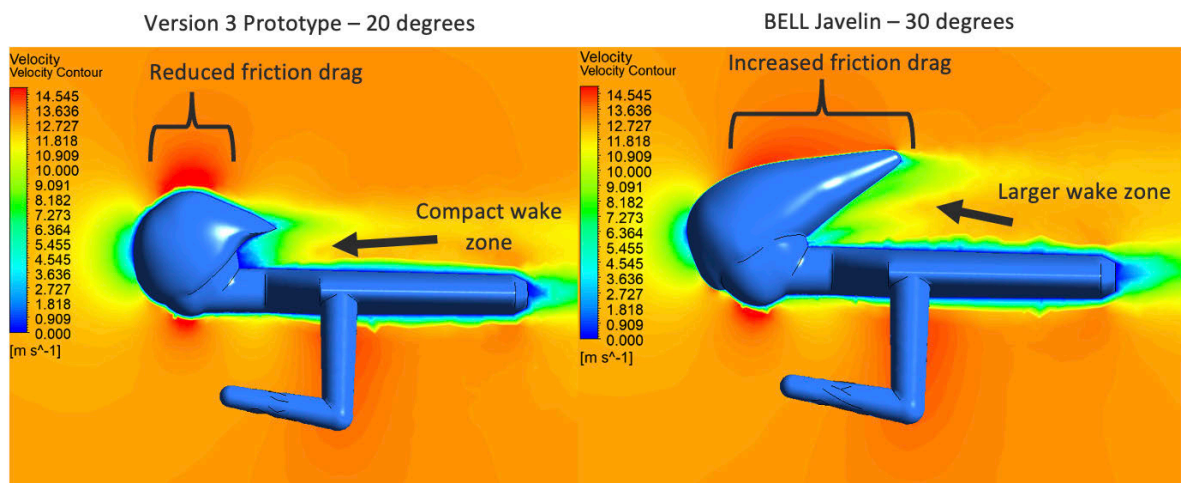


Figure 80 – Velocity contour plot for best and worst performing helmet

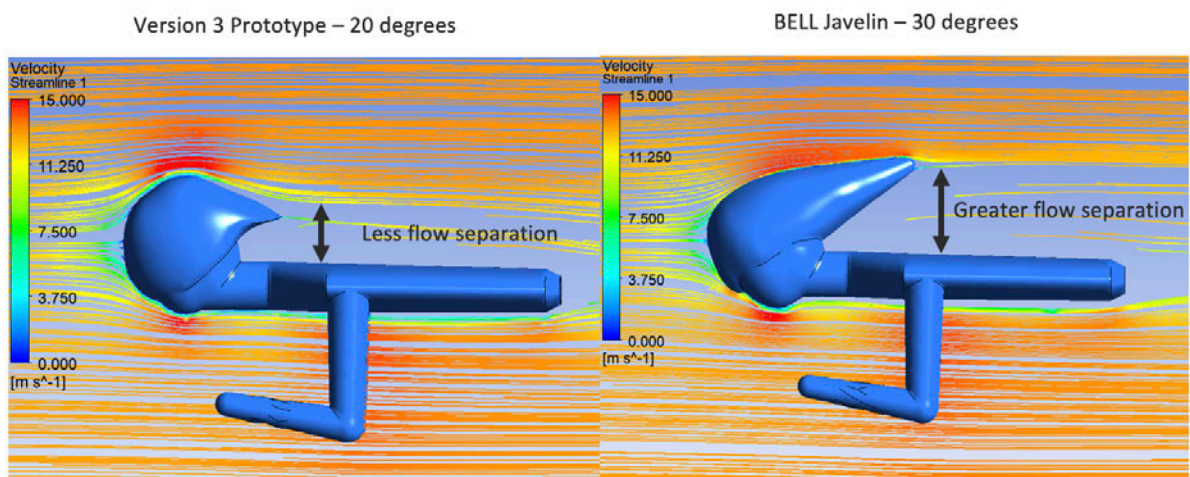


Figure 81 – Velocity streamline plot for best and worst performing helmet

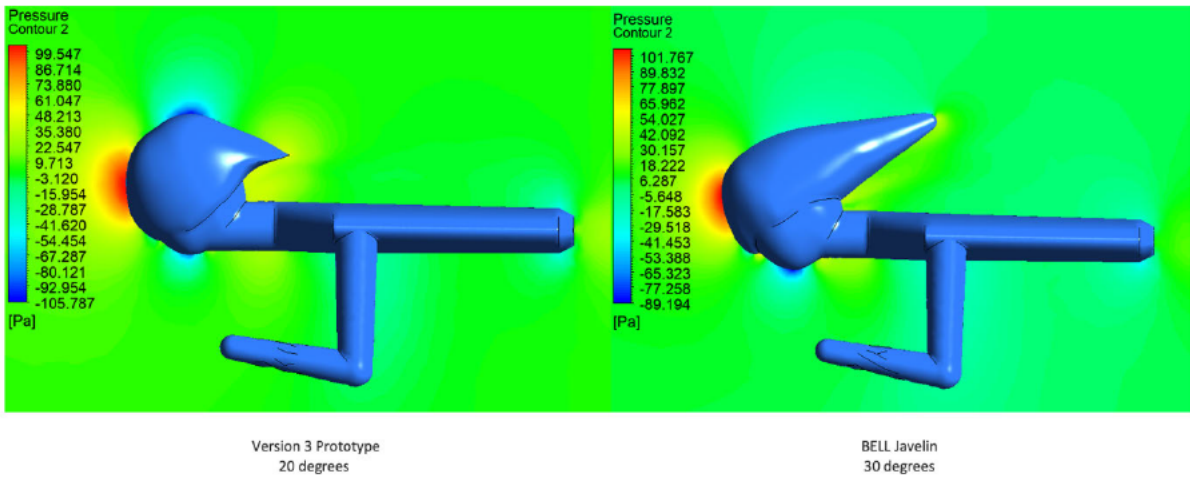
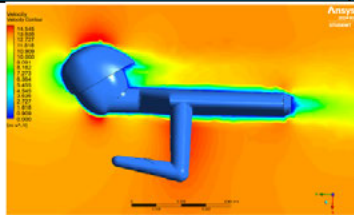

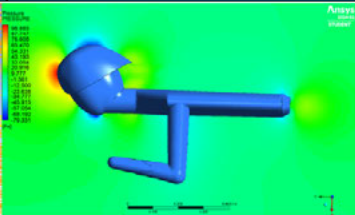
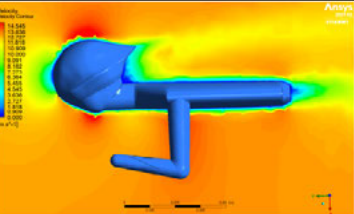

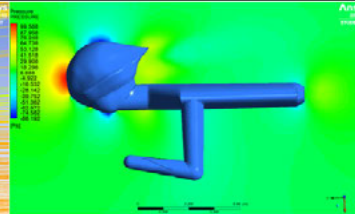
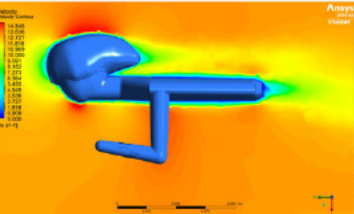
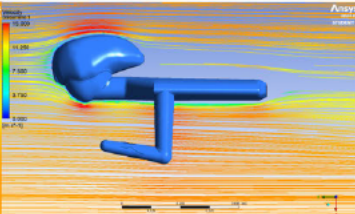
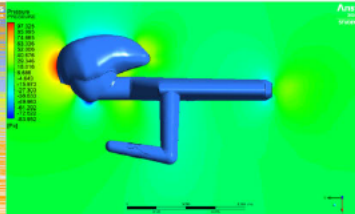
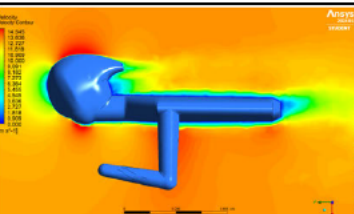
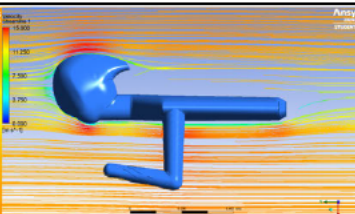
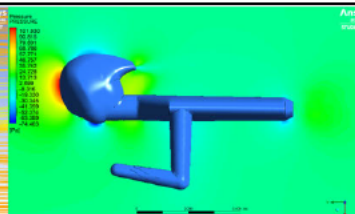


Figure 82 – Pressure contour plot for best and worst performing helmet

Table 23 – Visualisations of remaining helmets at 20 degrees

Helmet	Velocity Contour	Velocity Streamline	Pressure Contour
HJC			
POC			
Vers 1			
Vers 2			

Table 24 – Visualisations of remaining helmets at 30 degrees

Helmet	Velocity Contour	Velocity Streamline	Pressure Contour
HJC			
POC			
Vers 1			
Vers 2			

4.3 – Time Savings Model

Refer to Table 25, which shows the complete TT time savings model which provides drag force, velocity, total time, time gap and the ranking of all helmets when a rider of equal size and output is considered for the use of each over a 40 km TT. Refer to Figure 83, which shows a graphical comparison of all helmets at both angles. The helmets were ranked against each other which included their performance across both head angle positions of 20 and 30 degrees.

Table 25 – Time savings theoretical model

Time savings over 40km TT when P = 400 W								
Angle	Helmet	Helmet Drag Force (N)	Total Resistive Forces (N)	Velocity (m/s)	Velocity (km/h)	Total Time (mm:ss)	Time gap (mm:ss.ss)	Rank
20°	Vers 3 Prototype	3.18	28.18	14.19	51.09	46:58.58	-	1
	Vers 1 Prototype	3.33	28.33	14.12	50.83	47:13.13	00:15.15	3
	HJC Adwatt	3.39	28.39	14.09	50.71	47:19.19	00:21.21	5
	POC Tempour	3.46	28.46	14.05	50.59	47:26.26	00:28.28	6
	Vers 2 Prototype	3.47	28.47	14.05	50.58	47:27.27	00:28.28	7
	BELL Javelin	3.60	28.60	13.99	50.36	47:40.40	00:41.41	10
30°	HJC Adwatt	3.31	28.31	14.13	50.86	47:11.11	00:13.13	2
	Vers 2 Prototype	3.34	28.34	14.11	50.81	47:14.14	00:16.16	4
	Vers 1 Prototype	3.53	28.53	14.02	50.48	47:33.33	00:34.34	8
	Vers 3 Prototype	3.59	28.59	13.99	50.36	47:39.39	00:41.41	9
	POC Tempour	3.62	28.62	13.98	50.32	47:42.42	00:43.43	11
	BELL Javelin	3.66	28.66	13.95	50.24	47:46.46	00:48.48	12

TT time savings model, P = 400 W

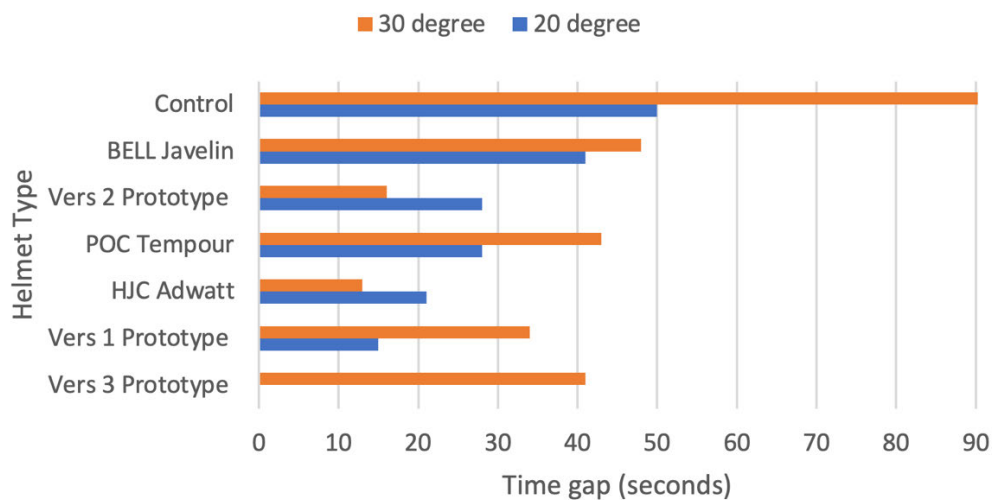


Figure 83 – Graphical comparison of time gap of all helmets at both angles

4.4 – Steady State vs Transient Solver

The main results considered for this project were the steady state simulations, which all the above results were obtained from. Refer to Table 26 and Table 27, which show the results when using a transient solver for all helmets at 20 and 30 degrees. Refer to Figure 84, which shows a graphical comparison of these results.

Table 26 – 20 degree position transient simulation results

CFD transient simulations for 20 degree head angle @ 13 m/s						
Helmet Type	Angle (°)	20 Degrees	Drag Coefficient	Frontal area incl. rider (m ²)	Percentage Drag Force Improvement Compared to Control	Rank
None	20	3.153921	5.1492589	0.1246537		
Control	20	3.7340113	6.096345	0.1426161		
HJC Adwatt	20	3.5010062	5.7159285	0.1332361	6.2	3
BELL Javelin	20	3.5476586	5.7920957	0.1341381	5.0	5
POC Tempour	20	3.5341362	5.7700183	0.1474832	5.4	4
Vers 1 Prototype	20	3.4192733	5.5824871	0.13732076	8.4	2
Vers 2 Prototype	20	3.6318554	5.9295598	0.1319908	2.7	6
Vers 3 Prototype	20	3.3218369	5.4234073	0.1326649	11.0	1

Table 27 – 30 degree position transient simulation results

CFD transient simulations for 30 degree head angle @ 13 m/s						
Helmet Type	Angle (°)	30 Degrees	Drag Coefficient (-)	Frontal area incl. rider (m ²)	Percentage Drag Force Improvement Compared to Control	Rank
None	30	3.7778042	6.1678436	0.1267121		
Control	30	4.247676	6.9349813	0.1419186		
HJC Adwatt	30	3.3508974	5.4708529	0.1326154	21.1	2
BELL Javelin	30	3.5316268	5.7659213	0.1392865	16.9	4
POC Tempour	30	3.6534965	5.9648923	0.1480469	14.0	5
Vers 1 Prototype	30	3.4860677	5.691539	0.134128	17.9	3
Vers 2 Prototype	30	3.347058	5.4645845	0.1309996	21.2	1
Vers 3 Prototype	30	3.6718756	5.9948989	0.1332187	13.6	6

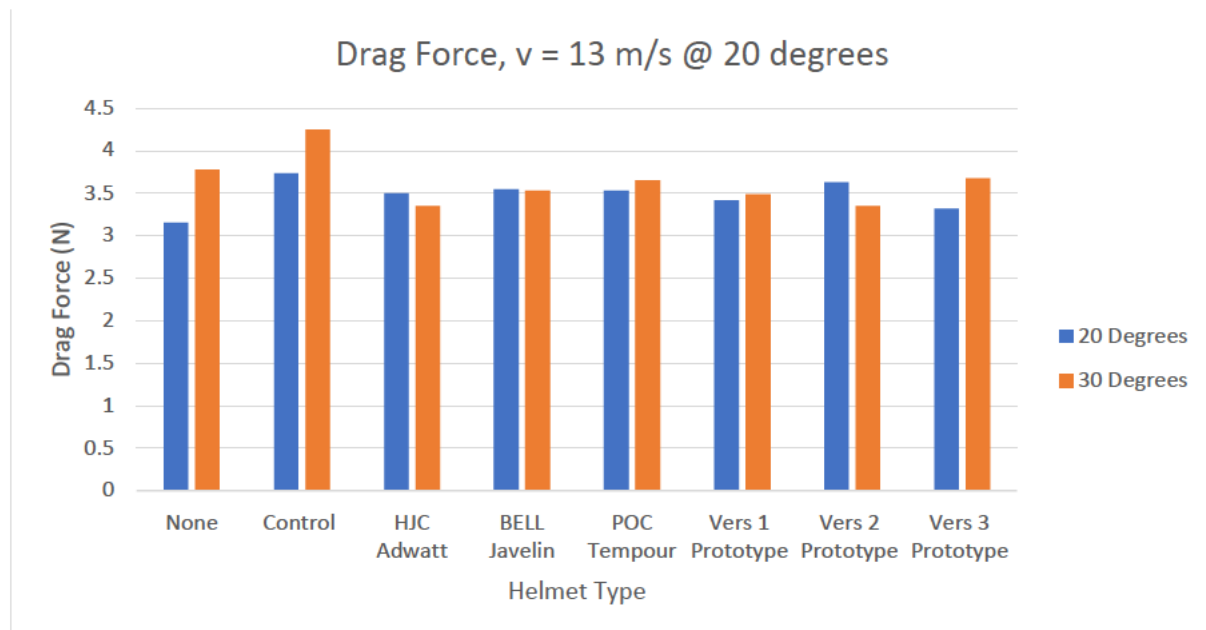


Figure 84 – Graphical representation of transient results for both angles

4.5 – Chapter Summary

This chapter has provided all the results that were obtained from the simulations and the subsequent application to the time savings model. The results are discussed further in the next section of the report.

Chapter 5 – Discussion

5.1 – Chapter Overview

This chapter will provide discussion on all results which will include the best and worst performing helmet, the application of the results to the time savings model, changes in head angle, performance of remaining helmets and the comparison of steady state with transient simulations.

5.2 – Results Analysis

The best and worst performing helmets were assessed by their drag force value, regardless of head angle. The percentage improvements and rankings were made relative to each group of helmets under their respective head angles.

5.2.1 – Best Performing helmet

Overall, the best performing helmet was the version 3 prototype at a head angle of 20 degrees with a drag force of 3.184581 N. This helmet showed a 13.7% improvement when compared with the control helmet and an 11.2% improvement when compared to the worst performing helmet at 20 degrees. Refer to Figure 85, where the velocity contour and streamline visualisations of this helmet have been combined for ease of reading.

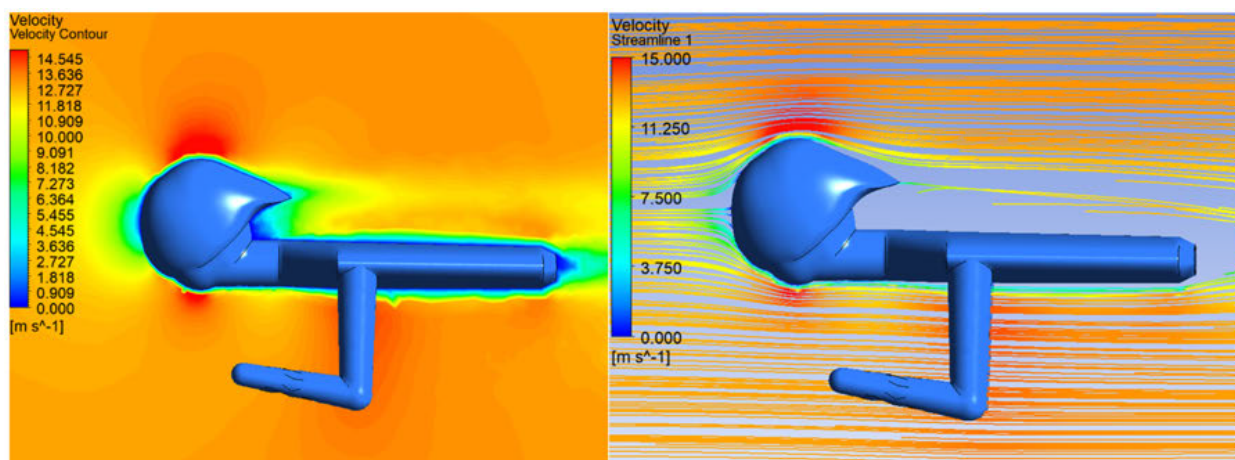


Figure 85 – Version 3 prototype visualisations

An analysis of the CFD visualisations and the design itself indicate the following:

- Velocity contour: Due to the shorter tail of this helmet design, friction drag is reduced when compared to the BELL Javelin, therefore reducing the overall drag force of the design. Although the wake zone behind the helmet showed a lower velocity, it is compact in comparison, therefore, enhancing the overall performance of the helmet.
- Velocity streamline: Observation indicated streamlines remain close to the surface of the helmet which indicates minimal flow separation. This provides an enhanced performance for this helmet as it reduces the low pressure area behind the cyclist which causes an increase in drag. Furthermore, reduced turbulence can be observed around the helmet as there is minimal disruptive flow patterns.

5.2.2 – Worst Performing helmet

The worst performing helmet was the BELL Javelin at a head angle of 30 degrees with a drag force of 3.66462 N. This helmet showed the lowest improvement when compared to the control at 30 degrees of 10.7% which was 8.6% less efficient than the top performing helmet at 30 degrees. Refer to Figure 86, where the velocity contour and streamline visualisations of this helmet have been combined for ease of reading.

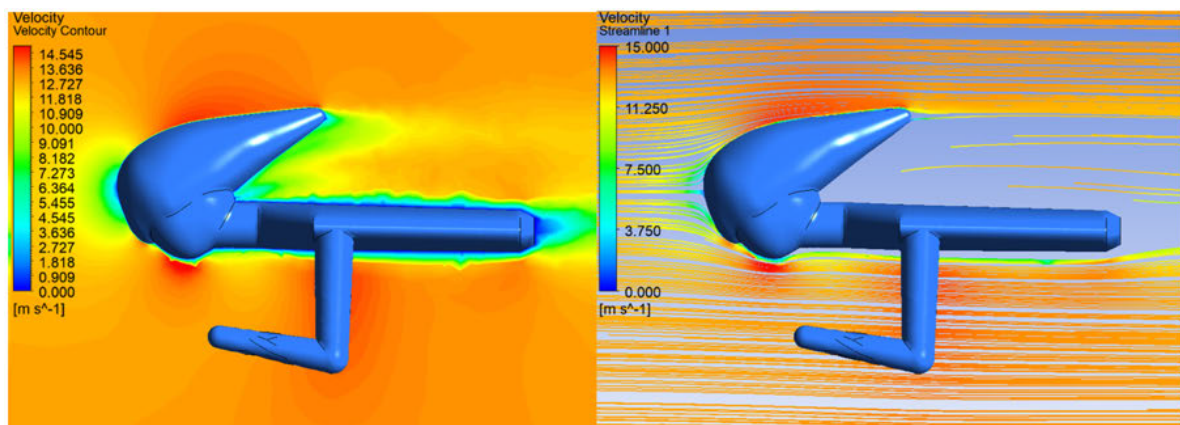


Figure 86 – BELL Javelin visualisations

An analysis of the CFD visualisations and the design itself indicate the following:

- **Velocity contour:** Due to the longer tail of this helmet when compared to the version 3 prototype, it has increased friction drag. Furthermore, drag force is increased due to the large wake zone despite the wake velocity not being as low as the best helmet. Large areas of flow deceleration can be observed over the face of the helmet, which indicated a greater disruption to airflow resulting in an increase in aerodynamic resistance.
- **Velocity streamline:** The tail of the helmet displays early flow separation and a larger wake, which results in a larger low pressure area behind the cyclist. This causes drag force to be increased significantly, to which an increase in the head angle would be a contributing factor of. Furthermore, the increase of turbulence behind the helmet due to the large flow separation contributes to a larger eddy formation.

5.2.3 – Remaining helmets performance

Whilst the focus of the research was finding an optimal design that offered a lower value of C_{dA} than its commercially available competitors, the visualisations offer great insight into how each shape and design impact the aerodynamic efficiency of the helmet. Refer to Figure 87, which shows how the difference in flow separation between each design is quite significant.

The HJC performs consistently through both angles with flow separation minimised which would result in less drag. The POC helmet performs poorly due to a large flow separation. It appears that shifting the head position or adjusting the way the helmet is worn could facilitate significant improvements to its results. However, at the tested angles in this project it results in an inefficient design.

The version 1 prototype performs consistently across both angles and even with its large bulbous design, minimises flow separation resulting in less drag. The version 2 prototype indicates that a longer tail would assist in reducing the flow separation which resulted in an improved aerodynamic efficiency.

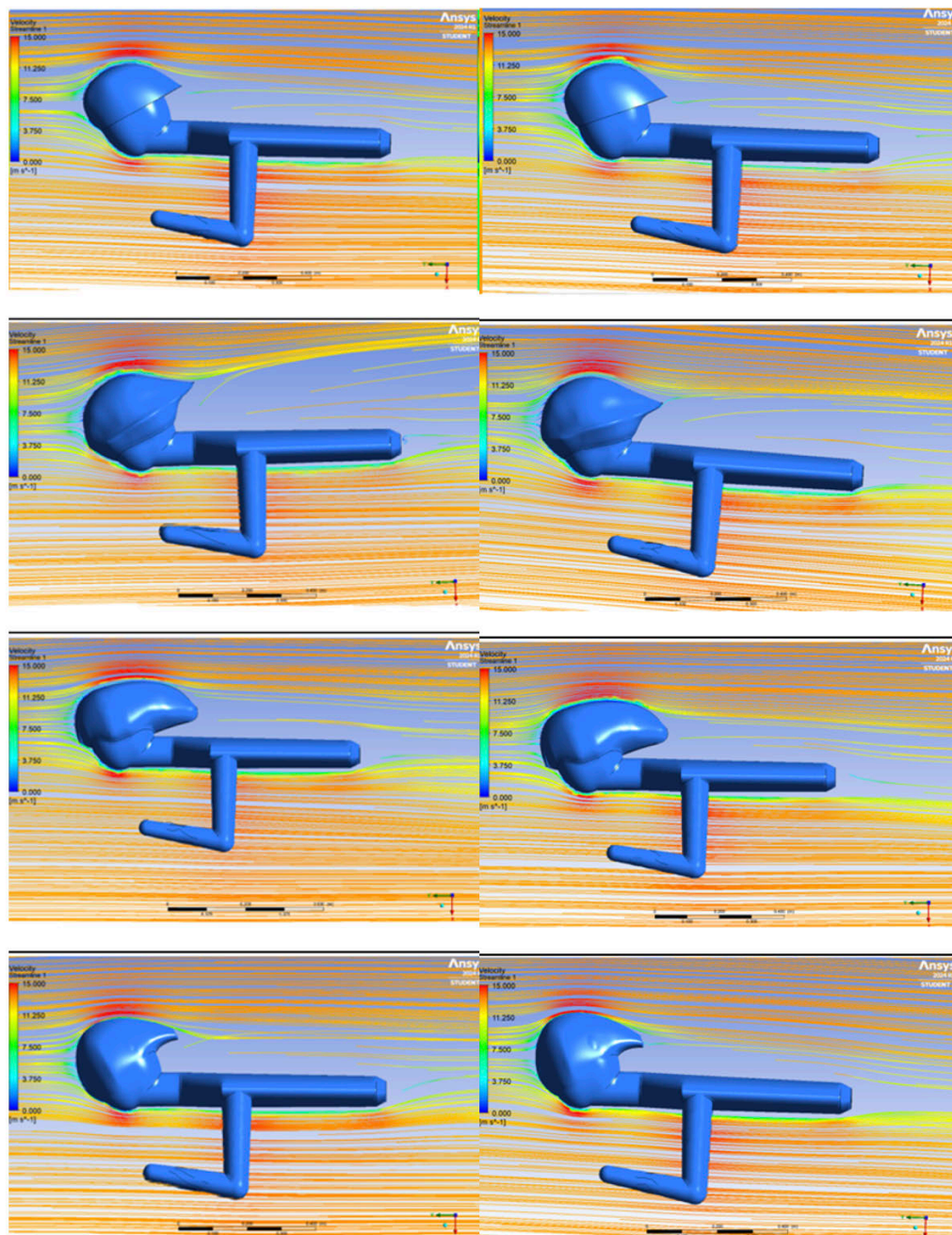
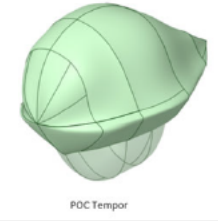
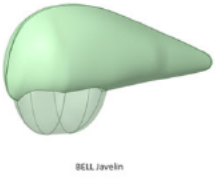
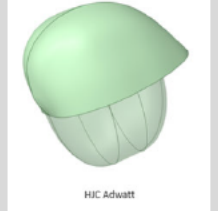
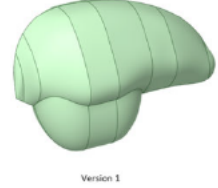

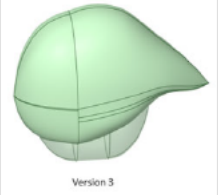


Figure 87 – Velocity streamline or remaining helmets at 20 (left) and 30 degrees (right)

5.2.4 – Optimal helmet shape designs

From observation of the results for both the replica helmets and the prototypes certain characteristics were highlighted. Refer to Table 28, which discusses how shapes suggest certain aerodynamic performance and flow behaviour.

Table 28 – Helmet shape designs and their characteristics

Helmet	Design Feature	Aerodynamic Characteristics
 <p>POC Tempor</p>	<ul style="list-style-type: none"> - Elongated rear section - Wide surface area 	<ul style="list-style-type: none"> - Streamlines air flow well when rider position is rigid and consistent - May perform poorly in cross winds
 <p>BELL Javelin</p>	<ul style="list-style-type: none"> - Tear drop design - Small frontal area 	<ul style="list-style-type: none"> - May perform well if there is minimal gap between tail and rider - Would perform poorly in cross wind - Changes in head position impact results
 <p>HJC Advant</p>	<ul style="list-style-type: none"> - Minimalist design - Aggressive tail 	<ul style="list-style-type: none"> - Would perform consistently in a range of wind conditions - Performs consistently in different head angles
 <p>Version 1</p>	<ul style="list-style-type: none"> - Rounded shape - Large volume - Blunt tail 	<ul style="list-style-type: none"> - Large volume may assist air dispersion - The flat tail may cause drag pockets - Would perform poorly in cross winds
 <p>Version 2</p>	<ul style="list-style-type: none"> - Sharp tail leading to flat end - Smooth shapes transition to riders face 	<ul style="list-style-type: none"> - Smaller design allows for consistency in performance of different wind conditions
 <p>Version 3</p>	<ul style="list-style-type: none"> - Streamlined profile - Sharp Tail - Uniformly smooth 	<ul style="list-style-type: none"> - Minimal disruption to airflow - Changes in head angle impact results

5.2.5 – Time savings results

The application of the above results into the TT time savings model provide context for how much of an impact the helmet can make in a TT. The results indicate that the best performing helmet, version 3 prototype (20 degrees), would complete the 40 km TT in a time of 46 min and 58.58 sec. The worst performing helmet, BELL Javelin (30 degrees), would complete the 40 km TT in a total time of 47 min and 46.46 sec with a time gap to the lead helmet of 48.48 sec.

Whilst this model was built using theoretical calculations and many assumptions and simplifications have been made, it highlights the importance of an optimally designed TT helmet. Some points for consideration for the accuracy of results from this model include:

- Rider position: Positions will change drastically depending on factors which include, fatigue, cornering, terrain, or wind behaviour.
- Rider power output: Power output will change constantly due to factors such as adrenaline, gradient of the road, cornering, or external encouragement from team directors.
- Change of drag: The value for drag would be subject to change due to the movement of the cyclists legs as this model considered a uniform value for drag throughout the TT.

5.2.6 – Change in head angle

The change in head angle and the resulting values of drag highlight some interesting results for each helmet. The overall best performing helmet, when tested at 30 degrees, becomes the 9th ranked helmet overall with a time gap of 41.41 sec. In a real world setting, the top performing version 3 prototype may not perform optimally when compared to some of the other designs which offer greater consistency of optimal drag values when head angle is changed throughout the test.

This research and testing indicated that HJC Adwatt is the best performing helmet across different positions when compared to the subjects used in this project. It was ranked 5th at 20 degrees and 2nd at 30 degrees. Also performing consistently, the version 1 prototype ranked 3rd at 20 degrees and 8th at 30 degrees. The variance in results for each angle have contributed

significant foundation to the need for further work and research in this area which will be expanded on in the next section.

5.2.7 – Change in velocity

The results from the testing at different velocities as seen in Table 22 and Figure 79 show that the version 3 prototype remains consistent as the top performer as velocity increases. It can be observed that the aerodynamic advantages of this helmet become more noticeable at higher speeds. As velocity reaches 18 m/s, the difference in drag force compared to the control is 0.92 N which has a significant impact to aerodynamic efficiency with an improvement of 13.12%.

The overall behaviour of the helmets with respect to an increase in velocity shows a nonlinear trend. This is particularly evident in the increase from 16 to 18 m/s, which is attributed to the relationship between drag force and speed as drag force is proportional to the square of speed.

5.2.8 – UCI Design Compliance

Each prototype design was created with the UCI helmet template as seen in Figure 46 as the defining limitations for size. Therefore, each helmet was compliant in accordance with those dimensions. Refer to Figure 88, Figure 89 and Figure 90, which shows the dimensions for all three prototype helmets respectively.

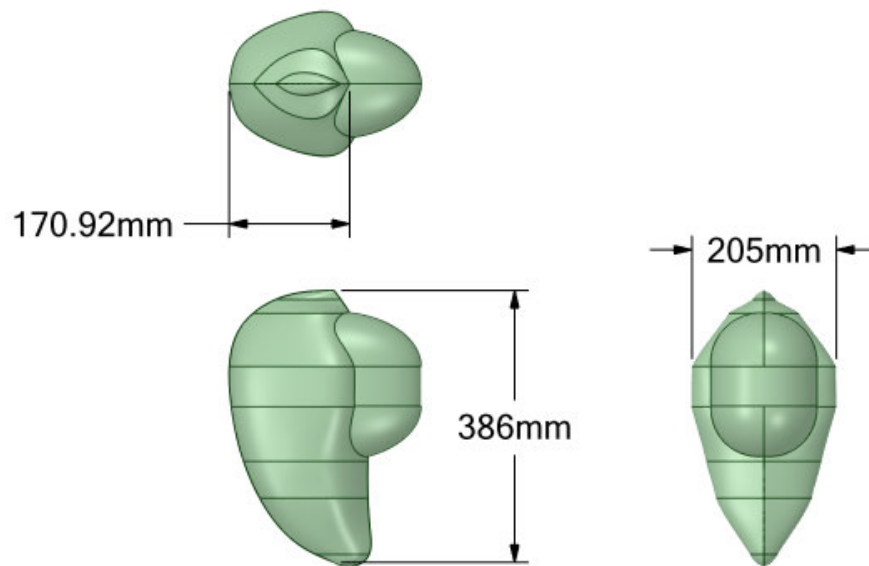


Figure 88 – Version 1 prototype helmet dimensions

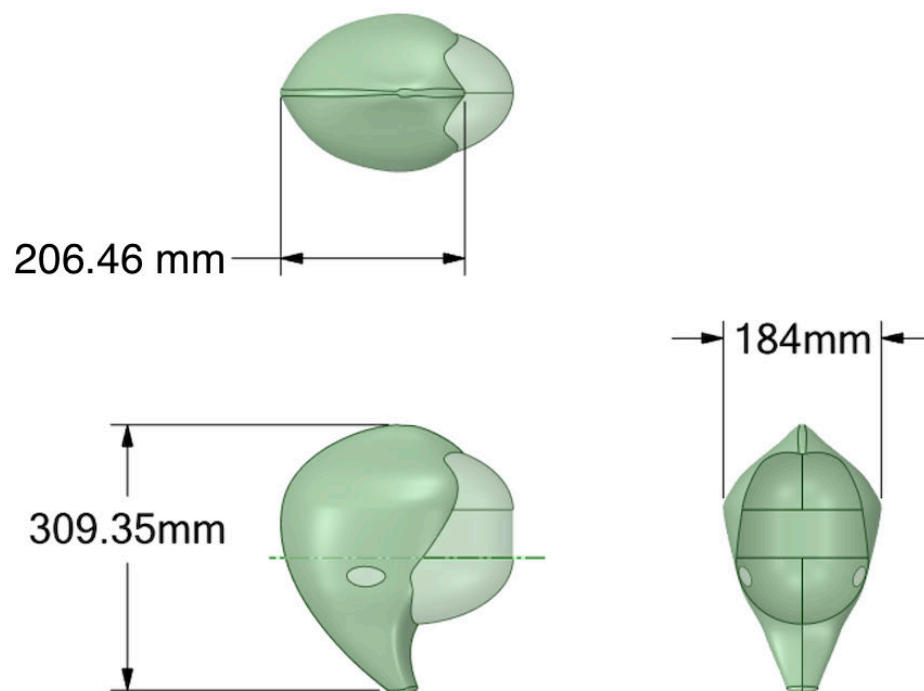


Figure 89 – Version 2 prototype helmet dimensions

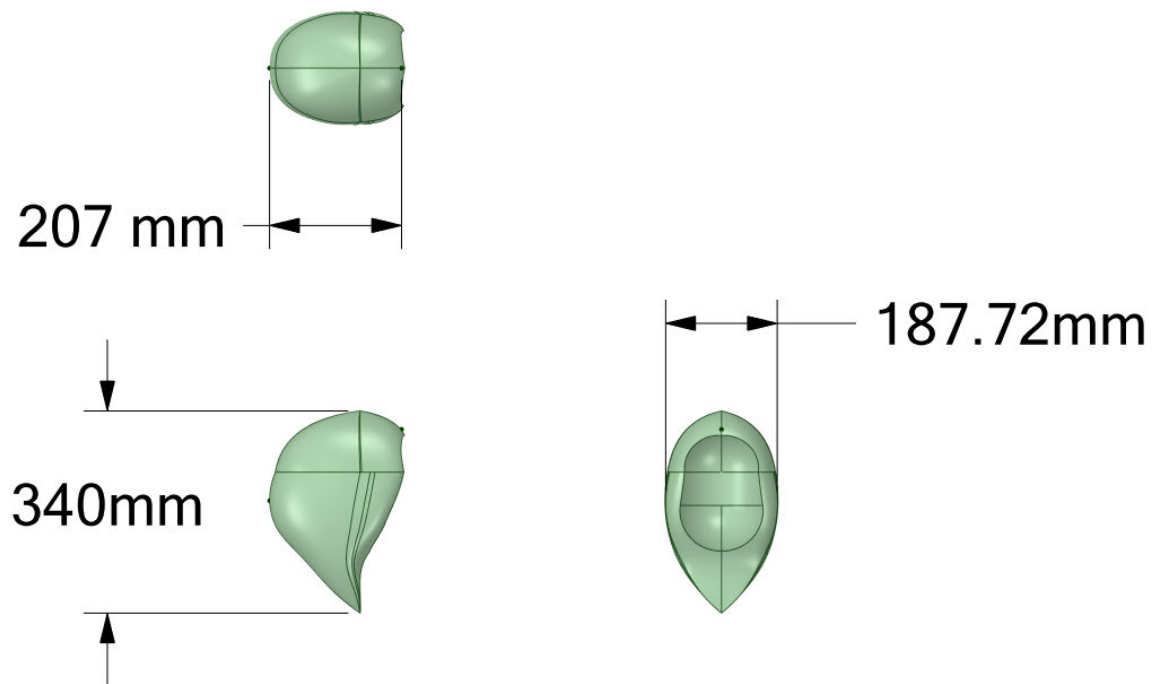


Figure 90 – Version 3 prototype helmet dimensions

5.2.9 – Average of Results

To provide some values to suggest the best all round performing helmet, the average of results at each head angle was calculated. Refer to Table 29, which shows the calculated average values of each helmet and ranks their performance. These are compared to the average results of the control helmet. Refer to Figure 91, which shows a graphical comparison of the average results.

Table 29 – Calculated average of results from both head angles showing performance consistency

Average of all helmets at both angles @ 13 m/s						
Helmet Type	Angle (°)	Drag Force (-N)	Drag Coefficient (-)	Frontal area incl. rider (m ²)	Percentage improvement with control (%)	Rank
None	30	3.5615485	5.81477305	0.1256829		
Control	30	3.8965886	6.3617773	0.14226735		
HJC Adwatt	30	3.3537942	5.47558235	0.13292575	13.9	1
BELL Javelin	30	3.6300802	5.92666155	0.1367123	6.8	6
POC Tempour	30	3.5421133	5.7830421	0.14776505	9.1	5
Vers 1 Prototype	30	3.42779845	5.5964056	0.13572438	12.0	4
Vers 2 Prototype	30	3.4042403	5.55794335	0.1314952	12.6	3
Vers 3 Prototype	30	3.3893967	5.53769025	0.1329418	13.0	2

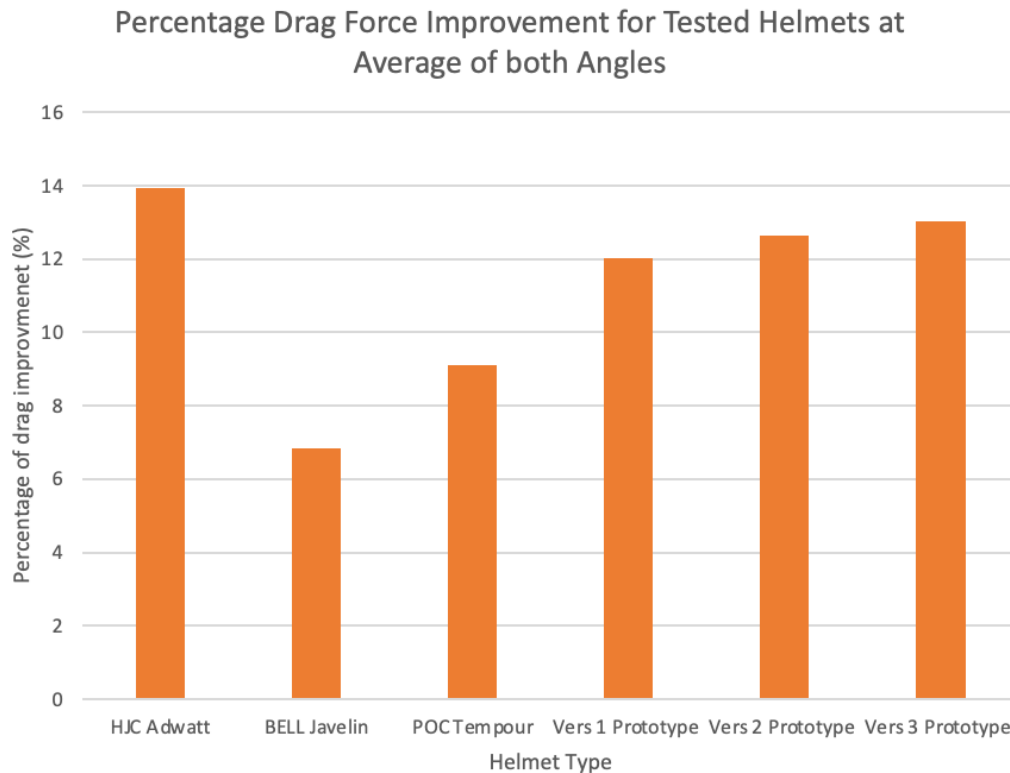


Figure 91 – Percentage drag force improvement of the average performance of all helmets through both angles

5.2.10 – Transient Result Comparison

Refer to Table 30, which provides a data analysis of the difference in results of steady state vs transient at both angles for drag force and the percentage improvement compared to control at 20 degrees. Refer to Figure 92, which shows a graphical comparison of drag force at 20 degrees. Refer to Figure 93, which shows a graphical comparison of the percentage improvement when compared to the control at 20 degrees. These results indicated that the version 3 prototype remains the optimal design overall, however, its percentage improvement was reduced. Furthermore, the results indicated that the BELL Javelin is not the worst helmet at 20 degrees and instead was replaced by the version 2 prototype.

Table 30 – Steady vs transient result comparison at 20-degrees

Steady State vs transient @ 20 Degrees, V=13 m/s						
Helmet Type	Angle (°)	Drag Force (N)		% Improvement		Rank
		Steady state	Transient	Steady state	Transient	
HJC Adwatt	20	3.3940434	3.5010062	8.0	6.2	3
BELL Javelin	20	3.5955404	3.5476586	2.5	5.0	5
POC Tempour	20	3.4648672	3.5341362	6.1	5.4	4
Vers 1 Prototype	20	3.3299316	3.4192733	9.7	8.4	2
Vers 2 Prototype	20	3.467814	3.6318554	6.0	2.7	6
Vers 3 Prototype	20	3.184581	3.3218369	13.7	11.0	1

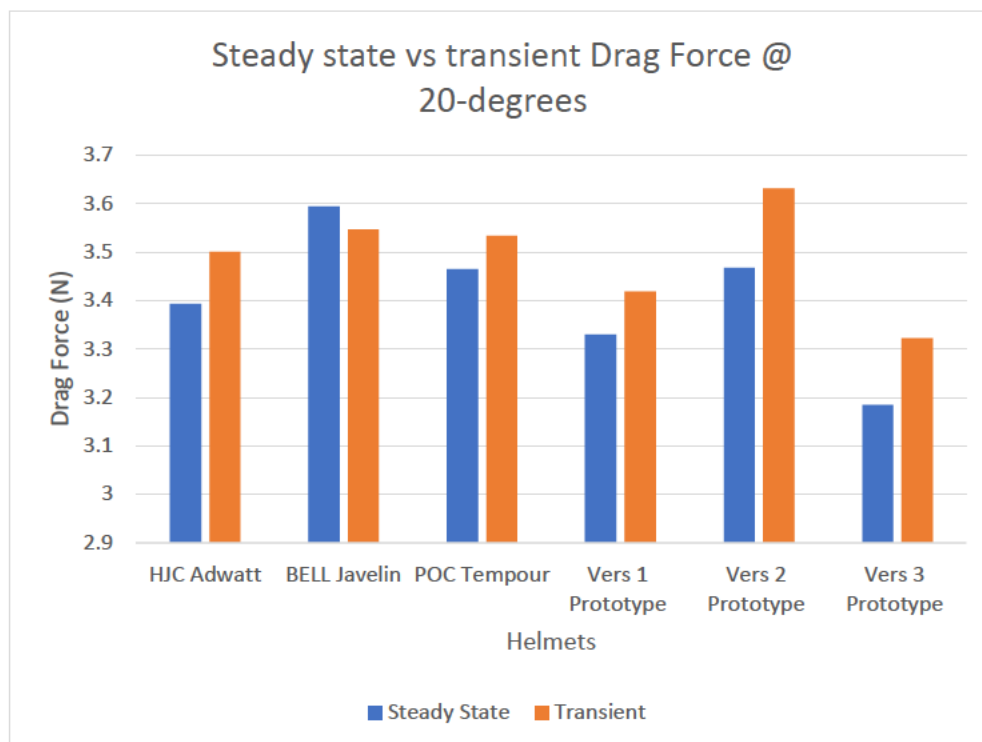


Figure 92 – Steady vs transient drag force result graphical comparison at 20-degrees

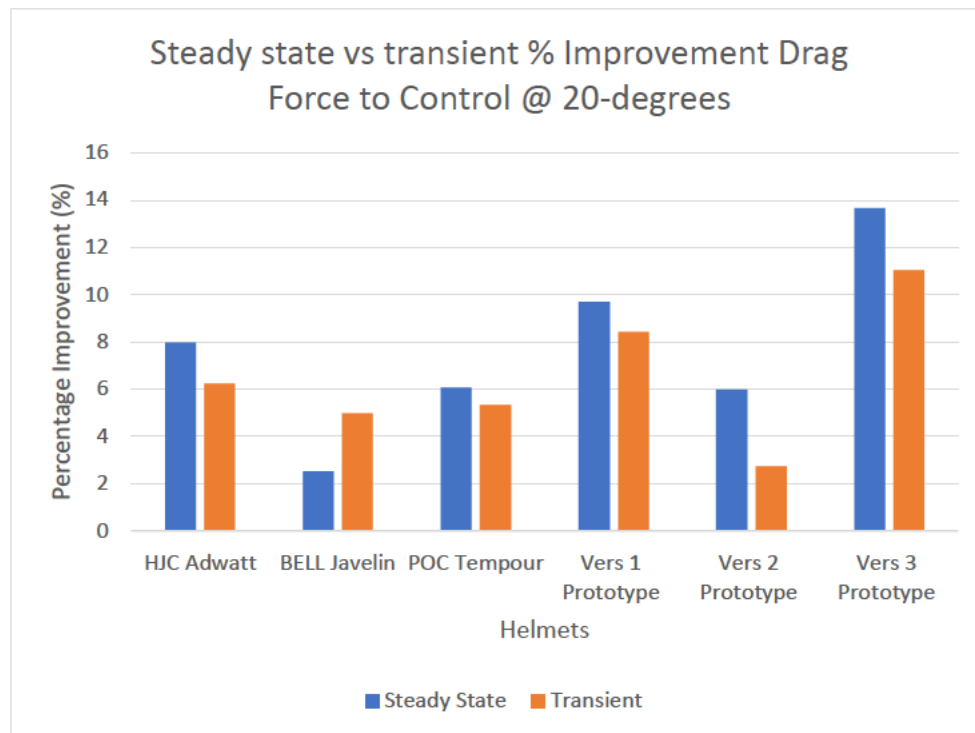


Figure 93 – Steady vs transient percentage improvement graphical comparison at 20-degrees

Refer to Table 31, which provides a data analysis of the difference in results of steady state vs transient at both angles for drag force and percentage improvement compared to control at 30 degrees. Refer to Figure 94, which shows a graphical comparison of drag force at 30 degrees. Refer to Figure 95, which shows a graphical comparison of the percentage improvement when compared to the control at 30 degrees. These results showed a drastic change with the version 3 prototype performing the worst. The BELL Javelin helmet still performed poorly; however, it performed better than the POC Tempour also. The choice of solver can be largely attributed to geometry and available computational resources. These findings contributed to the conclusion.

Table 31 – Steady vs transient result comparison at 30-degrees

Steady State vs transient @ 30 Degrees, V=13 m/s						
Helmet Type	Angle (°)	Drag Force (N)		% Improvement		Rank
		Steady state	Transient	Steady state	Transient	
HJC Adwatt	20	3.313545	3.3508974	19.3	21.1	2
BELL Javelin	20	3.66462	3.5316268	10.7	16.9	4
POC Tempour	20	3.6193594	3.6534965	11.8	14.0	5
Vers 1 Prototype	20	3.5256653	3.4860677	14.1	17.9	3
Vers 2 Prototype	20	3.3406666	3.347058	18.6	21.2	1
Vers 3 Prototype	20	3.5942124	3.6718756	12.4	13.6	6

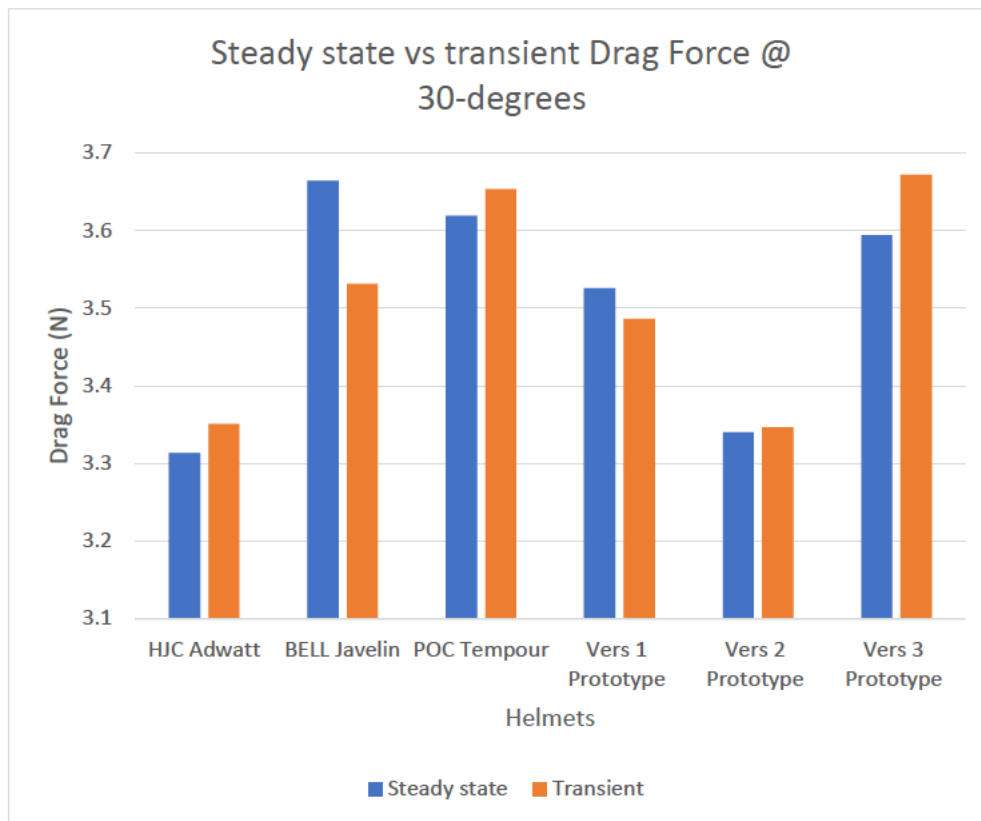


Figure 94 – Steady vs transient drag force result graphical comparison at 30-degrees

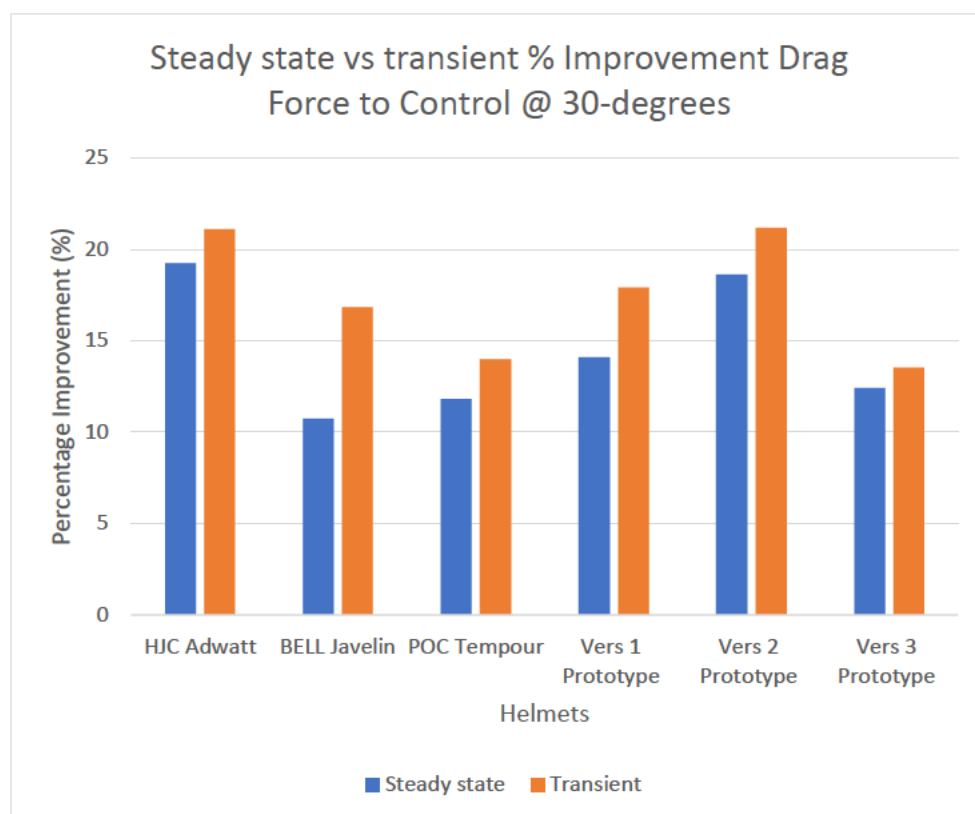


Figure 95 – Steady vs transient percentage improvement graphical comparison at 30-degrees

5.3 – Chapter Summary

This chapter provided discussion of the results that were presented during Chapter 4. This built the foundation for the conclusion, limitations to this research and the further work required in this area of research.

Chapter 6 – Conclusion and Further Work

6.1 – Conclusion

The results of the research identified four main components that contributed to the conclusion which are listed below:

1. Helmet performance is directly related to rider position, regardless of size or shape of the helmet.
2. For future design and work in this topic, it would be recommended to utilise transient simulations. This would be largely dependent on the computational resources available.
3. Helmet design is and should be terrain dependent. Having a helmet that performs well in a perfect aerodynamic position on a flat stage would not be optimal for a TT stage that consists of lots of undulating terrain or climbing.
4. To counteract the change in position from the rider during a race, there is need for further testing and research into viable technology. Currently technology exists that allows the rider to get a live value for their C_{dA} , however, it does not provide any form of direction to address that. A method proposed is sensors in the helmet which provide prompts to the rider on how and where to adjust their position to so they can maintain optimal aerodynamic efficiency.

6.2 – Performance Analysis

The improvement to road cycling performance in design through aerodynamics using CFD was achieved using ANSYS Fluent. The model utilised a velocity inlet of 13 m/s in which three commercially available replica helmets and three prototype design helmets were tested at head angles of 20 and 30 degrees. Initially the project specification and work plan provided prior to commencing this research was aimed to obtain the most optimal performing helmet which research indicated was the HJC Adwatt. However, in the early stages of the literature review it became clear that it would be impossible to compare results from any research without having their exact model for the helmet and what they used for a cyclist model. A decision was made early to adopt the plan listed above.

Section 1.4 – Research Goals details the objectives and expected outcomes of this research and a summary of them and how they were achieved has been listed below.

Conduct literature review to build a theoretical model for cycling aerodynamics to determine helmet performance. An extensive literature review was conducted which highlighted many elements to consider for carrying out research and testing in this area for this type or problem. From this it was determined that the CFD simulations would obtain frontal area, drag force and drag coefficient. There would be a need for an enclosure and wake with appropriate dimensions. A suitable riding position was selected for the rider and an understanding of cyclist power was established. The difference in helmet designs was established and anthropometric data was identified to obtain average sizes of professional cyclists. The available turbulence models were identified, and the most suitable model was selected within the context of this level of project. The Australian standard for helmet design was identified and the UCI regulations were defined for design later in the process. All governing equations for this problem were established and a theoretical model was created. The theoretical model facilitated an understanding of the performance of helmets at different dimensions and angles which set a starting point for the CFD simulations. From the theoretical model, a TT time savings model was created to determine the performance of each helmet against each other which would provide their velocity and time savings.

Design a basic control helmet to compare all tests to. Prior to designing a control helmet, a cyclist was created in the form of a blank torso, arms and head, which was based off a larger male cyclist. Prior to simulations, the enclosure and wake dimensions were set, and a velocity of 13 m/s was selected which is a common average speed of TT races. A basic design control model was created and tested to set a reference point for all other simulations. This was achieved by performing some initial simulations to confirm the operation of ANSYS and the input conditions. It was determined at this point that a head angle of 20 and 30 degrees would be tested to provide a greater understanding of the aerodynamic behaviour of each helmet.

Obtain 3 commercially available designs for testing. The literature review provided no credible sources for helmet performance so three popular designs, each unique in their shape and design were selected. The three different commercially available designs selected were the HJC Adwatt, POC Tempor and BELL Javelin. They were replicated using ANSYS Spaceclaim as accurately as possible. Once each was created and simulated, the results were tabulated to set the criteria for future prototypes to be compared to.

Design a prototype helmet which performs optimally compared to the control and commercial designs. It took three different prototypes to reach a design that provided a more optimal value of drag force than the replicas. If the research failed to design a helmet that did not offer a more optimal value of drag force, the project would have shifted focus as to why the designs did not perform better than their commercially available counterparts. Excel was used to collate all results and provided an efficient means to ranking performance of each helmet. The top performing helmet was the version 3 prototype at 20 degrees with an improved aerodynamic efficiency of 13.7% compared to the control.

Rank the performance of all helmets in a race scenario of a 40km TT. From the governing cycling aerodynamic equations obtained during the literature review and the results from simulations of each helmet, a TT time savings model was created using Excel. This provided a platform to convert the CFD values into a practical application which would rank each helmet against each other on a 40 km TT when a cyclist of equal power output, size, and conditions is considered.

The results show that the version 3 prototype helmet was the best performing helmet at a head angle of 20 degrees, however, it did not perform optimally at 30 degrees. Furthermore, the consistency of performance over different head angles was not the focus for this research, however, these observations were covered in the results discussion and are further elaborated in this section of the report. Whilst the version 3 prototype performed optimally using either steady state or transient simulations, there are a significant variance in results to consider for future research and work in this area.

6.3 – Further Work

Whilst the results have provided some great insight into this problem, the method has many limitations which will be covered in detail in this section. Furthermore, the results have also identified a large scope of further work required to establish more accurate results of these designs and how to establish a greater understanding of improving aerodynamic performance of TT helmets.

6.3.1 – Commercial Design Replication

An attempt was made to reach out to the manufacturer HJC to share a CAD file of their helmet, but due to privacy and copyright, they did not fulfill the request. The method in which the commercially available helmets were replicated was crude in the context of engineering research. Whilst this allowed for reasonable replications of each design to facilitate subsequent CFD simulations, the dimensions would not be exact. Therefore, it would be dismissive to take these results into consideration as absolute, reliable values. An option to counteract this for further work could be to procure the helmets and use a 3D scanner to obtain a more accurate CAD file. However, this poses its own challenges as it would be a challenge to assign a mesh.

6.3.2 – Human model

As previously mentioned throughout the report, the simulations were done using the same size head, torso and arms which was modelled off a larger-sized male cyclist. The cyclist was in the same position each simulation, in which hands were rested on top of the hoods of the bicycle handlebars. Testing with more positions would provide more data to give a wider range of insight into each helmet.

To continue widening the insight into characteristics of each helmet, it would require simulating with multiple models of both genders and multiple sizes. Furthermore, the addition of legs would have given more realistic results. However, this would require more considerations to different leg positions due to the pedalling motion of the cyclists legs. This model did not include any additional cyclist equipment such as socks, gloves, suit/uniform, all of which can make significant impact to the aerodynamic performance.

6.3.3 – Bicycle model

The addition of a bicycle will drastically change the results for future simulations. However, it was not considered in this project, as the main value desired was the performance of each helmet and how they compare against each other. Refer to Table 32, which shows how the addition of a bicycle and other equipment can drastically impact the aerodynamic performance of the complete system.

Table 32 – Examples of additional considerations for simulating with a full bicycle system

Description	Example		
TT bars	 (Mackinnon, 2021)	 (Sexty, 2024)	 (Look, 2024)
Frame	 (CADEX, 2023)	 (CICLIMATTIO, 2024)	 (Excel Sports, 2018)
Wheels	 (Elite Wheels, 2024)	 (Elite Wheels, 2024)	 (Elite Wheels, 2024)
Equipment	 (Rapha Cycling, 2024)	 (Bikebug, 2024)	 (BSpoke Velo, 2024)

6.3.4 – Simulation refinements

Due to the academic licence that was used for this research as mentioned throughout this report, it puts limitations on the quality of the mesh. For future work, it would require a professional licence and sufficient computational power to facilitate assigning a highly refined mesh. Due to the small differences in drag force for these simulations, the higher quality mesh would provide more accurate results which may give teams the marginal gain advantage over their competitors.

6.3.5 – Non-uniform wind flow

During this research, only uniform wind flow in the opposing direction of the moving cyclist was considered and simulated. Further testing would require complex wind patterns such as cross winds at multiple angles, gusts of wind and tail winds at a minimum. Realistically the cyclist would rarely be riding through perfect wind conditions and selecting a prototype helmet for performance would require considering these conditions and simulating all of them.

6.3.6 – Simulations of cyclist in paceline

Refer to Figure 96, which shows cyclists in a team time trial format which would be an important consideration for future work and subsequent CFD simulations. This consideration would not be as important as the standalone performance of the helmet, however, it would be worthwhile determining performance in this format as it could encourage the development of a team time trial helmet. This design may differ from an individual design as it could perform more optimally in this scenario.



Figure 96 – TTT drafting

6.4 – Further testing

For the current research to move forward to the next stage of design and development, some crucial steps would have to be carried out to ensure performance is consistent throughout the simulated environment into the real world.

6.4.1 – 3D Prototype WT

To assist in determining prototypes that would be suitable in taking them to the next stage of the design, 3D printing could be used at a scaled model size and tested in a small WT. This would facilitate experimental validation of the results obtained in CFD simulations.

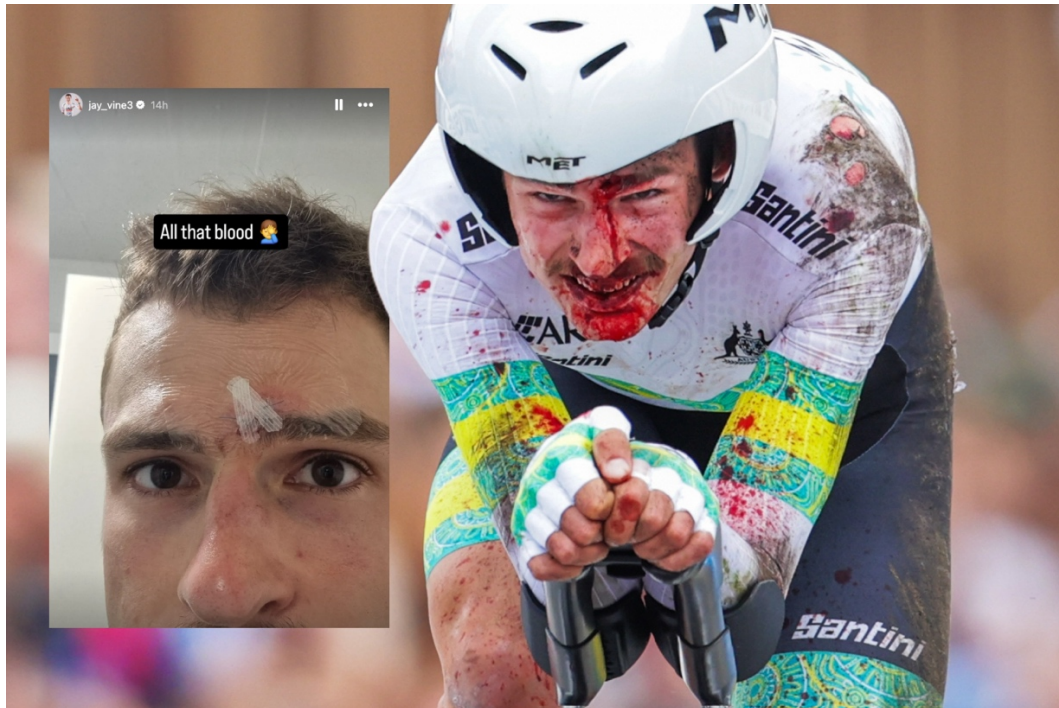
6.4.2 – Human WT

As a full size prototype is developed, it could be first tested in a full size WT with either a full model dummy or human where the safety of the helmet is not yet a concern in the design stage. This would further validate results obtained from the CFD and the scaled model WT testing.

6.4.3 – Strength and safety testing

Prior to any on road testing, the strength and safety testing would have to occur through Finite Element Analysis (FEA). This would involve many complex design considerations, such as determining material properties, structural integrity and how the helmet might perform if a crash occurs. Furthermore, the FEA will facilitate material selection which will ensure sufficient performance under stress conditions such as compression, deformation and impact. This process may influence the shape of the design as a minimum strength and safety standard would have to be adhered to.

Due to the intensity that TT events are raced at, cyclists tend to take more risks and crashes occur frequently. Refer to Figure 97, which shows a recent crash at the UCI World Championship TT. During this race Australian Rider, Jay Vine, took a significant risk which resulted in him crashing and suffering severe lacerations and grazes. Refer to Figure 98, which shows Stefan Kung's crash at the European TT championships which further demonstrated the importance of the strength and safety of TT helmets.



*Figure 97 – Jay Vine's recent TT crash at UCI World Championship
(Davidson, 2024)*



*Figure 98 – Stefan Kung's TT crash at the European Championship
(Cash, 2023)*

6.4.4 – On road testing

Once all the above design stages have been successfully completed, on road testing would have to occur to determine the true behaviour and performance gains of the helmet. This would allow for testing on multiple terrains, wind and heat conditions. For a helmet to successfully pass all stages of design, it would require sufficient on road testing to completely validate all experimental results.

6.4.5 – Helmet designs

This research has highlighted that throughout all the available literature, there is insufficient research and/or data on what types of helmet designs perform optimally. This could largely be attributed to manufacturers keeping their own research on their design private to not provide an advantage or secrets to competitors. As shown by some of the data in this research, utilising a high performing helmet can give a significant advantage to cyclists which can be critical to their success.

References

Alam, F, Chowdhury, H, Wei, HZ, Mustary, I, & Zimmer, G, 2014. *Aerodynamics of ribbed bicycle racing helmets*, *Procedia engineering*, 72, pp. 691-696.

Albornoz, C.P., Soberanis, M.E., Rivera, V.R. and Rivero, M., 2022. Review of atmospheric stability estimations for wind power applications. *Renewable and Sustainable Energy Reviews*, 163, p.112505.

ANSYS, 2010, *Introduction to ANSYS Fluent - Turbulence Modelling*. [online] imechanica.org. Available at: https://imechanica.org/files/fluent_13.0_lecture06-turbulence.pdf [Accessed 5 Oct. 2024].

ANSYS, 2020, *ANSYS Fluent Mosaic Technology Automatically Combines Disparate Meshes with Polyhedral Elements for Fast, Accurate Flow Resolution*. [online] ANSYS. Available at: <https://www.ansys.com/content/dam/resource-center/white-paper/ansys-fluent-mosaic-technology-wp.pdf> [Accessed 5 Oct. 2024].

Arthur, D. 2015, *POC release Tempor Time Trial helmet*, *road.cc*. Available at: <https://road.cc/content/news/62798-poc-release-tempor-time-trial-helmet?page=347> (Accessed: 12 April 2024).

AusCycling, 2020, *AusCycling Technical regulations: General*. Available at: <https://assets.auscycling.org.au/s3fs-public/2020-12/auscycling-technical-regulations-general.pdf> (Accessed: 04 March 2024).

Barry, N, Burton, D, Sheridan, J, Thompson, M & Brown, NA 2015, *Aerodynamic performance and riding posture in road cycling and triathlon*, *Proceedings of the Institution of Mechanical Engineers, Part P: Journal of Sports Engineering and Technology*, vol. 229, no. 1, pp. 28-38.

Bassett Jr, DR, Kyle, CR, Passfield, L, Broker, JP & Burke, ER, 1999, Comparing cycling world hour records, 1967-1996: modeling with empirical data. *Medicine and Science in Sports and Exercise*, 31(11), pp.1665-1676.

Beaumont, F, Taiar, R, Polidori, G, Trenchard, H, & Grappe, F, 2018. Aerodynamic study of time-trial helmets in cycling racing using CFD analysis. *Journal of biomechanics*, 67, pp.1-8.

Bikebug (2024). *XLab Aero TT Cage and Bottle Frame System Black/Black 590mL*. [online] Bikebug. Available at: <https://www.bikebug.com/xlab-aero-tt-cage-and-bottle-frame-system-black-black-590ml.html> [Accessed 1 Oct. 2024].

Blocken, B, Defraeye, T, Koninckx, E, Carmeliet, J, Hespel, P, 2013, CFD simulations of the aerodynamic drag of two drafting cyclists. *Comput. Fluids* 71, 435–445.

Blocken, B, van Druenen, T, Toparlar, Y, Malizia, F, Mannion, P, Andrianne, T, Marchal, T, Maas, GJ, & Diepens, J, 2018. Aerodynamic drag in cycling pelotons: New insights by CFD simulation and WT testing. *Journal of Wind Engineering and Industrial Aerodynamics*, 179, pp.319-337.

Brett, M, 2023, *Check out Remco Evenepoel's Specialized S-Works Shiv TT*. [online] road.cc. Available at: <https://road.cc/content/feature/check-out-remco-evenepoels-specialized-s-works-shiv-tt-301129> [Accessed 2 Oct. 2024].

BSpoke Velo, 2024, *76 Projects - TT Mount 3.0 - Modular Cycling Computer Mount NEW*. [online] Bspoke Velo. Available at: <https://bspokevelo.com.au/products/copy-of-76-projects-tt-mount-2-0-modular-computer-mount> [Accessed 1 Oct. 2024].

CADEX, 2023, *CADEX Tri Frameset*. [online] CADEX. Available at: <https://www.cadex-cycling.com/au/cadex-tri-frameset-2023> [Accessed 1 Oct. 2024].

Casey, M, & Wintergerste, T, 2000, Best Practice Guidelines. ERCOFTAC Special Interest Group on “Quality and Trust in Industrial CFD”, ERCOFTAC.

Cash, D, 2023, *Stefan Küng in scary crash at Euro TT Championships - Escape Collective*. [online] Escape Collective. Available at: <https://escapecollective.com/stefan-kung-in-scary-crash-at-euro-tt-championships/> [Accessed 1 Oct. 2024].

Chowdhury, H, & Alam, F, 2014, An experimental study on aerodynamic performance of time trial bicycle helmets. *Sports Engineering*, 17, pp.165-170.

CICLIMATTIO, 2024, *Frame Kit Colnago TT1*. [online] Ciclimattio.com. Available at: <https://ciclimattio.com/en/p/colnago/tt1-frame-kit-without-appendices-uae-s> [Accessed 1 Oct. 2024].

Crouch, TN, Burton, D, LaBry, ZA, & Blair, KB, 2017, *Riding against the wind: a review of competition cycling aerodynamics*, Sports Engineering, 20, pp. 81-110.

Croxton, J, 2024, *Just when we thought TT helmets couldn't get any weirder: Giro leaves us speechless*. [online] cyclingnews.com. Available at: <https://www.cyclingnews.com/news/just-when-we-thought-tt-helmets-couldnt-get-any-weirder-unreleased-giro-lid-leaves-us-speechless/> [Accessed 1 Oct. 2024].

Cyclestore, 2016, Bell Javelin Aero Helmet, Cyclestore. Available at: https://www.cyclestore.co.uk/bell_javelin_aero_tt_helmet-ID_68721 (Accessed: 12 April 2024).

Dave, DP, 2024, *Advances in Vehicular Aerodynamics*. Doctoral dissertation, Purdue University Graduate School.

Davidson, T, 2024, *Jay Vine receives three stitches for head wound suffered in World Championships crash*. [online] cyclingweekly.com. Available at: <https://www.cyclingweekly.com/racing/jay-vine-receives-three-stitches-for-head-wound-suffered-in-world-championships-crash> [Accessed 1 Oct. 2024].

Debraux, P, Grappe, F, Manolova, AV, & Bertucci, W, 2011, *Aerodynamic drag in cycling: methods of assessment*, Sports biomechanics, 10(3), pp. 197-218.

Defraeye, T, Blocken, B, Koninckx, E, Hespel, P, Carmeliet, J, 2010, Aerodynamic study of different cyclist positions: CFD analysis and full-scale wind-tunnel tests. J. Biomech. 43, 1262–1268.

Defraeye, T., Blocken, B., Koninckx, E., Hespel, P. and Carmeliet, J., 2010. Computational fluid dynamics analysis of cyclist aerodynamics: Performance of different turbulence-modelling and boundary-layer modelling approaches. *Journal of biomechanics*, 43(12), pp.2281-2287.

Defraeye, T, Blocken, B, Koninckx, E, Hespel, P, Carmeliet, J, 2011, Computational fluid dynamics analysis of drag and convective heat transfer of individual body segments for different cyclist positions. *J. Biomech.* 44, 1695–1701.

di Prampero, P.E. and Ferretti, G., 2023. Cycling, Swimming and Other Forms of Locomotion on Land and in Water. In *Exercise, Respiratory and Environmental Physiology: A Tribute from the School of Milano* (pp. 171-221). Cham: Springer International Publishing.

Dumas, L., 2008. CFD-based optimization for automotive aerodynamics. In *Optimization and computational fluid dynamics* (pp. 191-215). Berlin, Heidelberg: Springer Berlin Heidelberg.

Edelstein, S, 2021, *The Bugatti Bolide's air scoop was designed like a golf ball.* [online] Motor Authority. Available at: https://www.motorauthority.com/news/1130680_the-bugatti-bolide-s-air-scoop-was-designed-like-a-golf-ball.

Elite Wheels, 2024, *TT Rim Brake Bundle.* [online] Elitewheels. Available at: <https://www.elite-wheels.com/product/time-trial-triathlon-wheels-tt-rim-brake-bundle/> [Accessed 1 Oct. 2024].

Epton, T, 2022, *Best time trial and Triathlon Helmets 2024: We test them so you don't have to,* *cyclingweekly.com.* Available at: <https://www.cyclingweekly.com/group-tests/best-time-trial-and-triathlon-helmets-2022-we-test-them-so-you-dont-have-to> (Accessed: 13 May 2024).

Excel Sports, 2018, *Pinarello Bolide TT Frameset 2018 Excel Sports I Shop Online From Boulder Colorado.* [online] Excelsports.com. Available at: <https://www.excelsports.com/pinarello-bolide-tt-frameset-2018> [Accessed 1 Oct. 2024].

Fintelman, DM, Hemida, H, Sterling, M, & Li, FX, 2015, CFD simulations of the flow around a cyclist subjected to crosswinds. *Journal of Wind Engineering and Industrial Aerodynamics*, 144, pp.31-41.

Fitzgerald, S, Kelso, R, Grimshaw, P, & Warr, A, 2019, Measurement of the air velocity and turbulence in a simulated track cycling team pursuit race. *Journal of Wind Engineering and Industrial Aerodynamics*, 190, pp.322-330.

GIRO Helmets, 2024, *Aerohead Mips Helmet*. [online] Giro.com. Available at: <https://www.giro.com/p/aerohead-mips-road-bike-helmet/100000000300000048.html> [Accessed 4 Oct. 2024].

Glendenning, B, 2012, *50 stunning Olympic moments No43: Chris Boardman's Golden Barcelona*, The Guardian, viewed 05 October 2023, <<https://www.theguardian.com/sport/blog/2012/jun/27/50-stunning-olympic-moments-chris-boardman>>

Godo, M., Corson, D. and Legensky, S., 2010, January. A comparative aerodynamic study of commercial bicycle wheels using CFD. In 48th AIAA aerospace sciences meeting including the new horizons forum and aerospace exposition (p. 1431).

HJC Sports, 2024, Adwatt Aero Helmet: TT & Triathlon, HJC Sports. Available at: <https://www.hjcsports.com/helmets/adwatt/> (Accessed: 12 April 2024).

Javadi, A, Buckrell, AJ, & Peterson, SD, 2020, Improving numerical estimation of cyclist drag area in static conditions using unsteady RANS. In *Proceedings* (Vol. 49, No. 1). MDPI.

Jobson, SA, Nevill, AM, Palmer, GS, Jeukendrup, AE, Doherty, M, & Atkinson, G, 2007, The ecological validity of laboratory cycling: Does body size explain the difference between laboratory-and field-based cycling performance?. *Journal of Sports Sciences*, 25(1), pp.3-9.

Kamarudin, KM, Basri, MSM, Maidin, NA, & Ab Rahman, MH, 2020, Aerodynamic Drag Study of Time-Trial Cycling Helmets Using CFD Analysis. *Journal of Advanced Research in Fluid Mechanics and Thermal Sciences*, 72(1), pp.21-31.

KASK, 2022, *Mistral / Kask*. [online] Kask.com. Available at: https://www.kask.com/en-es/Mistral/CHE00050V.html?srsId=AfmBOopgbhfkDilnourz8iZEpnSf3ows8zZQC5sAoV_NUjB0Mcc-qjk- [Accessed 4 Oct. 2024].

Kuhlmann, K, Sinn, C, Siebert, JMU, Wehinger, G, Thöming, J, & Pesch, GR, 2022, From μ CT data to CFD: an open-source workflow for engineering applications, *Engineering Applications of Computational Fluid Mechanics*, 16(1), pp. 1706-1723.

Laughlin, R.M, 2022, *Optimising Ganna: CFD, CdA, CORE & Bigham*. [online] Velo. Available at: <https://velo.outsideonline.com/road/road-racing/optimising-ganna-cfd-cda-core-bigham/> [Accessed 3 Oct. 2024].

LAZER Sports, 2024, *Victor KinetiCore I Lazer*. [online] Lazer Sport. Available at: <https://www.lazersport.com/oc/helmets/on-road/victor-kineticore> [Accessed 4 Oct. 2024].

Li, L., Xu, X., Wang, W., Lau, R. and Wang, C.H., 2022. Hydrodynamics and mass transfer of concentric-tube internal loop airlift reactors: A review. *Bioresource Technology*, 359, p.127451.

Look, 2024, *Dolan Bikes*. [online] <https://www.dolan-bikes.com>. Available at: <https://www.dolan-bikes.com/alpina-carbon-tt-handlebars/> [Accessed 1 Oct. 2024].

Lueck, R, 2013, Calculating the rate of dissipation of turbulent kinetic energy. *Rockland Scientific International Tech. Note TN-028*, 18.

Lukes, RA, Chin, SB & Haake, SJ, 2005, *The understanding and development of cycling aerodynamics*, Sports engineering, vol. 8, pp. 59-74.

Mackinnon, K, 2021, *\$6,000 aero bars? Custom bars used by the pros - Triathlon Magazine Canada*. [online] Triathlon Magazine Canada. Available at: <https://triathlonmagazine.ca/gear/6000-aero-bars-custom-bars-used-by-the-pros/> [Accessed 1 Oct. 2024].

Maier, T, Schmid, L, Müller, B, Steiner, T, & Wehrlin, JP, 2017, Accuracy of cycling power meters against a mathematical model of treadmill cycling. *International Journal of Sports Medicine*, 38 (06), pp.456-461.

Malizia, F, & Blocken, B, 2020, *Bicycle aerodynamics: History, state-of-the-art and future perspectives*, Journal of Wind Engineering and Industrial Aerodynamics, 200, p. 104134.

Malizia, F, & Blocken, B, 2021, Cyclist aerodynamics through time: Better, faster, stronger. Journal of Wind Engineering and Industrial Aerodynamics, 214, p.104673.

Mathieu, A, Chauchat, J, Bonamy, C, & Nagel, T, 2019, Two-phase flow simulation of tunnel and lee-wake erosion of scour below a submarine pipeline. *Water*, 11(8), p.1727.

MET Helmets, 2024, *Triathlon and Aerodynamic Road Helmets*. [online] MET Helmets. Available at: <https://www.met-helmets.com/en/class/cycling-helmets/tri-aero-helmets/> [Accessed 4 Oct. 2024].

Othmer, C., 2014. Adjoint methods for car aerodynamics. *Journal of Mathematics in Industry*, 4(1), p.6.

Padilla, S, Mujika, I, Angulo, F, & Goiriena, JJ, 2000, Scientific approach to the 1-h cycling world record: a case study. *Journal of applied physiology*, 89(4), pp.1522-1527.

Passfield, L, Hopker, JG, Jobson, S, Friel, D, & Zabala, M, 2017, *Knowledge is power: Issues of measuring training and performance in cycling*, *Journal of sports sciences*, 35(14), pp. 1426-1434.

Piechna, J, 2021, A review of active aerodynamic systems for road vehicles. *Energies*, 14(23), p.7887.

Pompliano, J, 2023, *Tour de France: How the world's Most challenging race became a \$100 million business*, viewed 06 October 2023, <<https://huddleup.substack.com/p/tour-de-france-how-the-worlds>>

Rahpa Cycling, 2024, *Pro Team TT Mitts*. [online] Rahpa Cycling. Available at: <https://www.rapha.cc/eu/en/shop/pro-team-tt-mitts/product/BKA01XXHRIMED> [Accessed 2 Oct. 2024].

Resolved Analytics, n.d., *Steady-State vs. Transient Flow for CFD*. [online] Available at: <https://www.resolvedanalytics.com/cfd-physics-models/steady-vs-unsteady-flow>.

RUDY Project, 2024, *RUDY Project I The Wing TT Helmet*. [online] RUDY Project. Available at: <https://rudypoint.com.au/products/the-wing-time-trial-helmet> [Accessed 4 Oct. 2024].

Schröder, M, Bätge, T, Bodenschatz, E, Wilczek, M. and Bagheri, G., 2024. Estimating the turbulent kinetic energy dissipation rate from one-dimensional velocity measurements in time. *Atmospheric Measurement Techniques*, 17(2), pp.627-657.

Sexty, J, 2024, *Clip-on aerobars: 12 of the best reviewed for triathlon*. [online] 220 Triathlon. Available at: <https://www.220triathlon.com/gear/bike/accessories/aerobars/best-aero-bars> [Accessed 1 Oct. 2024].

Shaw, KK, Kesarwani, Y, & Chakravarty, P, 2020, Study of dimple effect on aerodynamic drag characteristics of a car. *Prepr. Int J Innov Res Sci Eng Technol*, 9, pp.4628-4637.

Sims, BW, Jenkins, PE, 2011, Aerodynamic bicycle helmet design using a truncated air foil with trailing edge modifications. In: ASME 2011 International Mechanical Engineering Congress and Exposition, Vol. 6: Fluids and Thermal Systems; Advances for Process Industries, Parts A and B, pp. 453– 462.

SMITH Optics, 2024, *SMITH Jetstream TT Helmet*. [online] Smith Optics. Available at: https://www.smithoptics.com/en_CA/p/helmet/jetstream-tt-mips%C2%AE-new/E007439KS5155.html?yoReviewsPage=5 [Accessed 4 Oct. 2024].

Tew, GS, & Sayers, AT, 1999, *Aerodynamics of yawed racing cycle wheels*, Journal of Wind Engineering and Industrial Aerodynamics, 82(1-3), pp. 209-222.

UCI, 2024, *UCI Equipment*. Available at: <https://www.uci.org/equipment/bh2JJzw1eB0n876rX2iB1> (Accessed: 04 March 2024).

UCI, 2023, *UCI Clarification on the Technical Regulation Guide* . Available at: <https://www.uci.org/regulations/3MyLDDrwJCJJ0BGGOFzOat> (Accessed: 04 March 2024).

Van Dijk, H., Van Megen, R. and Vroemen, G., 2017. The secret of cycling: maximum performance gains through effective power metering and training analysis. Meyer & Meyer Sport, p.54

van Druenen, T, & Blocken, B, 2024, *CFD simulations of cyclist aerodynamics: Impact of computational parameters*. Journal of Wind Engineering and Industrial Aerodynamics, 249, p.105714.

Wang, W, Cao, Y, & Okaze, T, 2021, Comparison of hexahedral, tetrahedral and polyhedral cells for reproducing the wind field around an isolated building by LES. *Building and Environment*, 195, p.107717.

Wilson, M, 2022, *Best tour de france finish ever: Why LeMond's '89 win Reigns Supreme*, GearJunkie, viewed Accessed: 05 October 2023, <<https://gearjunkie.com/biking/best-tour-de-france-finish-ever-1989-greg-lemond>>

Wood, R, 2019, *Body size of cyclists in the Tour de France*, Top End Sports. Available at: <https://www.topendsports.com/sport/cycling/anthropometry-tourdefrance.htm> (Accessed: 04 March 2024).

Yang, C., Tian, X., Liu, T., Cao, Y. and Li, D., 2017. '3D printing for continuous fiber reinforced thermoplastic composites: mechanism and performance', *Rapid Prototyping Journal*, vol. 23, no. 1, pp.209-215.

Zaidi, H, Taiar, R, Fohanno, S & Polidori, G, 2008, Analysis of the effect of swimmer's head position on swimming performance using computational fluid dynamics. *Journal of Biomechanics*, 41(6), pp.1350-1358.

Zaidi, H, Fohanno, S, Taiar, R, & Polidori, G, 2010, Turbulence model choice for the calculation of drag forces when using the CFD method. *Journal of biomechanics*, 43(3), pp.405-411.

Appendix A

A.1 – Project Specification and Work Plan

Specification and Work Plan

Title: Improving Road Cycling Performance in Design Through Aerodynamics Using Computational Fluid Dynamic Methods

Name: Robert Campbell

Student ID: [REDACTED]

Supervisors: Assoc Prof Andrew Wandel (Lead), Dr Khalid Saleh (Second)

Introduction and Background:

Within the sport of road cycling, aerodynamics can sometimes be a deciding factor in who succeeds to victory. Athletes work with sponsors and manufacturers to obtain the most aerodynamic bicycles and equipment to achieve marginal gains over their competitors. The critical role aerodynamics plays in cycling became evident in the 1989 Tour De France, in which Greg Lemond famously won the tour by beating Laurent Fignon. Lemond was 50 seconds behind Fignon on the last day on the tour in which the stage consisted of a 25 km time trial (TT). Lemond, competed in an aerodynamic TT helmet, triathlon bars and a back disc wheel, whilst Fignon competed with conventional TT bars of the time without any helmet on. Lemond was able to beat Fignon by 58 seconds, to which, began the evolving development of aerodynamics in the world of cycling (Tew & Sayers, 1999).

Studies have shown that aerodynamic drag is a significant contributing factor in the total resistance the cyclist must overcome and is responsible for up to 80% of the force. Furthermore, the time trial helmet is responsible for up to 8% of the total aerodynamic resistance the cyclist must overcome (Beaumont, et al., 2018).

Within engineering and design, CFD is widely used to allow observation of fluid flow, temperature and/or species fields inside of and surrounding objects (Kuhlmann, et al., 2022). In the context of bicycle helmet design and manufacture, CFD can reduce the number of prototypes from 100 down to 10. Whilst wind tunnel testing is considered the final step in testing for design of helmets and bicycles (Pogni & Petrone, 2016), studies have shown that CFD results are within accordance of wind tunnel results (Blocken, et al., 2013).

The sport of cycling is governed by the Union Cycliste International (UCI), who is responsible for the evolving rules and regulations for design to enforce an even playing field for teams at a professional level. Effectively applied CFD can reduce the amount of wind tunnel testing required and facilitate companies being able to adapt to changes in response of UCI regulations (Godo, et al., 2010).

Whilst there is sufficient research available in this area, it is still reasonably limited which could most be attributed to manufacturers trying to withhold their design secrets to not give any advantage to their competitors (Crouch, et al., 2017). This gap confirmed the demand for the research.

Objectives and Aims:

This research project proposes to produce a time trial helmet with a lower value of drag force than popular designs currently available, in particular the HJC ADWATT. The design will be tested using Computational Fluid Dynamic (CFD) methods with a human model wearing the helmet. The design must conform with UCI regulations.

Specific Objectives:

- Literature review and research to determine what has been tested
- Obtain control model of the HJC ADWATT and popular designs helmet to be utilised for CFD
- Produce prototype model helmet
- Calculate cyclist power and speed savings

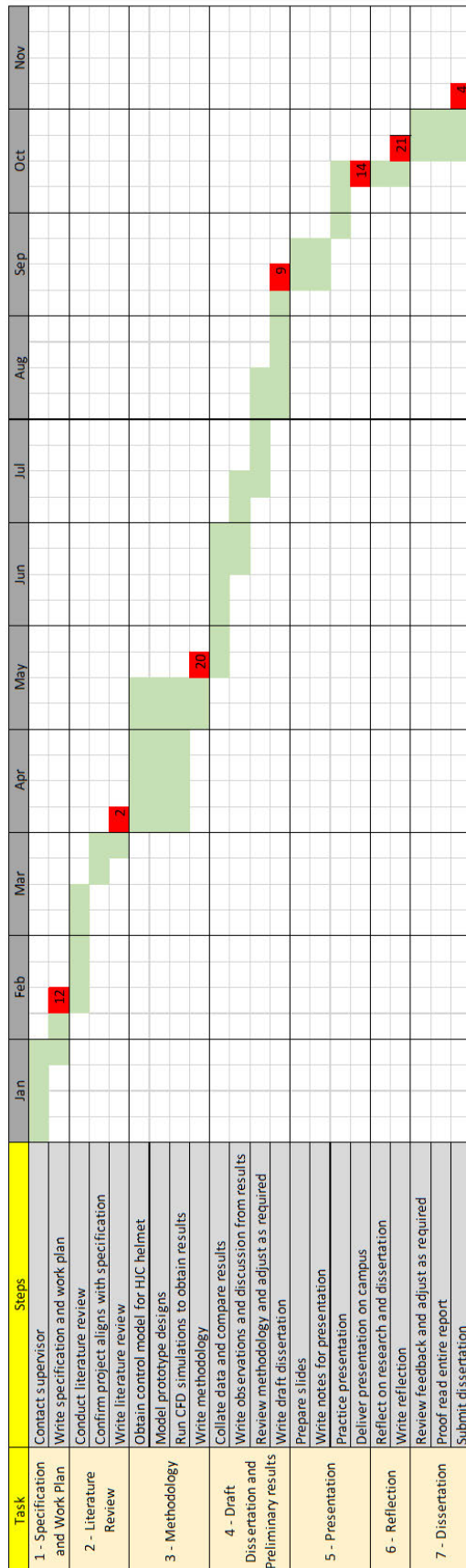
Expected Outcomes:

- A prototype helmet that has tested a lower value of CdA than the control on CFD platform
- The time and speed advantage for the cyclist using the prototype helmet over a flat 40 km time trial race

Resources Required:

- **Equipment:**
 - Desktop computer (CFD compatibility)
 - 3D printer (if time permits physical model)
 - USQ wind tunnel (if time permits physical model)
- **Software:**
 - Microsoft Excel
 - Microsoft Word
 - Creo (Modelling)
 - Ansys (CFD)
 - MATLAB
 - Endnote

A.2 – Timeline



A.3 – Risk Assessment



University of Southern Queensland

Offline Version

USQ Safety Risk Management System

Note: This is the offline version of the Safety Risk Management System (SRMS) Risk Management Plan (RMP) and is only to be used for planning and drafting sessions, and when working in remote areas or on field activities. It must be transferred to the online SRMS at the first opportunity.

Safety Risk Management Plan – Offline Version				
Assessment Title:	ENP4111 - Improving Road Cycling Performance in Design Through Aerodynamics Using Computational Fluid Dynamic Methods		Assessment Date:	15/05/2024
Workplace (Division/Faculty/Section):	School of Engineering		Review Date:(5 Years Max)	15/05/2029
Context				
Description:				
What is the task/event/purchase/project/procedure?	Improving road cycling performance by enhancing aerodynamics through design of time trial helmets			
Why is it being conducted?	Required testing for capstone project			
Where is it being conducted?	Personal residence, Mcdowall QLD			
Course code (if applicable)	ENP4111	Chemical name (if applicable)	N/A	
What other nominal conditions?				
Personnel involved	Robert Campbell			
Equipment	MacBook Air 1.4 GHz Dual-Core Intel Core i5			
Environment	Indoor, private residence			
Other	ANSYS			
Briefly explain the procedure/process	To produce bicycle helmet on ansys and then test their aerodynamics using CFD fluent			
Assessment Team - who is conducting the assessment?				
Assessor(s)	Andrew Wandel			
Others consulted:	N/A			

This document is uncontrolled once printed and may not be the latest version. Access the online SRMS for the latest version. Safety Risk Management Plan V1.1

Step 1 (cont)	Step 2	Step 2a	Step 2b	Step 3			Step 4				
Hazards: From step 1 or more if identified	The Risk: What can happen if exposed to the hazard without existing controls in place?	Consequence: What is the harm that can be caused by the hazard without existing controls in place?	Existing Controls: What are the existing controls that are already in place?	Risk Assessment: Consequence x Probability = Risk Level			Additional controls: Enter additional controls if required to reduce the risk level	Risk assessment with additional controls:			
				Probability	Risk Level	ALARP? Yes/no		Consequence	Probability	Risk Level	ALARP? Yes/no
Example											
Working in temperatures over 35° C	Heat stress/heat stroke/exhaustion leading to serious personal injury/death	catastrophic	Regular breaks, chilled water available, loose clothing, fatigue management policy.	possible	high	No	temporary shade shelters, essential tasks only, close supervision, buddy system	catastrophic	unlikely	mod	Yes
Poor posture from continuous sitting - Ergonomic	Repetitive strain injury	Minor	Regular breaks, activation exercises	Unlikely	Low	Yes	Mandatory breaks every 40 min, mouse and keyboard set up to appropriate levels. Every 3 hours take 30 min break	Insignificant	Rare	Low	Yes
Excessive work periods looking at screen - Ergonomic	Vision impairment/headache	Minor	Regular breaks, try to take focus off screen every 10 mins, room is well lit, natural light if possible	Unlikely	Low	Yes	Mandatory breaks every 40 min, screen set up to appropriate height. Every 3 hours take 30 min break	Insignificant	Rare	Low	Yes
Computer overheating from high CPU requirements	Damage to computer, loss of data	Minor	Ensure computer has sufficient CPU for simulations, close all other programs	Unlikely	Low	Yes	Ensure computer is well ventilated, run appropriate mesh sizes for simulations that don't require excessive CPU	Insignificant	Rare	Low	Yes
Fall hazard from cluttered workspace	Minor fall injury	Minor	Ensure workspace is clean with nothing left on floor	Unlikely	Low	Yes	Workspace cleaned prior to conducting any research, Family members to keep clear of workspace to avoid any clutter or rubbish from entering it	Insignificant	Rare	Low	Yes